UNIVERSITÉ DE STRASBOURG

ÉCOLE DOCTORALE 182 : Physique et Chimie-Physique

Institut Charles Sadron, UPR 22

THÈSE présentée par :

Alexandre DOCHTER

soutenue le : **23 septembre 2014**

pour obtenir le grade de : **Docteur de l'université de Strasbourg**

Discipline/ Spécialité : **CHIMIE-PHYSIQUE**

Polymer films and brushes self-construction by electrochemically triggered morphogens.

THÈSE dirigée par :

Pierre SCHAAF Professeur, université de Strasbourg

RAPPORTEURS :

Tomaso ZAMBELLI Chercheur, ETH Zürich

Pierre LABBE Professeur, Université Joseph Fourier

AUTRES MEMBRES DU JURY :

Michel NARDIN Directeur de recherche, CNRS

A ma femme Tere

et à mon fils Lucas,

REMERCIEMENTS

Ce travail a été effectué à l'Institut Charles Sadron (CNRS, UPR 22) en étroite collaboration avec l'unité INSERM 1121 « Biomatériaux et Bioingénierie ». Je tiens à remercier les directeurs Jean-François Legrand, Jean-Michel Guenet et Pierre Schaaf de m'avoir accueilli dans leurs laboratoires respectifs.

Je tiens particulièrement à remercier mon directeur de thèse, le Professeur Pierre Schaaf pour m'avoir accueilli au sein du laboratoire ainsi que pour son encadrement régulier tout au long de ma thèse. Je le remercie pour toutes ses contributions scientifiques lorsque je rencontrais des difficultés ainsi que pour sa forte disponibilité. Je le remercie également pour les nombreuses corrections qu'il a apportées à ce manuscrit ainsi qu'aux articles qui y sont rattachés.

Je remercie également le Dr. Fouzia Boulmedais pour son encadrement au quotidien, sa disponibilité et ses conseils. Ses corrections ont permis l'obtention de ce manuscrit tel qu'il est aujourd'hui et sa présence lors de mes répétitions de soutenance m'a permis d'améliorer grandement mes qualités de communication. Son aide s'est révélée précieuse dans le cadre de mes travaux de recherche et ses conseils ont menés à l'obtention de la plupart de mes résultats. Je la remercie également de sa patience lors de cet encadrement qui, je le sais, n'a pas toujours été facile.

Mes plus profonds remerciements vont au Dr. Loïc Jierry qui a toujours été présent pour moi dans les bons comme dans les mauvais moments. Ses compétences scientifiques en chimie ont permis la genèse de ce travail et de ces projets mais je tiens avant tout à le remercier pour les qualités humaines qu'il a démontrées tout au long de ces trois années. Sans son soutien et ces conseils avisés, cette thèse n'aurait probablement pas aboutie.

Je suis très sensible à l'honneur que me font les membres de mon jury en acceptant d'évaluer ce travail. Je tiens à témoigner toute ma reconnaissance au Dr. Tomaso Zambelli de l'ETH Zürich et au Professeur Pierre Labbé de l'université Joseph Fourrier d'avoir accepté d'intervenir en tant que rapporteur de la thèse. Je garde par ailleurs les meilleurs souvenirs de mon passage dans le laboratoire LBB de l'ETH ou j'ai effectué mon stage de dernière année d'ingénieur. J'y ai trouvé un excellent cadre scientifique et humain et conserve encore certaines amitiés de cette expérience. J'adresse toute ma reconnaissance au Directeur de recherche Michel Nardin d'avoir accepté de présider ce jury en tant qu'examinateur. Je remercie également le Dr. Fouzia Boulmedais d'avoir participé à ce jury en tant qu'invitée.

Je tiens à remercier tout particulièrement le Dr. Tony Garnier avec lequel j'ai partagé mon bureau. Ses compétences en chimie ont permis l'obtention de la quasi-totalité des polymères que j'ai utilisés pendant ma thèse et ses conseils en chimie m'ont énormément apporté (l'addition de Michael entre autre). Son esprit « brésil », sa bonne humeur transmissible et ses anecdotes ont participé à cette ambiance du laboratoire qui me manque déjà. Je n'oublierai pas les diners et les sorties hors de l'ICS, et, s'il lit ces remerciements, je tiens à lui rappeler qu'une surface est quadratique.

Des personnes qui ont rendu cette thèse agréable, je n'oublierai pas mes deux autres compagnons thésard : Johan Longo et Lydie Séon avec lesquels j'ai beaucoup partagé. Ces deux amis ont eux aussi connus les joies et les difficultés de la thèse dont nous parlions abondamment autour d'un café. J'ai aimé les sorties que nous avons faites ensemble même si je n'étais pas aussi présent hors du

laboratoire que je l'aurai souhaité. J'espère que nous nous reverrons souvent au cours des années à venir !

Des personnes du laboratoire, je remercie également Clément Maerten, Eric Lutz, Olga Siscan et Fabien Gaudière pour leur bonne humeur et les anecdotes partagées. Ils ont tous contribués à la bonne ambiance générale et ont su rendre la thèse plus agréable. Je pense en particulier à Clément à qui il reste encore à écrire le manuscrit et soutenir: courage !!!

Je tiens également à remercier le Dr.Damien Mertz qui m'a donné le goût de la recherche lorsque je n'étais qu'un jeune universitaire. C'est lui qui m'a transmis la passion et l'intérêt de la recherche en matériaux et m'a introduit au sein du laboratoire. Je lui dois beaucoup scientifiquement et je n'oublierai jamais nos discussions scientifiques et personnelles au cours de ces huit années.

Enfin, des personnes externes au laboratoire je remercie ma femme pour sa patience, sa disponibilité et ses encouragements tout au long de la thèse. C'est elle, parmi tous, qui a vécu au plus près les joies et difficultés de cet exercice. Toujours présente, elle a, d'une certaine manière, contribué à la rédaction de ce manuscrit et à la préparation de ma soutenance.

Table of contents

Table of contents

LIST OF ABBREVIATIONS

Chemical compounds

Macromolecules

PAH	poly(allylamine hydrochloride)
PAHc	PAH grafted with citraconic functions
PAHd	PAH grafted with dimethylmaleic functions
PEDOT	poly(3,4-ethylenedioxythiophene)
PEI	poly(ethylene immine)
PEI-Br	PEI modified with bromo-isobutyramide functions
PEG	poly(ethylene glycol)
PSS	poly(styrene sulfonate)

Other compounds

HEPES	2-[4-(2-hydroxyethyl)piperazin-1-yl]ethanesulfonic acid
MeO_2MA	2-(2-methoxyethoxy)ethyl methacrylate
OEGMA	oligo(ethylene glycol) methyl ether methacrylate
TBAB	tetra n-butylammonium bromide
TPMA	tris(2-pyridylmethyl)amine
PNP	para-nitrophenylphosphate

Methods

AFM	atomic force microscopy
CAP	continuous assembly of polymers
LbL	layer-by-layer
QCM-D	quartz crystal microbalance with dissipation
EC-QCM-D	electrochemical quartz crystal microbalance with dissipation
NMR	nuclear magnetic resonance
SAM	self-assembled monolayer
XPS	X-ray photoelectron spectroscopy

Usual abbreviations

Pdiff	potential difference
CE	counter electrode
Ip	isoelectric point
RE	reference electrode
WE	working electrode

RÉSUMÉ DES TRAVAUX

RESUME DES TRAVAUX

CONTENTS

1.1 CONTEXTE DE L'ÉTUDE

L'auto-construction exclusivement près de surfaces de films dépassant la monocouche représente un réel défi car cela requiert des molécules complémentaires qui interagissent entre elles. Or comment restreindre ces interactions entre molécules au voisinage de la surface et donc les éviter en solution? Dans la nature, certaines molécules spécifiques appelées morphogènes contrôlent le développement des tissus biologiques par l'établissement d'un gradient de concentration.

Récemment, une nouvelle approche a été introduite qui consiste à construire des films polymériques en une seule étape (one-pot) par électrochimie. Se basant sur un travail consistant à construire un film par électrochimie click en faisant réagir des alcynes sur des azides via la formation d'un gradient de Cu(I), catalyseur de la réaction et morphogène, par électrochimie (Rydzek et al. 2011, Rydzek 2012, Rydzek et al. 2012), nous avons voulu élargir cette approche à d'autres réactions chimique.

Mes travaux de thèse portent donc sur la généralisation de cette approche par le développement de trois systèmes : (1.2) la polymérisation radicalaire contrôlée basée sur des liaisons covalentes, (1.4) la construction de films de polyélectrolytes bioactifs et (1.3) la construction de films de polyampholytes ces deux dernières approches étant basées sur des interactions électrostatiques.

1.2 POLYMERISATION RADICALAIRE PAR TRANSFERT D'ATOME INITIE EN SURFACE PAR ELECTROCHIMIE.

Le chapitre 3 de cette thèse est focalisé sur la construction par électrochimie de brosses de polymères par polymérisation radicalaire par transfert d'atome initiée en surface (eSI-ATRP).

L'ATRP est une technique de polymérisation radicalaire contrôlée qui fût introduite pour la première fois simultanément par Matyjaszewski et Sawamoto en 1995 (Kato et al. 1995, Wang et al. 1995). Cette technique est basée sur un équilibre entre un "état dormant" où les chaînes de polymères contenant un halogène n'ont pas de radicaux et ne polymérisent pas et un "état vivant" où la chaîne de polymère contient un radical et polymérise. Le passage de l'"état dormant" des chaînes de polymères à l'"état vivant" se fait par le biais d'un catalyseur, le plus souvent le cuivre(I).

Récemment, il a été montré qu'il était possible d'effectuer une polymérisation par ATRP en milieu aqueux par électrochimie (eATRP) (Bortolamei et al. 2011). Dans ce cas, le catalyseur, i.e. le cuivre(I) est généré par électrochimie et la croissance des polymères a lieu en solution. La Figure 1a détaille cette réaction eATRP.

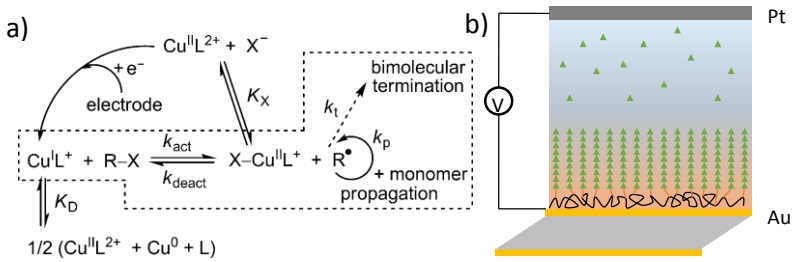

Figure 1 Réaction électrochimique d'une polymérisation radicalaire par transfert d'atome (eATRP) (a). Schéma du projet: construire des brosses de polymère par ATRP depuis une surface conductrice en utilisant un macro-initiateur polymérique et en générant un gradient de catalyseur par électrochimie (morphogène) (b).

La généralisation de cette technique aux surfaces a constitué mon premier objectif de thèse.

Pour assurer une réaction d'eSI-ATRP, un macro-initiateur polymérique est déposé sur une électrode de travail. Un potentiel électrique est alors appliqué à cette électrode en contact avec une solution contenant des monomères et des ions Cu(II). Au voisinage de l'électrode, des ions Cu(I) sont générés à partir du Cu(II) en solution. La liaison C-Br du macro-initiateur est alors clivée, générant le radical nécessaire à la réaction d'ATRP. La Figure 1b décrit schématiquement cette technique d'assemblage.

Le choix du macro-initiateur polymérique s'est porté sur un poly(éthylène immine) sur lequel une fonction bromo-isobutyramide a été greffée. L'une des premières conditions requise pour construire des brosses de polymère par ATRP depuis une surface est la compréhension de l'influence du catalyseur, i.e. le Cu(I) sur le contrôle de la cinétique de construction.

L'influence de différents sels de cuivre sur le signal électrochimique par voltammétrie cyclique (CV) a d'abord été étudiée afin de déterminer le meilleur sel à utiliser pour la réaction d'eSI-ATRP. Une réaction de polymérisation d'un monomère éthylène glycol méthacrylate a été suivie par microbalance à cristal de quartz avec mesure de la dissipation (QCM-D) et par voltammétrie cyclique afin de déterminer le potentiel à appliquer nécessaire pour générer les ions Cu(I). Il a été mis en évidence que la différence de potentiel électrique doit être inférieure à une valeur critique de -250 mV (vs une électrode de référence de type Ag/AgCl).

Des brosses d'homopolymères ont été construites en introduisant une solution de monomères au voisinage de l'électrode et en modulant le stimulus électrochimique. Les propriétés anti-adsorbante vis-à-vis des protéines des brosses d'éthylène glycol construites ont été mises en évidence.

L'utilisation d'un sel bromé a permis d'améliorer la cinétique de construction.

Suite à la publication de travaux très similaires par un groupe chinois à ceux que nous avons menés, ce sujet n'a pas donné lieu à une publication scientifique (Li et al. 2012, Li et al. 2013a, Li et al. 2013b). L'intégralité de ces travaux est disponible au chapitre 3 de ce présent manuscrit.

1.3 AUTO-ASSEMBLAGE TOUT-EN-UN D'UN FILM DE POLYANIONS/POLYCATIONS PAR ELECTROCHIMIE

Le second projet de cette thèse, décrit dans le Chapitre 4, est basé sur l'auto-construction de films de polyélectrolytes par approche morphogénique. Dans ce cas, un poly(allylamine hydrochlorique) protégé avec un groupement diméthylmaléique (**PAHd**, synthèse: Dr. Tony Garnier) a été synthétisé. Le PAHd, chargé négativement en milieu neutre et basique, se charge positivement en milieu acide et devient un polycation (Figure 2).

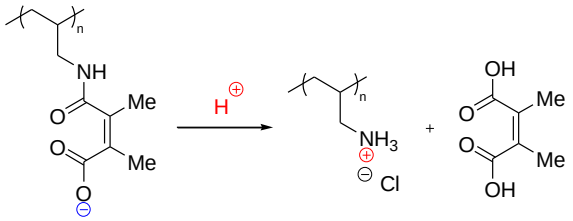

Figure 2 Réaction de déprotection du polyanion PAHd en polycation.

Le polycation généré peut alors se complexer avec un partenaire polyanionique présent simultanément en solution ce qui conduit à la formation d'un film. Des études par QCM-D, AFM, chronopotentiométrie et XPS ont été effectuées.

Le polyanion PAHd a été mis en solution en présence d'hydroquinone et d'un autre polyanion, le poly(styrène sulfonate) (PSS), dans une solution saline. Lors de l'application d'un courant, le PAHd se déprotège et forme le polycation qui complexe avec le PSS à l'interface.

La croissance du film PAH/PSS au cours du temps à partir d'une solution de PAHd/PSS pour un courant fixe de -100 µA a été obtenue. Une augmentation de la cinétique de construction des films est observée par augmentation de l'intensité du courant appliqué.

Le polyanion PSS utilisé peut être remplacé par une enzyme chargée négativement telle que l'alcaline phosphatase (AP). Dans ce cas, le film formé PAH/AP conserve une activité enzymatique et possède une épaisseur de 105 nm pour un courant appliqué de -100 µA appliqué pendant une heure.

Une augmentation de l'activité pour des temps de constructions croissants d'un film PAH/AP a été mise en évidence montrant une relation entre la quantité d'AP immobilisée et l'activité.

Des constructions de films PAH/PSS et PAH/AP sur des micro-électrodes ont été réalisées démontrant ainsi la localisation de la construction des films par électrochimie.

L'intégralité des résultats de ce projet est disponible au chapitre 4 de ce présent manuscrit.

1.4 AUTO-ASSEMBLAGE TOUT-EN-UN D'UN FILM DE POLYAMPHOLYTE PAR ELECTROCHIMIE

Le dernier projet présenté dans ce manuscrit au chapitre 5 consiste en l'auto-assemblage de polyampholytes basé sur la génération d'un gradient de protons par oxydation de l'hydroquinone (Figure 3a). Un polyanion de synthèse, le poly(allylamine hydrochlorique) protégé par une fonction anhydride citraconique (**PAHc**, synthèse: Dr. Tony Garnier), est présent dans la solution. Ce polyanion, chargé négativement en milieu neutre et basique, se charge partiellement positivement en milieu acide et devient un polyampholyte (Figure 3b). La formation du polyampholyte est due à une double cinétique de déprotection du polymère.

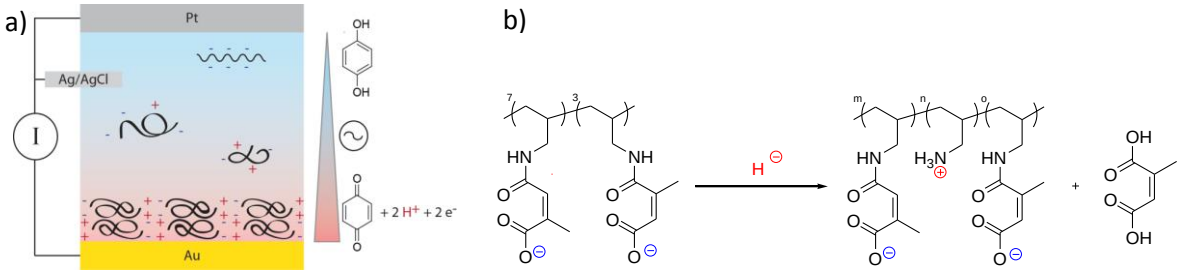

Figure 3 But du projet: construction d'un film de polyampholyte par génération électrochimique d'un gradient de protons (morphogène) (a). Réaction chimique de déprotection partielle du PAHc produisant le polyampholyte (b).

Le polyampholyte généré peut alors former des complexes intra-moléculaires et inter-moléculaires ce qui conduit à la formation d'un film. Des études par QCM-D, Microscopie à force atomique (AFM), chronopotentiométrie et spectrométrie d'émission de photons X (XPS) ont été effectuées.

Le polyanion PAHc a été mis en présence d'hydroquinone dans une solution saline. Lors de l'application d'un courant fixe de -100 µA (chronopotentiométrie), un film de polyampholyte croît à la surface de l'électrode de travail. Une variation linéaire de l'épaisseur du film formé au cours du temps a été obtenue.

Le gradient de proton généré par l'oxydation électrochimique de l'hydroquinone peut être contrôlé grâce à la valeur de l'intensité du courant appliqué. Plus l'intensité du courant appliqué est élevée, plus la quantité de protons générée est grande et donc plus l'acidité à proximité de l'électrode de travail va être importante menant à une construction plus rapide. L'augmentation de la cinétique de construction pour une intensité de courant appliquée croissante a été mise en évidence. Une vitesse de construction maximale correspondant à un courant appliqué de -100 µA a été observée. L'épaisseur des films construits est de l'ordre de 350 nm pour un courant de -100 µA appliqué pendant une heure.

Les films de polyampholytes formés ne sont pas stables lors du rinçage. Une réticulation thermique de ces films permet de les rendre plus robustes.

L'intégralité des résultats obtenus dans le cadre de ce projet est disponible au chapitre 5 de ce présent manuscrit.

RÉFÉRENCES

Bortolamei, N., A. A. Isse, A. J. Magenau, A. Gennaro and K. Matyjaszewski (2011). "Controlled Aqueous Atom Transfer Radical Polymerization with Electrochemical Generation of the Active Catalyst." Angewandte Chemie, International Edition in English **50**(48): 11391-11394.

Kato, M., M. Kamigaito, M. Sawamoto and T. Higashimura (1995). "Polymerization of Methyl-Methacrylate with the Carbon-Tetrachloride Dichlorotris(Triphenylphosphine)Ruthenium(Ii) Methylaluminum Bis(2,6-Di-Tert-Butylphenoxide) Initiating System - Possibility of Living Radical Polymerization." Macromolecules **28**(5): 1721-1723.

Li, B., B. Yu, W. T. Huck, W. Liu and F. Zhou (2013a). "Electrochemically Mediated Atom Transfer Radical Polymerization on Nonconducting Substrates: Controlled Brush Growth through Catalyst Diffusion." Journal of the American Chemical Society **135**(5): 1708-1710.

Li, B., B. Yu, W. T. Huck, F. Zhou and W. Liu (2012). "Electrochemically Induced Surface-Initiated Atom-Transfer Radical Polymerization." Angewandte Chemie, International Edition in English **51**(21): 5092-5095.

Li, B., B. Yu and F. Zhou (2013b). "In Situ Afm Investigation of Electrochemically Induced Surface-Initiated Atom-Transfer Radical Polymerization." Macromolecular Rapid Communications **34**(3): 246-250.

Rydzek, G. (2012). Assemblage De Films Polymères Par Réaction Click Électrocontrôlée.

Rydzek, G., L. Jierry, A. Parat, J. S. Thomann, J. C. Voegel, B. Senger, J. Hemmerle, A. Ponche, B. Frisch, P. Schaaf and F. Boulmedais (2011). "Electrochemically Triggered Assembly of Films: A One-Pot Morphogen-Driven Buildup." Angewandte Chemie, International Edition in English **50**(19): 4374-4377.

Rydzek, G., A. Parat, P. Polavarapu, C. Baehr, J. C. Voegel, J. Hemmerle, B. Senger, B. Frisch, P. Schaaf, L. Jierry and F. Boulmedais (2012). "One-Pot Morphogen Driven Self-Constructing Films Based on Non-Covalent Host-Guest Interactions." Soft Matter **8**(2): 446-453.

Wang, J. S. and K. Matyjaszewski (1995). "Controlled Living Radical Polymerization - Atom-Transfer Radical Polymerization in the Presence of Transition-Metal Complexes." Journal of the American Chemical Society **117**(20): 5614-5615.

GENERAL INTRODUCTION

Surface coatings obtained by molecule deposition is studied since the 30s. Their interest resides in the possibility to confer specific properties to material surfaces. Since the beginning of the 90s, the layer-by-layer technique, consisting in an alternate adsorption of polycations and polyanions on surfaces, have known a striking development. This approach allows to easily obtain multilayer films with a thickness ranging from nano to micrometer on substrate with various chemical compositions and topographies. These assemblies have been used in various fields such as biomaterials, nanofiltration devices, surface catalysis and energy production. More recently, a new generation of multilayer films have emerged with stimuli responsive properties towards electric fields, irradiation or physical/chemical properties of the medium.

However, the application of the layer-by-layer technique have been slowed down by two major limitations: the coatings must be resistant towards the physical and chemical constraints of their environment and their buildup must be fast and cheap.

In the last years, several research in polyelectrolyte multilayers have been oriented to provide a faster deposition process and robust films. A new strategy based on the electrochemical generation of a catalyst gradient triggering the self-assembly of polymer films have been introduced by our team: the **one-pot morphogen approach**. In chemistry, a **morphogen** can be defined as a molecule or an ion that is produced at an interface, that diffuses into the solution, creating a gradient and which induces locally a chemical process.

This approach was successfully applied to buildup polymer films constituted of two interacting polymers through covalent and non-covalent bonding. The role of the morphogen was played by copper (I) which was electrochemically generated at an electrode to catalyze a click reaction between azide and alkyne bearing polymers.

The purpose of this PhD was to extend this strategy to other systems. The one-pot morphogenic approach was successfully applied to buildup polymer brushes by the copper (I) catalyzed atom transfer radical polymerization. It was also used to buildup polycation/polyanion and polyampholyte films by an electrochemically triggered proton catalyzed reaction.

This manuscript is composed of five chapters. The first chapter briefly reviews the state-of-the-art in the latest development of the layer-by-layer technique and in the field of electro-deposited coatings. The second chapter presents the material and methods used during this PhD. The third chapter reviews the latest development in the field of atom transfer radical polymerization and presents the application of this technique for building up polymer brushes from a surface with an electrochemical generation of the catalyst. The self-construction of polycation/polyanion films triggered by an electrochemical gradient of catalyst is exposed in chapter four. The latest chapter focuses on the self-construction of polyampholyte films by an electrochemically triggered gradient of catalyst.

The first chapter presents the state-of-the-art in current research on multilayer films obtained by the Layer-by-Layer (LbL) technique. The improvements of the technique to provide faster buildup mechanisms and robust films are briefly exposed. The contribution of our team on the development of such films by a strategy based on electrochemically triggered morphogens is discussed. In this context, the literature of the community on morphogenic buildups of polymer and biomacromolecules films is reviewed.

The second chapter presents the material and methods used during this PhD. The commercial and synthesized polymers/biomacromolecules used in the later buildups are described. The common characterization and construction methods are explained. The signal analysis of the characterization and construction techniques are detailed in this chapter as well as in the following chapters when necessary.

The third chapter focuses on the buildup of polymer brushes by an electrochemically triggered morphogen. The buildup is based on a control radical polymerization process, namely, atom transfer radical polymerization. This process is based on a copper (I) catalysis like in the Huisgen-Sharpless click chemistry but relies on more complex equilibria that are discussed there. The electrochemical production of this catalyst constitutes the morphogen used to trigger the polymer brushes construction. Polymer brushes are thus obtained by an electrochemical surface initiated atom transfer radical polymerization (eSI-ATRP). Investigation of the buildup kinetic and of the surface morphology confirmed that the polymer brushes obtained are likely to be constructed by eSI-ATRP. The functionalized surface exhibits antifouling properties toward proteins thus confirming the chemical nature of the formed polymer brushes. Parameters influencing the buildup kinetic are discussed.

The fourth chapter presents the self-assembly of polycation/polyanion films by an electrochemically triggered morphogen. In this chapter and in the following one, the morphogen role is played by protons obtained during the electrochemical oxidation of a small molecule. The one-pot construction of this film is studied and the parameters influencing the buildup kinetic are discussed. The obtained

complexes films thicknesses are shown to be controlled by the electrochemical stimulus parameters such as the applied intensity and the construction time. Chemical composition of the film is investigated and confirms the proposed model for the film buildup.

The last chapter introduces the buildup of films based on polyampholytes generated by an electrochemical triggered morphogen. As in chapter four, the protons, i.e. the morphogens, are obtained by the electrochemical oxidation of a small molecule. The catalyst gradient generated at the interface is demonstrated to lead to a polyampholyte film buildup. The electrochemical parameters influencing the buildup kinetic are studied. The hydrosoluble films formed are proved to be cross-linkable by a thermic post treatment. The chemical composition of the films confirms the proposed mechanism for the film construction.

CHAPTER 1: BIBLIOGRAPHIC REVIEW

1 BIBLIOGRAPHIC REVIEW

CONTENTS

1.1 CONTEXT OF THE STUDY.

Polyelectrolyte multilayers are films obtained by the alternate deposition of polyanions and polycations on solid substrates. They were introduced in 1991 by G. Decher and have since received considerable attention from the scientific community (Decher et al. 1992, Decher 1997). They constitute a very versatile tool to functionalize surfaces: they can be applied on almost any kind of surface even with complex geometry and allow conferring specific properties that cover a large range of applications (biomaterials, optical properties, sensors, wetting properties, self-cleaning properties and many others) (Decher 2012, Seyrek et al. 2012) (Kerdjoudj et al. 2010) (Sassolas et al. 2012) (Mertz et al. 2009). Yet the step-by-step buildup process has not only advantages, it is also a tedious procedure. Creating a film made of 30 polyanion/polycation bilayers can take as long as 2 days if one uses the dipping method (dipping the substrate alternately in a polyanion and a polycation solution with rinsing steps in between). In order to speed-up the buildup process different improvements were introduced: deposition by spraying (Schlenoff et al. 2000, Bucur et al. 2006a, Lefort et al. 2011) or spin-coating (Bucur et al. 2006b) of the constituents, building up the film by using polyelectrolyte complexes instead of polyelectrolyte chains (Schaaf et al. 2012) (Krogman et al. 2009). Yet, the Holy Grail in the field would be to mix all the film constituents in solution and have a film building up spontaneously in a one pot procedure. This idea was, to our knowledge, first formulated by Rubner, one of the leaders in polyelectrolyte multilayers during a dinner at the 236th ACS Meeting at Philadelphia (reported by P. Schaaf). The question is then: **how to mix constituents that should not interact in solution and interact exclusively near the substrate in such a way as to buildup a film?**

One solution to solve this challenge is to use a strategy widely developed by nature, namely a morphogen driven buildup. A morphogen is a chemical species that is produced locally, diffuses into a solution and influences cellular processes in biology and chemical reactions in chemistry. We worked on step-by-step covalently cross-linked polyelectrolyte multilayers based on Sharpless click chemistry where a reaction between azide and alkyne groups is catalyzed by Cu(I). Our group progressively went from a chemical reduction of Cu(II) into Cu(I) by sodium ascorbate (El Haitami et al. 2010) to an electrochemically triggered step-by-step buildup where Cu(I) is generated electrochemically at an electrode from Cu(II) (Rydzek et al. 2010). Finally, because the azide-alkyne reaction takes place only in the presence of Cu(I) and because Cu(I) is generated exclusively in the vicinity of the electrode, it can play the role of a morphogen and trigger the film construction between alkyne bearing and azide bearing chains exclusively near the electrode (Rydzek et al. 2011a). Both polymers can then be present simultaneously in the solution free of Cu(I). Figure 1.1 schematically represents this process. It

constituted the first example of one pot buildup where the concept of morphogen buildup was clearly formalized, even if other morphogen buildup processes were used previously in other contexts.

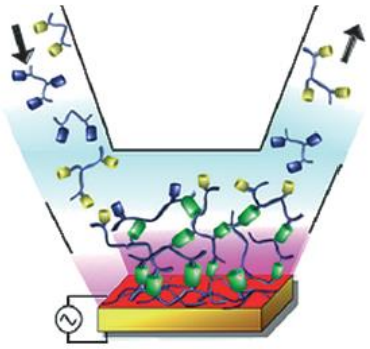

Figure 1.1 Schematic representation of the one pot morphogen buildup process between azide-bearing polymers (blue barrels) and alkyne bearing polymers (yellow barrels) leading to the formation of triazole groups (green barrels) through a reaction catalyzed by the Cu(I) gradient (purple) generated at the electrode from Cu(II) (blue) (Rydzek et al. 2011b).

Because Atom Transfer Radical Polymerization (ATRP) is a polymerization process that can be catalyzed by Cu(I), our idea was to use electrochemically generated Cu(I) from Cu(II) at an interface to buildup polymer brushes at an electrode, extending the concept of morphogen film buildup to surface localized ATRP brushes buildup using a morphogenic approach (Chapter 3). This was the initial goal of my thesis. Yet, one year after the beginning of my PhD, a series of papers by Li et al. (Li et al. 2012, Li et al. 2013a, Li et al. 2013b) were published on this subject using very similar systems than ours. We thus decided to change our goal and to address the problem of morphogen film buildup of non-covalent polyanion-polycation or polyampholyte complex films (Chapter 4 and 5). This subject lies in the continuity of the morphogen ATRP since we also intended to address this problem by generating morphogens, namely protons, through electrochemistry.

The introduction chapter will thus be divided in two parts: I will first review briefly the work of our laboratory to bring my studies in this context. I will then review major results obtained in the field of non-covalent electrochemically triggered morphogen buildups. The bibliography of the morphogen driven buildup of polymer brushes by atom transfer radical polymerization will be reviewed in chapter 3.

1.2 ONE-POT MORPHOGEN BUILDUP: RESULTS FROM OUR GROUP.

1.2.1 The layer-by-layer morphogen approach.

As already mentioned, our group worked since more than 10 years on polyelectrolyte multilayers. These films are obtained from the alternate deposition of polyanions and polycations and the buildup process can be summarized in Figure 1.2.

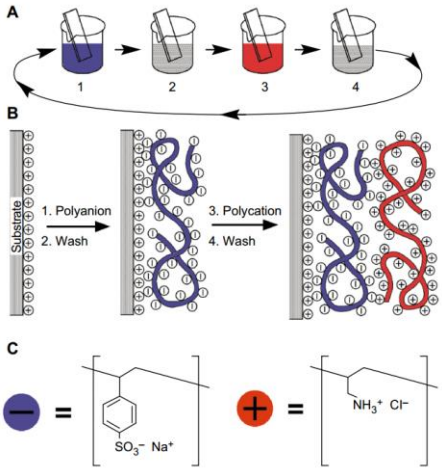

Figure 1.2 Schematic representation of the polyelectrolyte multilayer buildup (Decher 1997).

Such a film can be seen as an assembly of polyanion/polycation complexes which are, in certain cases, nicely stratified (Decher 1997). Despite the great versatility of the method and its numerous potential applications, it has so far been seldom applied industrially. One of the reasons for the difficulty to get out from the academic world into the industrial sphere is due to mechanical robustness of polyelectrolyte multilayers. Based on non-covalent electrostatic interactions, they are sensitive to water and to mechanical stress (Richert et al. 2004, Mertz et al. 2007). To circumvent this drawback, films had to be cross-linked. In 2006, our laboratory thus started to work on the buildup of polyelectrolyte multilayers constituted of polyelectrolytes bearing azide and alkyne groups. These groups react one with each other in the presence of Cu(I) to form a triazole through a reaction called Huisgen-Sharpless click. First, Cu(I) was generated from Cu(II) by using a reducing agent, namely, sodium ascorbate. Figure 1.3 schematically represents the triazole formation process by the Huisgen-Sharpless click reaction.

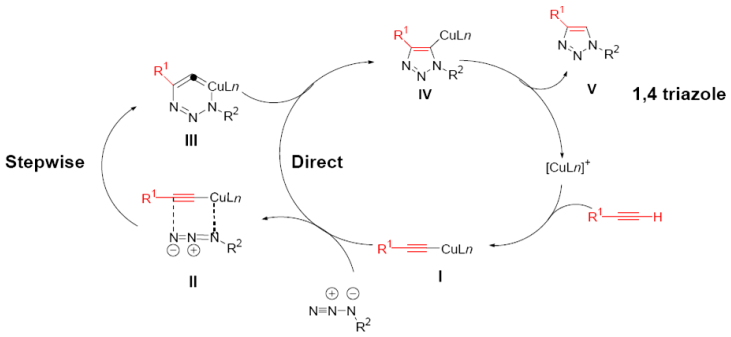

Figure 1.3 Schematic representation of the triazole formation by the Huisgen-Sharpless click reaction between an alkyne and an azide catalyzed by Cu(I) (Rostovtsev et al. 2002) (Sonogashira et al. 1975) (Tornøe et al. 2002).

This process was then extended to the step-by-step buildup of polymers or polyelectrolytes bearing azide groups and poly(ethylene oxide) bis alkyne chains as schematically represented in Figure 1.4.

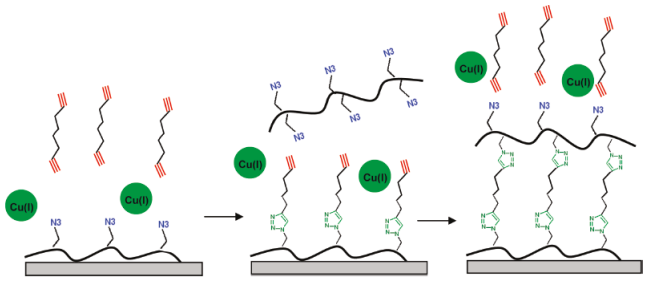

Figure 1.4 Schematic representation of the step-by-step buildup of a polymer film based on the formation of triazole by the Huisgen—Sharpless click reaction between polymer chains bearing azide groups and a spacer bearing alkyne groups. The copper(I) catalyst of the reaction is generated by the chemical reduction of copper(II) by sodium ascorbate (El Haitami et al. 2010).

Yet the buildup process based on the production of Cu(I) from Cu(II) by using sodium ascorbate is tedious due to the use of fresh solution of ascorbate. In 2006 Collmann et al. proposed the first electrochemically triggered Sharpless click reaction. They attached ethynylferrocene on azide terminated self-assembled monolayers. The Cu(I) catalyst was generated at an electrode through the reduction of Cu(II) by the application of a reduction potential (Figure 1.5).

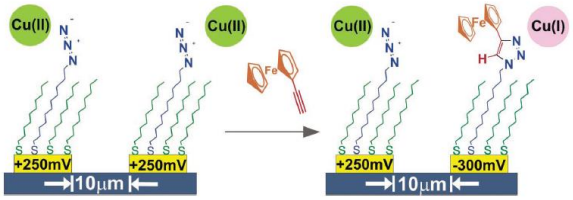

Figure 1.5 Electro-click reaction of a self-assembled monolayer bearing azide group with ethynylferrocene bearing alkyne groups. The copper(I) catalyst is electrochemically generated by the reduction of copper(II) (Devaraj et al. 2006).

This inspired our group to use a similar strategy to generate Cu(I) from Cu(II) for the step-by-step buildup of covalently cross-linked polyelectrolytes multilayers using polyelectrolytes bearing azide and alkyne groups (Figure 1.6). This can be called the first morphogen buildup of polyelectrolyte multilayer even if at this moment the concept of morphogen construction was still not mentioned.

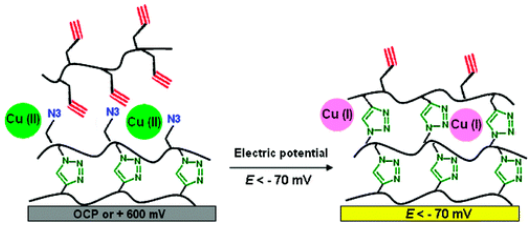

Figure 1.6 Construction of a layer-by-layer film by electrochemically triggered click chemistry. The polymer containing respectively azide or alkyne is brought in contact of the film together with copper(II). A reduction potential is applied at each deposition step to reduce copper(II) into copper(I) and catalyze the click reaction (Rydzek et al. 2010).

1.2.2 The one pot morphogenic approach.

The previous results highlight that the reaction between the azides and alkynes groups takes place only in the presence of Cu(I) and that this species is localized near the electrode when produced electrochemically from Cu(II). Therefore, one can mix simultaneously two neutral polymers or eventually two polyelectrolytes of similar charge, one bearing azides and the other alkynes in solution in the presence of Cu(II), apply a reduction potential and have a film building up at the electrode. This film would be constituted by the two types of polymer chains covalently coupled through triazole groups. The concept was established in 2011 with different systems: poly(acrylic acid) (PAA), poly(allylamine) hydrochloride (PAH) and poly(N-hydroxypropylmethacrylamide) (PHPMA), all functionalized at around 5% with N_3 and C≡C moieties. Different films could be constructed in this way: ($PAA_{C\equiv C}$, PAA_{N3}), ($PHPMA_{C\equiv C}$, $PHPMA_{N3}$), ($PAH_{C\equiv C}$, PAH_{N3}), ($PAA_{C\equiv C}$, $PHPMA_{N3}$), ($PHPMA_{C\equiv C}$, PAA_{N3}). It is in this work that the concept of morphogen film buildup was clearly introduced (Rydzek et al. 2011a).

This work was followed by a series of papers where the concept was generalized to other systems. First it was generalized to the self-construction of films composed of poly(acrylic acid) functionalized with alkyne groups and homobifunctionalized spacers bearing azide groups (Figure 1.7).

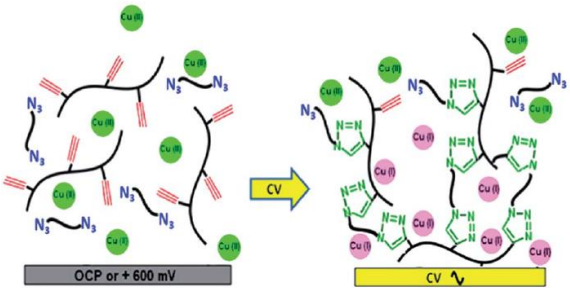

Figure 1.7 Morphogen driven electrochemically triggered click reaction of functionalized poly(acrylic acid) bearing alkyne with an homobifunctionalized spacer bearing azide groups. The copper(I) catalyst is generated by the electrochemical reduction of copper(II) thus triggering the click reaction (Rydzek et al. 2012b).

These films proved to be pH responsive in a reversible way. When decreasing the pH from 3.5 to 9.5, the films swelled by a factor of more than 100% and returned to their original size when the pH was brought back to 3.5. This comes from the deprotonation of the carboxylic groups when the pH is increased.

Next, the concept was generalized to films whose integrity is due to non-covalent host-guest interactions. The self-construction was based on clickable host (cyclodextrin) and guests (ferrocene or adamantane) both functionalized by alkyne groups reacting with azides grafted on PAA chains. The film buildup is schematically represented in Figure 1.8

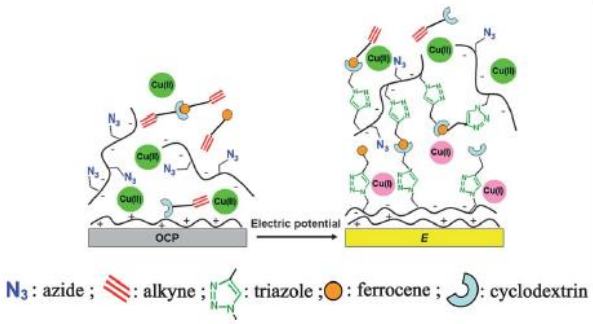

Figure 1.8 Morphogenic polymer film buildup based on non-covalent host-guest interactions (Rydzek et al. 2012a).

These films also proved to be pH responsive, being destroyed when the pH is increased from 3.5 to 9.5. As for the previous case, this is due to a deprotonation of the carboxylic groups when the pH is increased which leads to a repulsion between the PAA chains. The cyclodextrin-ferrocene (or adamantane) interactions are non-covalent and reversible inducing a film dissolution.

Finally, the concept was applied to the one-pot buildup of supramolecular polyrotaxane films. The initial solution used was composed of (i) PAA chains functionalized with $(EO)_{13}$-N_3 side chains where EO represents ethylene oxide units, (ii) cyclodextrins, as macro-cycles that can be threaded along the $(EO)_{13}$ arms forming polyrotaxanes, (iii) alkyne-functionalized stoppers (ferrocene or adamantane) to

cap the supramolecular polyrotaxane assembly by click chemistry and (iv) Cu(II). This one-pot mixture was brought in contact with an electrode and Cu(I) was generated by application of a reduction potential. The electrochemically triggered click reaction between alkyne functionalized stoppers and azide functionalized $(EO)_{13}$ arms led to the capping of the polyrotaxane chains, hindering the cyclodextrins to leave out of the $(EO)_{13}$ chains. The polyrotaxanes then self-assembled through lateral supramolecular interactions to form aggregates and ensure the cohesion of the forming film. Figure 1.9 schematically represents the whole concept.

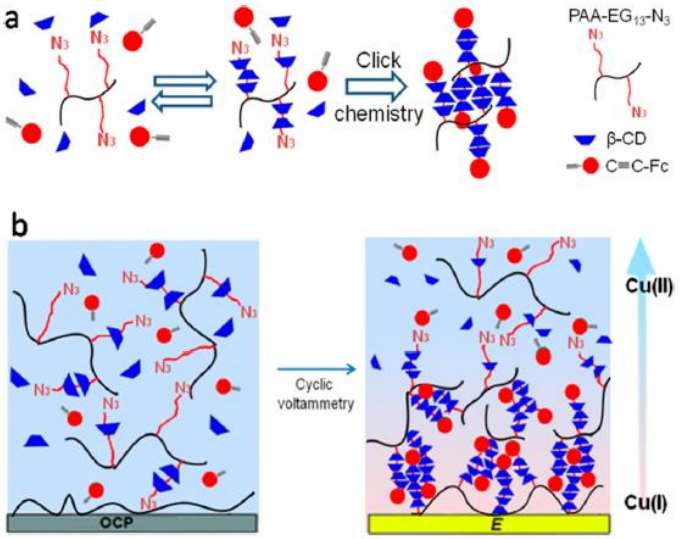

Figure 1.9 Morphogenic one-pot construction of polyrotaxane films based on electrochemically triggered click reaction and non-covalent host-guest interactions (Rydzek et al. 2013).

In all these cases, Cu(I) was generated at an electrode from Cu(II), diffused into the solution, catalyzing the click reactions in the vicinity of the electrode. The copper(I) catalyst thus played the role of morphogen. When applying the potential on a microelectrode instead of an electrode, Cu(I) will be generated very locally not only perpendicularly to the interface but also laterally then giving the whole sense of a morphogenic buildup.

The morphogen buildup strategy based on the Cu(I) catalyzed Huisgen-Sharpless reaction was used by the group of Huskens (Nicosia et al. 2013) to build chemical gradients along a substrate (Figure 1.10).

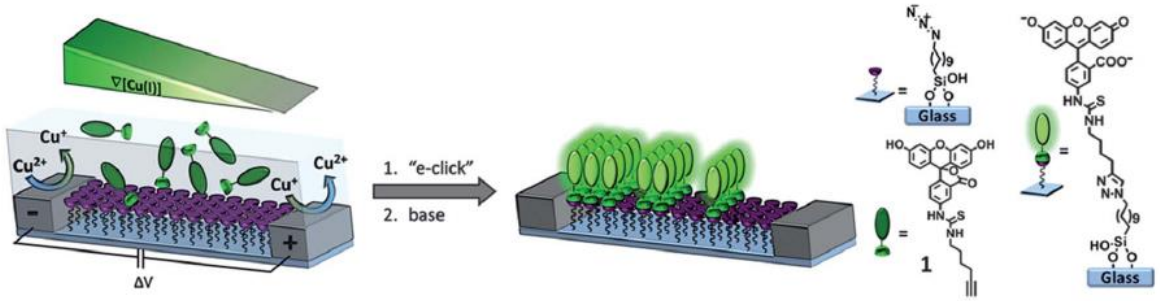

Figure 1.10 Schematic representation of the strategy used to create a chemical gradient along a surface by using a morphogen approach (Nicosia et al. 2013).

The authors used microelectrode arrays deposited on glass. A Cu(I) gradient was then established from the electrode to its adjacent neighbor through local electrochemical reduction of Cu(II) and oxidation of the generated Cu(I) back to Cu(II). The Cu(I) solution gradient, in the presence of alkyne functionalized molecules in solution and an azide functionalized monolayer on the glass between the two electrodes is then exploited for the surface-confined gradient fabrication *via* the click reaction. This procedure allows the generation of gradients with a control of the shape on the micron-scale as represented in Figure 1.11.

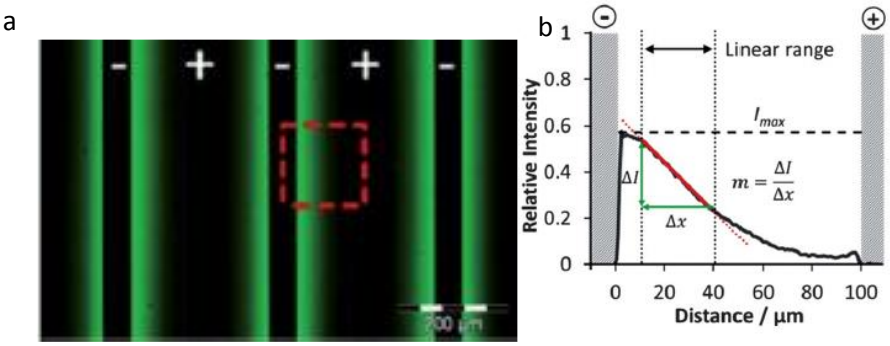

Figure 1.11 Image of several lateral gradients generated by using alkyne modified fluorescein (a); Relative intensity as a function of the distance from an electrode, highlighting the chemical gradient (b) (Nicosia et al. 2013).

Another way to generate chemical gradients along an electrode using Cu(I) as morphogen was presented by Inagi and coworkers (Shida et al. 2012). These authors polymerized PEDOT-N_3 on an indium tin oxide electrode, used as a bipolar electrode. Since the potential varies along the electrode, a Cu(I) gradient is generated. In the presence of molecules bearing azide groups, they generate a gradient of these molecules along the surface. The whole process is schematically represented in Figure 1.12. Such a process could be used to create films of variable thickness along the bipolar electrode by using the one-pot morphogen buildup of polymers presented previously.

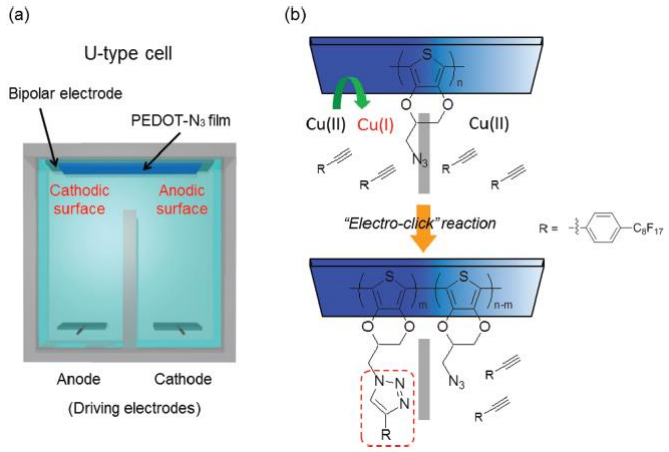

Figure 1.12 Schematic representation of the buildup of a gradient along a surface using a bipolar electrode (Shida et al. 2012).

1.3 MORPHOGEN BUILDUP OF NON-COVALENT FILMS.

1.3.1 General mechanism of electro-deposition and early works.

Electro-deposition, also called electrophoretic deposition is a method by which charged colloidal particles or macromolecules are deposited onto a surface by means of electrophoretic motion and a morphogen (Zhitomirsky 2002) (Boccaccini et al. 2010). The most widely used morphogens so far are the protons and the hydroxydes ions. They are generated electrochemically from oxidation or reduction of water following the two-half reactions at the cathode and anode:

Cathode: $$2H_2O + 2e^- \rightarrow H_2 + 2HO^-$$

Anode: $$2H_2O \rightarrow O_2 + 4H^+ + 4e^-$$

Figure 1.13 shows the pH gradient diffusion of the protons and hydroxides in an aqueous media respectively at the anode and cathode of a micro-channel by the mean of colorimetric indicator.

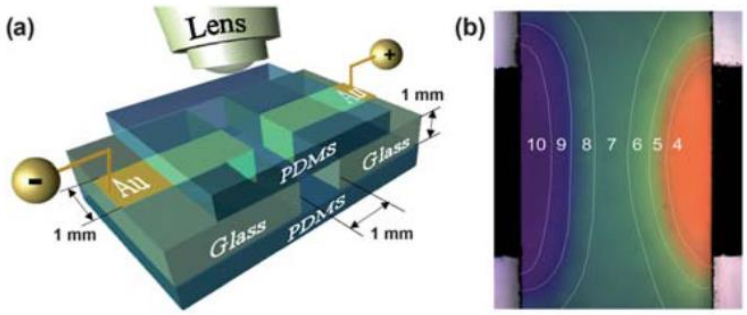

Figure 1.13 Schematic representation of the setup used to study the protons and hydroxide diffusion in the micro-channel. Microelectrodes made of gold (Au) and 1 mm thick are positioned in front of each other under a microscope lens (a). A pH-

sensitive colorimetric indicator is inserted in the micro-channel while a potential is applied that trigger the water electrolysis. The proton (red) at the anode and the hydroxide (blue) at the cathode gradients are displayed (b) (Cheng et al. 2010).

The electro-deposition of polymers occurs in two steps: (i) the dissolved polymers which are often charged, i.e. polyelectrolytes, diffuse to the surface by electrophoretic motion and (ii) once in the vicinity of the electrode, either carboxylic side chains of negatively charged polymers are protonated or amino side chains from positively charged polymers are deprotonated, leading to their precipitation on the electrode surface.

The deposited films can sometimes be submitted to a thermic post treatment to increase the homogeneity and density of the deposited layers by sintering.

This strategy is used since the 1970th in the car industry to deposit anti-corrosion protection films (Beck 1988) (Krylova 2001). This process was first applied to the functionalization of sensors by Schuhmann et al in 2002 (Kurzawa et al. 2002, Vilkanauskyte et al. 2002) who co-precipitated polymers used in the car industry with enzymes, glucose oxidase, lactate oxidase or pyruvate oxidase. They showed that the produced films were enzymatically active and that the procedure could be used to locally functionalize micro-band electrode arrays. The deposition was performed by applying a series of pulse potentials. The enzymatic activity of the film first increased with the number of deposition cycles (pulse) as long as the enzymes were close enough to the electrode to allow the transfer of electrons from the enzymes to the electrode. The formed biosensor was reproducible, exhibiting a high sensitivity and long term stability.

This technique was further developed using an electrochemical robotic system to improve the reproducibility of the biosensor fabrication (Reiter et al. 2004, Guschin et al. 2009). The versatility of the platform was shown by developing nitric oxide sensors based on metalloporphyrin (Isik et al. 2004), bi-functional biosensors based on glucose oxidase (Reddy et al. 2005), bi-layer and bi-enzyme biosensors based on peroxidase and alcohol oxidase (Alpeeva et al. 2005). All these biosensors exhibited a low sensitivity, effective electron transfer and provided stability of the enzymes. They also demonstrated that enzymes could be cross-linked (Alpeeva et al. 2005). The effect of the polymer matrix entrapping the glucose oxidase model enzyme was also investigated and confirmed that the sensors activities depended on the immobilization matrix (Ngounou et al. 2004, Ngounou et al. 2007).

1.3.2 Electro-deposition of chitosan.

In 2002 Payne and co-workers found that when chitosan is brought in contact with a negative electrode (potential ≤ -1V) it precipitates on the electrode forming a film whose thickness grows continuously with time (Wu et al. 2002). This is due to the fact that chitosan, a polycationic

polysaccharide, is only soluble below pH 6.5. Thus, when applying a negative potential, the reduction of water leads to the increase of the pH which propagates in the solution, inducing the precipitation of chitosan on the surface. Figure 1.14 schematically represents this process. The deprotonation of chitosan (Chit) which becomes insoluble is given by the following reaction:

$$Chit - NH_3^+ + HO^- \rightarrow Chit - NH_2 + H_2O$$

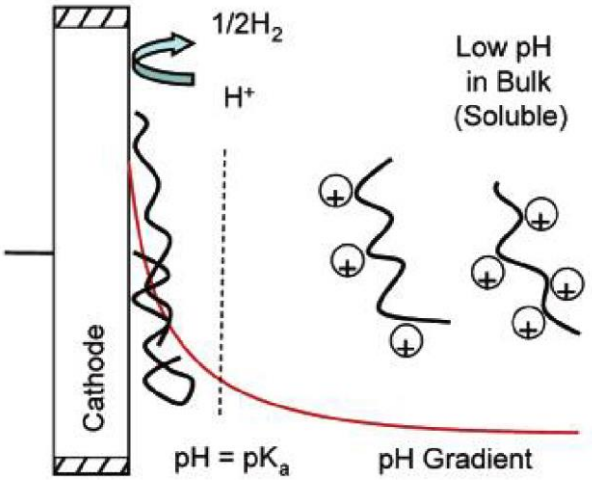

Figure 1.14 Schematic representation of the electro-deposition of chitosan: soluble protonated chitosan at pH < pK_a migrates to the cathode by electrophoresis. Once the soluble chitosan gets close to the cathode, the pH lowers under its pKa thus deprotonating the polymers which becomes insoluble and precipitates on the surface (Yi et al. 2005c).

The process of chitosan electro-deposition was extensively studied and demonstrated to be the combination of both the electrophoretic migration of chitosan to the electrode and the reaction with the hydroxide ions which makes it insoluble (Cheng et al. 2010). Figure 1.15 schematically shows the electro-deposition of chitosan under the application of an electrochemical potential. The gel growth at the electrode is denser close to the electrode due to the electrophoretic migration and the higher pH.

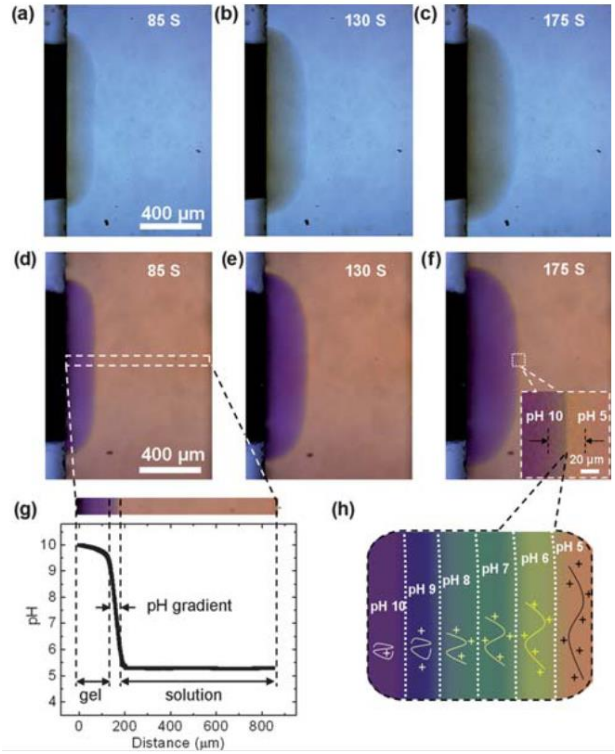

Figure 1.15 Process of the electro-deposition of chitosan: the positively charged chitosan diffuses towards the negative electrode due to electrophoretic motion and the high local pH progressively deprotonates the chitosan which becomes insoluble and precipitates onto the electrode (Cheng et al. 2010).

The group of Payne used the electro-deposition of chitosan in a large number of applications. They showed that it can be selectively deposited onto microelectrodes and further cross-linked with n-hydroxysuccinimide (NHS) (Wu et al. 2003). Figure 1.16 schematically shows the microelectrode array fabrication by photolithography and the further deposition of fluorescein labelled chitosan or un-labelled chitosan which is further cross-linked by labelled NHS.

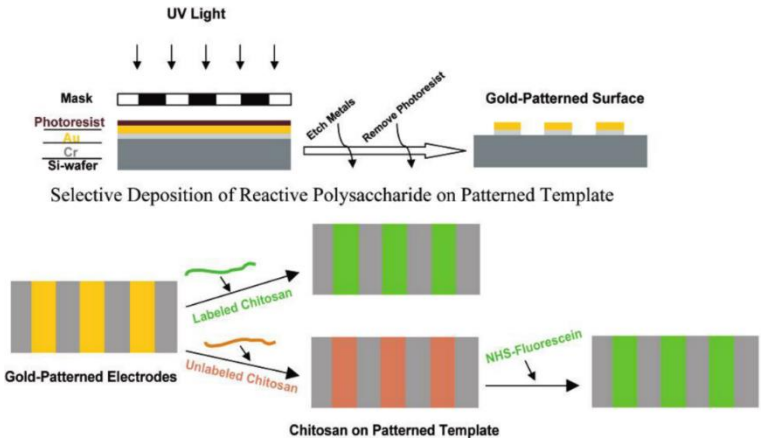

Figure 1.16 Schematic representation of the fabrication of patterned microelectrodes by photolithography (top). Electro-deposition with a spatial and temporal control of labelled and unlabelled chitosan on the microelectrodes array and further crosslinking of the unlabelled chitosan film by labelled NHS (bottom) (Wu et al. 2003).

When not cross-linked, the electro-deposited chitosan is dissolvable under mild acidic conditions (Fernandes et al. 2003).

The electro-deposited chitosan layer can serve as a template for covalently grafting DNA probes (Yi et al. 2004) to form a reproducible, quantifiable and robust biosensor that can be regenerated. Co-deposited latex nanoparticles allows to form stimuli responsive surfaces with reversible swelling/deswelling properties (Wu et al. 2005b). Viruses were grafted on the chitosan prior to its deposition to form virus templates (Yi et al. 2005a). Phenol reaction cascades were initiated to transfer a pattern onto a flexible chitosan film (Wu et al. 2005a). The electro-deposited chitosan film was cross-linked to allow its peeling (Wu et al. 2006).

Cross-linked electro-deposited chitosan films with catechols exhibit unusual electronic behaviour since they are insulating but can be used as an electron source. Such electron source can be depleted but can also be regenerated by the application of a short electrochemical treatment (Kim et al. 2010).

Electro-deposited chitosan films have also been used as specific food phenol detectors. In this last case, the chitosan films were brought in contact with phenols that are later oxidized at the electrode. Specific phenols oxidize and react with the chitosan films thus changing their absorbance (Liu et al. 2008).

The Zhitomirsky group and their associate extensively used the electro-deposition of chitosan as a platform (Simchi et al. 2009). They co-deposited hydroxyapatite (Pang et al. 2005) (Pang et al. 2007) (Pang et al. 2009), silica (Grandfield et al. 2008) and bioglass (Zhitomirsky et al. 2009) (Pishbin et al. 2011) together with the chitosan to form bioactive nano-composites with anti-corrosion properties. The depositions were performed on steel, NiTi and nitinol shape memory alloys. Investigation of the deposition yield highlighted the importance of both the applied field and the relative concentrations of the composite constituents. Co-electro-deposition of hydroxyapatite together with chitosan and silver allowed the formation of a film which slowly released Ag^{+} ions thus conferring anti-microbial properties to the anti-corrosion coatings (Pang et al. 2008). Functionally graded materials were prepared by the co-deposition of a first layer of chitosan and hydroxyapatite followed by a second layer of chitosan and heparin to provide bio-responsive coatings (Sun et al. 2009).

Other groups investigated this powerful electro-deposited chitosan platform to buildup composite hydrogels with bio-sensing properties. Chitosan was then electro-deposited together with glucose oxidase and gold nanoparticles (Luo et al. 2004), horseradish peroxidase and gold nanoparticles (Luo et al. 2005), glucose oxidase and ionic liquid (Zeng et al. 2009), horseradish peroxidase and ionic liquid (Xi et al. 2008), choline oxidase and manganese dioxide nanoparticles (Bai et al. 2007), hematite and

carbon nanotubes (Gong et al. 2008), horseradish peroxidase and glucose oxidase to form bi-enzyme biosensors (Li et al. 2009). The co-electro-deposition of chitosan together with silica nanoparticles was used as a template to immobilize hepatitis B surface antibodies by dissolving the nanoparticles and covalently grafting the antibodies with glutaraldehyde (Liang et al. 2008). Chitosan could also be chemically modified to obtain ferrocene-branched chitosan derivatives for co-electro-deposition with glucose oxidase and multi-walled carbon nanotubes (Liang et al. 2009) or with gold nanoparticles to further immobilize hepatitis B surface antibodies on the nanoparticles (Qiu et al. 2009). All the obtained biosensors exhibited a long durability and high sensitivity. It was proven that the biosensors sensitivity could be further enhanced by co-electro-depositing a first hydrogel layer of prussian blue together with chitosan which acts as a redox mediator followed by a bio-sensing top layer electro-deposited film made of glucose oxidase and chitosan (Wang et al. 2009). Electrochemical analysis of the electro-deposited chitosan films revealed that they did not possess any electro-activity but presented a permeability towards many electroactive redox probes (e.g. hexacyannoferrate) (Zangmeister et al. 2006).

Payne and coworkers also showed that electro-deposited chitosan films can serve to assemble proteins and nucleic acids onto this film (Yi et al. 2005b). First, working under cathodic conditions, the chitosan film was electro-deposited and rinsed. The formed film could be later coupled to Texas red-labelled gelatin or to green fluorescent protein by tyrosinase catalyzed conjugation. Another way to graft biomolecules was to activate the chitosan film with glutaraldehyde which later reacts with labelled DNA probes. This approach where the desired biomolecules are grafted on the chitosan after its electro-deposition was used for grafting proteins or peptides tether on the chitosan film in order to further bind the desired proteins or peptides (Yang et al. 2009). More recently, it was used to form biological nano-factories bearing bacteria specific antibodies (Fernandes et al. 2010).

The grafting of biomolecules onto chitosan can also be realized prior to its electro-deposition. Such approach was used to immobilize enzymes onto patterned micro-fluidic channels to form bio-micro-electromechanical systems (bioMEMs) (Luo et al. 2008). In this case, enzymes were grafted onto the chitosan prior to its electro-deposition on the patterned microelectrodes. The bioactive film thus formed maintained its enzymatic activity and the biosensor obtained could be later dissolved under mild acidic conditions. The washed microelectrodes were reused for other applications. Figure 1.17 schematically shows the formation and later dissolution of the bioMEMs bearing enzyme functionalized chitosan film.

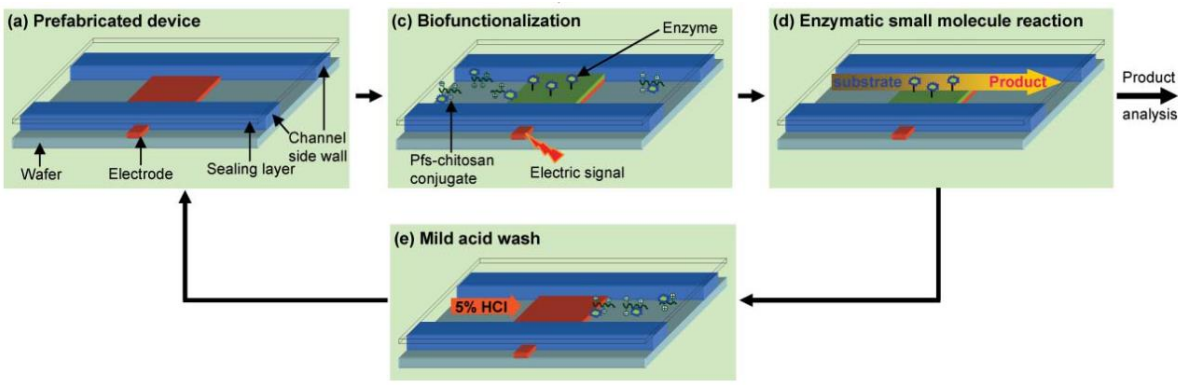

Figure 1.17 Fabrication of a bioMEMs: a micro-fluidic channel patterned with microelectrodes is brought in contact with a solution containing enzyme functionalized chitosan (a). Application of a potential electro-deposit the functionalized chitosan to form a bioresponsive film (c). When a solution containing the enzyme substrate is injected in the channel, the product is formed that can be analysed at the exit of the channel (d). The electro-deposited biofilm can be dissolved under mild acidic conditions (e) to obtain the uncoated micro-fluidic device (a) (Luo et al. 2008).

This process is limited since the high pH at the electrode interface can degrade the enzymes during the electro-deposition. To overcome this limitation, another technique was developed which used biotinylated functionalized chitosan (Shi et al. 2008). In that case, the chitosan bearing biotin is electro-deposited onto the patterned electrode surfaces. These films later reacts with streptavidin providing several reactive surfaces towards biotinylated proteins and antibodies. In that case, the molecular assembly of the biomolecules happens after the electro-deposition and in mild conditions thus avoiding the exposure of pH sensitive proteins or enzymes to high pH.

The grafting of biomolecules onto electro-deposited chitosan was later optimized to obtain a reagentless coupling (Shi et al. 2009b) (Gray et al. 2012). In this process, the chitosan film is electro-deposited as before and then rinsed. The film is then brought in contact with a phosphate buffer at pH 7 containing NaCl and an anodic potential (0.9V) is applied for short times. After rinsing the film, target proteins are brought in contact and assembled on the surface by simple incubation. In the absence of NaCl in the buffer solution during the anodic activation, no protein assembles on the surface. This behavior was explained by the production of reactive HOCl and ClO^- species at the electrode under anodic conditions. These species are known to selectively oxidize polysaccharides thus generating aldehyde and carboxylate functionalities. In this context, they can also be qualified as morphogens since they are produced at the electrode, diffuse from the electrode through the contacting film and react with this film. The so produced aldehydes can then further undergo Schiff-base formation with primary amines for covalent attachment of proteins. Figure 1.18 schematically represents the two step process involved.

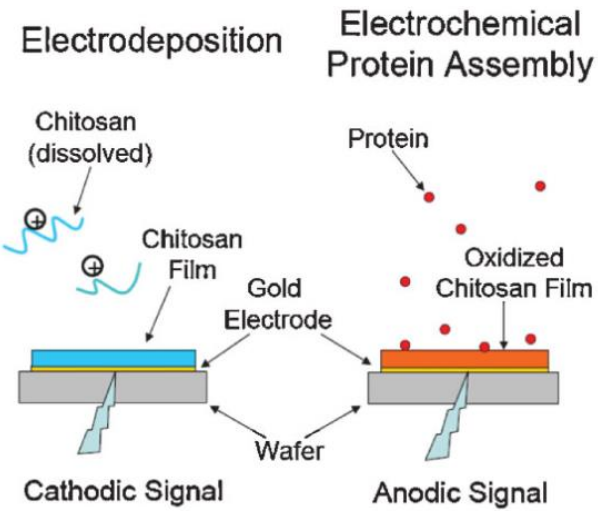

Figure 1.18 Schematic representation of the reagentless functionalization of an electrode with proteins in a two-step process making use of electro-deposition of chitosan. First, the chitosan is electro-deposited on the cathode. Then, an anodic potential is applied that produce the HOCl and ClO^- species which oxidize the chitosan that further reacts with the proteins and graft them (Shi et al. 2009b).

Such method has also been used to obtain a biosensor by grafting glucose oxidase together with chitosan (Gray et al. 2012).

More recently, it was reported the use of the electro-deposited chitosan platform as a template to further build a spatio-selective layer-by-layer film of chitosan/alginate. The chitosan platform served as a template to confer spatial selectivity for the LbL assembly whereas the LbL film possesses the advantages of providing a precise control of the thickness and to entrap labile biological components such as proteins. As an example, a model enzyme was immobilized in the LbL film that was built only on top of the chitosan film. Figure 1.19 schematically represents the buildup of the electro-deposited chitosan and the LbL film.

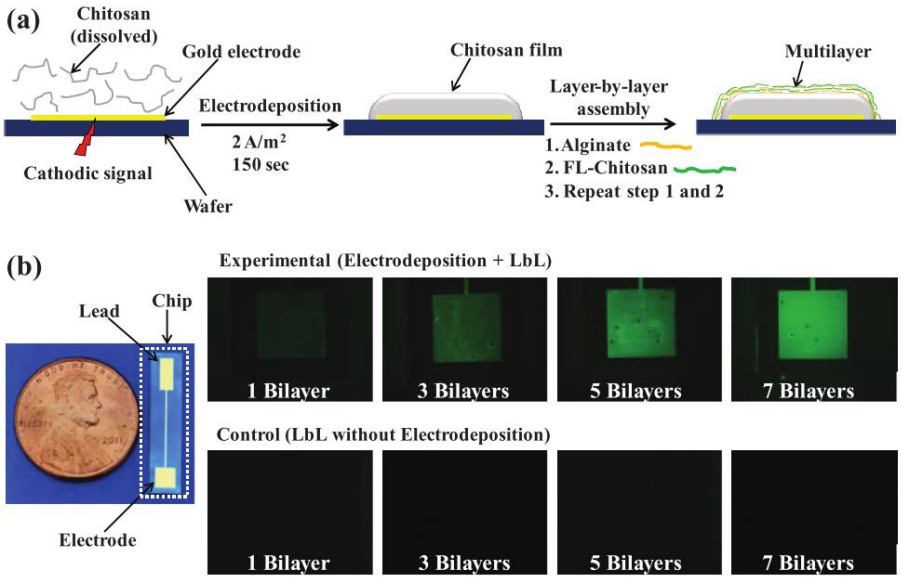

Figure 1.19 Schematic representation of the buildup: the chitosan is electro-deposited on top of the patterned microelectrodes and an LbL film of alginate and fluorescein labelled chitosan is assembled on top of it (a). The spatio-selective assembly of the LbL film is demonstrated to be due to the electro-deposited chitosan template (b).

Latest developments of the electro-deposited chitosan platform include the coupling of the polysaccharide film with an electro-click reaction (Shi et al. 2013). First, the aminopolysaccharide chitosan was electro-deposited on the patterned electrode surfaces and later chemically functionalized with alkyne groups. An azide tagged proteins (bovine serum albumin) bearing a fluorescent dye are then brought in contact with the micro-electrode array together with copper(II). Electrochemical reduction of the copper(II) in copper(I) triggers the Huisgen 1,3-dipolar cyclo-additions thus covalently grafting the protein onto the chitosan film scaffold (Figure 1.20).

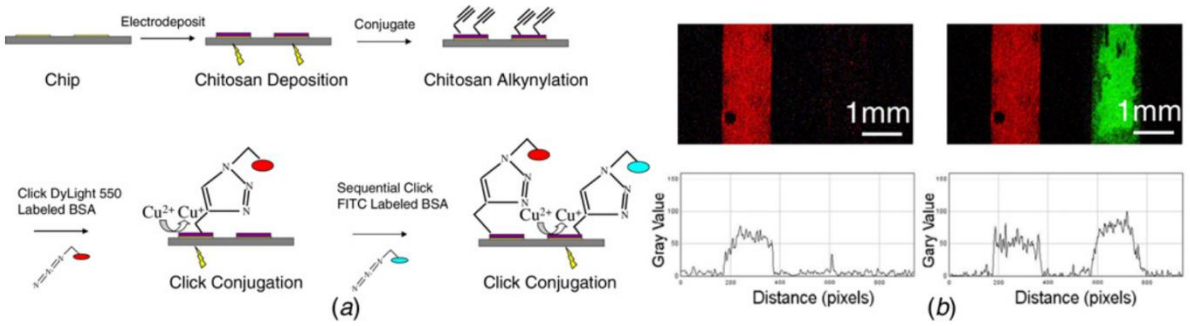

Figure 1.20 Schematic representation of the protein grafting on the chitosan film: chitosan is first electro-deposited on the top of a patterned micro-electrode array. The formed chitosan film is then chemically modified with alkyne groups. Labelled bovine serum albumin molecules bearing azides are brought in contact with the electrode together with copper(II). Application of a suited reductive potential on the desired electrode triggers the click cyclo-addition of the protein on the chitosan scaffold (a). Fluorescence microscopy measurements of two microelectrodes on which fluorescein and texas red labelled albumin molecules have been grafted (b) (Shi, Qiu et al. 2013).

Such a grafting method presents the advantage of occurring under mild conditions and thus represents a real advantage for the grafting of pH sensitive biomolecules.

1.3.3 Electro-deposition of alginate and alginic acid.

The electrochemical production of protons at the anode was also used by the group of Payne to electro-address the encapsulation of cells in a calcium alginate hydrogel. Alginate, a polyanionic polysaccharide, is known to form a gel when interacting with Ca^{2+} cations. These ions reticulate the alginate chains forming a gel. Payne et al. used a solution containing calcium carbonate and alginate which was brought in contact with an electrode. When applying an anodic potential, protons are formed, lowering the pH near the electrode. This leads to the dissolution of the calcium carbonate ($CaCO_3$) particles with the formation of Ca^{2+} cations following the reaction:

$$CaCO_3 + 2H^+ \rightarrow Ca^{2+} + H_2O + CO_2$$

The generated calcium ions diffuse into the medium and thus represent a morphogen that triggers the alginate gel buildup through a sol-gel transition (Figure 1.21).

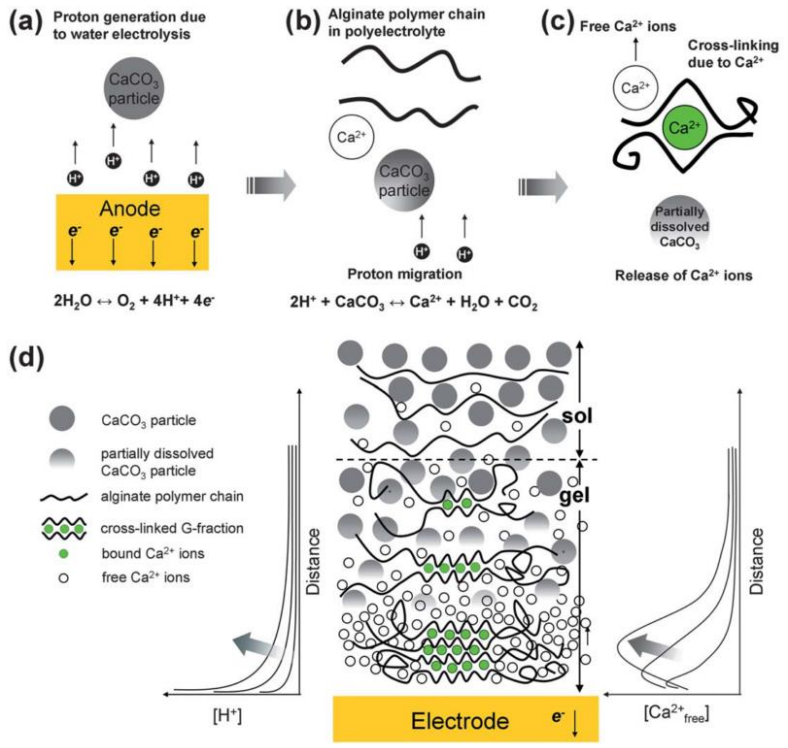

Figure 1.21 Schematic representation of the formation of an electrochemically triggered alginate deposition from solutions containing alginate and calcium carbonate. An anodic potential is applied that produces water electrolysis (a). The proton gradient dissolves the calcium carbonate particles thus generating Ca^{2+} cations that diffuse in the solution (morphogen) (b). The formed calcium cations react with the alginate chains and crosslink them (c). A gel is formed at the surface of the anode due to the sol-gel transition of alginate (d) (Cheng et al. 2011).

In the presence of cells, these are entrapped in the gel (Cheng et al. 2011) (Shi et al. 2009a) (Cheng et al. 2012).

This process can be performed locally on microelectrodes allowing for an addressable cell selective deposition (Shi et al. 2009a). When put in contact with sodium nitrate, a competition exists between the calcium and sodium ions which leads to the dissolution of the alginate film and the cell release. Such a system allows for spatiotemporally controllable assembly of cell populations thus providing a convenient platform for cell-based biosensing or the study of cell-cell signalling.

The alginate electro-deposition system was also used to co-deposit agarose together with alginate which also forms a gel upon temperature reduction. These two stimuli responsive film forming polysaccharides where used to entrap cell populations inside the film with potential applications in immunoanalysis (Yang et al. 2010).

The electro-deposition of alginate is particularly powerful when compared to chitosan since the generated protons are buffered by the calcium carbonate to generate the calcium ions. This then represents a powerful tool for the analysis of pH sensitive biomolecules or cells (Cheng et al. 2011) (Liu et al. 2010). The alginate platform was used for highly sensitive and stable biosensors fabrication by electro-co-deposition of alginate and horseradish peroxidase (Liu et al. 2009).

The group of Zhitormirsky also investigated the formation of alginate gels but with a different process. In their setup, alginate was not in the presence of calcium carbonate and the protons reacted directly with the negatively charged alginate to protonate it and form an alginic acid gel. Figure 1.22 shows the process differences between the formation of an alginic acid gel and of a cross-linked alginate gel.

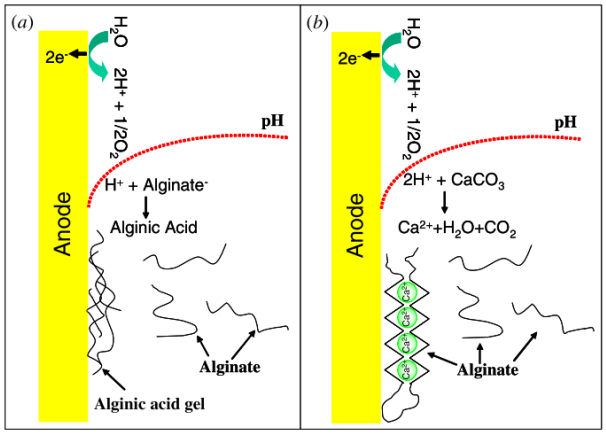

Figure 1.22 Schematic representation of the electro-deposition of an alginic acid and an alginate gel. The alginic acid gel is based on the protonation of the negatively charged alginate chains by the electrochemically generated protons at the anode (a). The alginate gel is a cross-linked gel formed by the interaction between Ca^{2+} ions formed by the dissociation of calcium carbonate in the acidic vicinity of the electrode together with the alginate chains (b) (Liu et al. 2010).

Such a gel was used to co-precipitate hydroxyapatite, titanium dioxide, chitosan (Cheong et al. 2008) and carbon nanotubes (Grandfield et al. 2009) in order to form nano-composite anti-corrosion coatings on NiTi and nitinol shape memory alloys. This group investigated the simultaneous co-deposition of chitosan, hydroxyapatite and bioglass at the cathode while co-depositing alginate, hydroxyapatite and bioglass at the anode to form two bio-responsive nano-composite films (Zhitomirsky et al. 2009). A similar process was developed to anodically electro-deposit hyaluronic acid together with bovine serum albumin (Ma et al. 2010).

1.3.4 Electro-gelation of silk fibroin.

Using a similar process than for alginic acid deposition, the electro-gelation of silk fibroin was reported (Servoli et al. 2008) (Leisk et al. 2010, Kojic et al. 2012). Indeed, silk fibroin has an isoelectric point of 4.2 and when the local pH becomes lower than the isoelectric point, a gel forms (e-gel). As described previously, the acidic pH is produced at the anode by water electrolysis leading to a macroscopic gel formation at the anode (Figure 1.23).

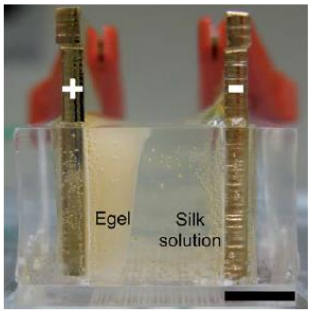

Figure 1.23 Silk fibroin gel electro-generated at an electrode by hydrolysis of water leading to a decrease of the local pH below the Ip of the protein. This results in the formation of a gel that expands from the electrode towards the solution (Kojic et al. 2012).

Silk fibers normally undergoes electrostatic repulsion when put in solution at a pH higher than their isoelectric point but investigation of the gelation process highlighted that the protonated silk fibers forms helices due to intermolecular electrostatic interactions. The formed helices entangled due to helical interactions thus forming micelles which later entangled to create intermicellar crosslinks. Figure 1.24 schematically shows the silk fibroin electro-gelation process.

The formed e-gel could later be dissolved with potential applications in drug delivery (Lu et al. 2011).

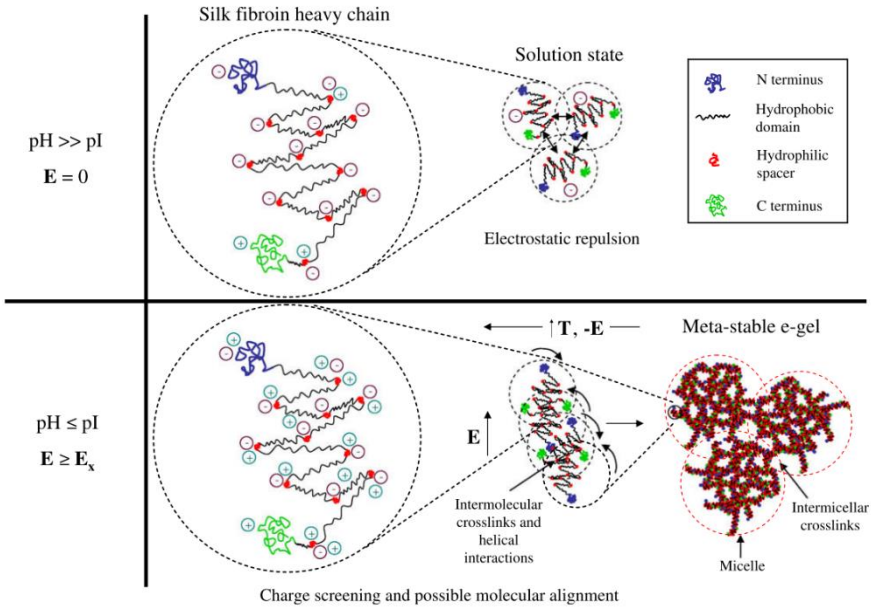

Figure 1.24 Schematic representation of the silk fibroin electro-gelation process. When the solution pH is higher than the isoelectric point of the silk fibers, their negative charge avoids the formation of a gel due to electrostatic repulsions (top). However, when a potential is applied that lowers the pH at the anode due to water electrolysis, the silk fibers protonate and form helices due to intra-molecular electrostatic interactions. These helices later assemble due to helical interactions thus leading to the formation of micelles. These micelles further entangle and the inter-micellar crosslink shows up by the formation of a macroscopic e-gel at the electrode surface (bottom) (Yucel, Kojic et al. 2010).

1.3.5 Self-assembly of dipeptides.

Still using a proton gradient, the group of Cameron proposed a directed self-assembly of dipeptides to form ultrathin hydrogen membranes (Johnson et al. 2010). This approach is different from the previously reported ones since it is not a precipitation of already present chains but it constitutes the formation of non-covalent chains starting from "monomeric bricks". They introduced a Fmoc-Leu-Gly-OH (Figure 1.25) dipeptide that was known to be a hydrogelator below pH 4 where the terminal carboxylic group is protonated and uncharged. In order to work under mild electrochemical conditions they used the oxidation of hydroquinone into 1,4-benzoquinone to generate the protons as presented in Figure 1.25. This method to generate electrochemically protons from the oxidation of hydroquinone was already introduced by Egeland et al. when discussing the confined patterning of surfaces (Egeland et al. 2002).

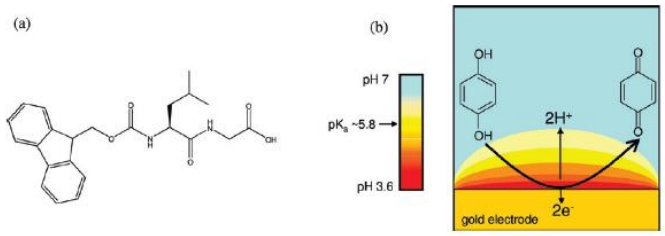

Figure 1.25 Chemical representation of the Fmoc-Leu-Gly-OH dipeptide (a) and schematic representation of the acidic pH gradient produced by the electrochemical oxidation of hydroquinone into 1,4-benzoquinone (Johnson et al. 2010).

When applying an oxidation current, a fiber hydrogel was formed on the electrode. This gel could be removed by application of a reduction current.

Soon after, Ulijn and Payne proposed to extend this method to Fmoc-phenylalanine which self-assembles under acidic conditions (Liu et al. 2011a). The electro-deposition process is very similar to that proposed by Cameron, namely based on the proton generation through hydroquinone oxidation. Payne proposed to use the electro-triggered self-assembly of Fmoc-Phe to co-assemble a neutral polysaccharide, agarose (Liu et al. 2011b). Agarose was then entrapped in the Fmoc-Phe gel which was produced at 37°C. After deposition, the gel was cooled down at room temperature and the peptide gelator could be removed by rinsing with a water solution at pH 8 thus leaving an agarose film on the surface. Figure 1.26 schematically represents the whole process.

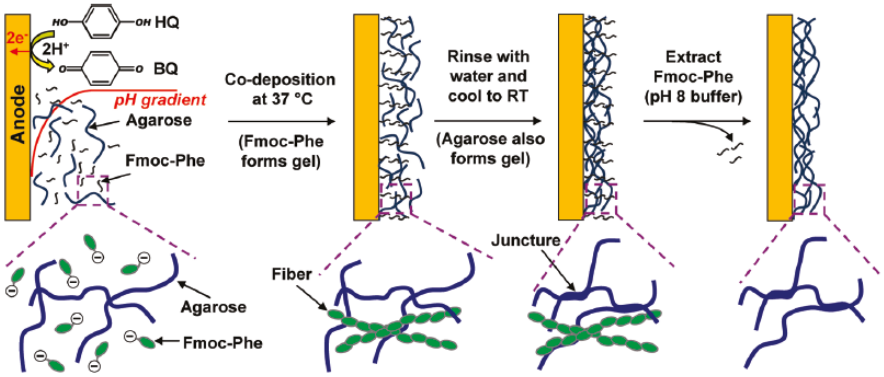

Figure 1.26 Schematic representation of the electrochemically triggered peptide self-assembly process associated with the deposition of an agarose film. Agarose is entrapped in the peptide self-assembled gel. The peptides gelator can be later removed from the deposit leaving behind an agarose film (Liu et al. 2011b).

1.3.6 Self-assembly of actin fibers.

Up to now, we have discussed morphogen buildup processes based on Cu(I) (from our group) or based on a pH trigger. Yet there are other morphogens possible to generate self-assembly. In 2007, Melosh proposed to use the ion double layer generated at an electrode under the application of a potential

to locally increase the concentration of ions present at low concentration in solution (Wong et al. 2007). They used actin, a protein that polymerizes into helical filaments upon addition of ions, particularly Mg^{2+}. They brought a low salt buffer solution containing actin monomers in contact with an electrode. The solution contained Mg^{2+} ions at a low enough concentration to keep the actin monomers in an inactive state. When applying a negative DC voltage on the electrode no buildup was observed. On the other hand, when an AC current was applied they observed the formation of actin fibers starting from the electrode (Figure 1.27). An AC current was necessary to lead to the formation of the fibers because AC currents cause the dominant species at the electrode surface, either Mg^{2+} or actin monomers, to exchange with a rate governed by the frequency of the applied current. This is due to the fact that Mg^{2+} and inactive actin monomer are oppositely charged. This allows the continuous activation of actin monomers by coupling with Mg^{2+} and their diffusion, in the active state, towards the solution. Thanks to this process, the actin fibers extended far beyond the electrical double layer (Wong et al. 2007) (Wong et al. 2008).

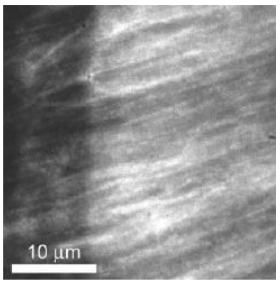

Figure 1.27 Actin fibers forming at the electrode under the action of a AC current in the presence of a low salt buffer solution containing a low concentration of Mg^{2+} ions (Wong et al. 2007).

In this work, the Mg^{2+} ions can be considered as the morphogen even if the buildup process is slightly more complex.

REFERENCES

Alpeeva, I. S., A. Vilkanauskyte, B. Ngounou, E. Csoregi, I. Y. Sakharov, M. Gonchar and W. Schuhmann (2005). "Bi-Enzyme Alcohol Biosensors Based on Genetically Engineered Alcohol Oxidase and Different Peroxidases." Microchimica Acta **152**(1-2): 21-27.

Bai, Y. H., Y. Du, J. J. Xu and H. Y. Chen (2007). "Choline Biosensors Based on a Bi-Electrocatalytic Property of Mno2 Nanoparticles Modified Electrodes to H2o2." Electrochemistry Communications **9**(10): 2611-2616.

Beck, F. (1988). "Electrodeposition of Polymer-Coatings." Electrochimica Acta **33**(7): 839-850.

Boccaccini, A. R., S. Keim, R. Ma, Y. Li and I. Zhitomirsky (2010). "Electrophoretic Deposition of Biomaterials." Journal of the Royal Society, Interface **7 Suppl 5**: S581-613.

Bucur, C. B., K. Hart and J. B. Schlenoff (2006a). "Sprayed Polyelectrolyte Multilayers." Abstracts of Papers of the American Chemical Society **231**: -.

Bucur, C. B., M. Tassabehji and J. B. Schlenoff (2006b). "Comparison of Polyelectrolyte Multilayers Built by Spin Coating and Inverted Spin Coating." Abstracts of Papers of the American Chemical Society **231**: -.

Cheng, Y., X. L. Luo, J. Betz, S. Buckhout-White, O. Bekdash, G. F. Payne, W. E. Bentley and G. W. Rubloff (2010). "In Situ Quantitative Visualization and Characterization of Chitosan Electrodeposition with Paired Sidewall Electrodes." Soft Matter **6**(14): 3177-3183.

Cheng, Y., X. L. Luo, J. Betz, G. F. Payne, W. E. Bentley and G. W. Rubloff (2011). "Mechanism of Anodic Electrodeposition of Calcium Alginate." Soft Matter **7**(12): 5677-5684.

Cheng, Y., C. Y. Tsao, H. C. Wu, X. L. Luo, J. L. Terrell, J. Betz, G. F. Payne, W. E. Bentley and G. W. Rubloff (2012). "Electroaddressing Functionalized Polysaccharides as Model Biofilms for Interrogating Cell Signaling." Advanced Functional Materials **22**(3): 519-528.

Cheong, M. and I. Zhitomirsky (2008). "Electrodeposition of Alginic Acid and Composite Films." Colloids and Surfaces a-Physicochemical and Engineering Aspects **328**(1-3): 73-78.

Decher, G. (1997). "Fuzzy Nanoassemblies: Toward Layered Polymeric Multicomposites." Science **277**(5330): 1232-1237.

Decher, G. (2012). Multilayer Thin Films Sequential Assembly of Nanocomposite Materials. Weinheim, Wiley-VCH.

Decher, G., J. D. Hong and J. Schmitt (1992). "Buildup of Ultrathin Multilayer Films by a Self-Assembly Process. Consecutively Alternating Adsorption of Anionic and Cationic Polyeletrolytes on Charges Surface." Thin Solid Films **210/211**: 831-835.

Devaraj, N. K., P. H. Dinolfo, C. E. D. Chidsey and J. P. Collman (2006). "Selective Functionalization of Independently Addressed Microelectrodes by Electrochemical Activation and Deactivation of a Coupling Catalyst." Journal of the American Chemical Society **128**(6): 1794-1795.

Egeland, R. D., F. Marken and E. M. Southern (2002). "An Electrochemical Redox Couple Activitated by Microelectrodes for Confined Chemical Patterning of Surfaces." Analytical Chemistry **74**(7): 1590-1596.

El Haitami, A. E., J.-S. Thomann, L. Jierry, A. Parat, J.-C. Voegel, P. Schaaf, B. Senger, F. Boulmedais and B. Frisch (2010). "Covalent Layer-by-Layer Assemblies of Polyelectrolytes and Homobifunctional Spacers." Langmuir **26**(14): 12351-12357.

Fernandes, R., X. Luo, C. Y. Tsao, G. F. Payne, R. Ghodssi, G. W. Rubloff and W. E. Bentley (2010). "Biological Nanofactories Facilitate Spatially Selective Capture and Manipulation of Quorum Sensing Bacteria in a Biomems Device." Lab Chip **10**(9): 1128-1134.

Fernandes, R., L. Q. Wu, T. H. Chen, H. M. Yi, G. W. Rubloff, R. Ghodssi, W. E. Bentley and G. F. Payne (2003). "Electrochemically Induced Deposition of a Polysaccharide Hydrogel onto a Patterned Surface." Langmuir **19**(10): 4058-4062.

Gong, J., L. Wang, K. Zhao and D. Song (2008). "One-Step Fabrication of Chitosan–Hematite Nanotubes Composite Film and Its Biosensing for Hydrogen Peroxide." Electrochemistry Communications **10**(1): 123-126.

Grandfield, K., F. Sun, M. FitzPatrick, M. Cheong and I. Zhitomirsky (2009). "Electrophoretic Deposition of Polymer-Carbon Nanotube–Hydroxyapatite Composites." Surface and Coatings Technology **203**(10-11): 1481-1487.

Grandfield, K. and I. Zhitomirsky (2008). "Electrophoretic Deposition of Composite Hydroxyapatite–Silica–Chitosan Coatings." Materials Characterization **59**(1): 61-67.

Gray, K. M., B. D. Liba, Y. Wang, Y. Cheng, G. W. Rubloff, W. E. Bentley, A. Montembault, I. Royaud, L. David and G. F. Payne (2012). "Electrodeposition of a Biopolymeric Hydrogel: Potential for One-Step Protein Electroaddressing." Biomacromolecules **13**(4): 1181-1189.

Guschin, D. A., H. Shkil and W. Schuhmann (2009). "Electrodeposition Polymers as Immobilization Matrices in Amperometric Biosensors: Improved Polymer Synthesis and Biosensor Fabrication." Analytical and bioanalytical chemistry **395**(6): 1693-1706.

Isik, S., J. Oni, V. Rjabova, S. Neugebauer and W. Schuhmann (2004). "Entrapment of Metalloporphyrins within an Electrodeposition Paint Layer as a Basis for Developing a Nitric Oxide Sensor." Microchimica Acta **148**(1-2): 59-64.

Johnson, E. K., D. J. Adams and P. J. Cameron (2010). "Directed Self-Assembly of Dipeptides to Form Ultrathin Hydrogel Membranes." Journal of the American Chemical Society **132**(14): 5130-5136.

Kerdjoudj, H., N. Berthelemy, F. Boulmedais, J. F. Stoltz, P. Menu and J.-C. Voegel (2010). "Multilayered Polyelectrolyte Films: A Tool for Arteries and Vessel Repair." Soft Matter **6**(16): 3722-3734.

Kim, E., Y. Liu, X. W. Shi, X. H. Yang, W. E. Bentley and G. F. Payne (2010). "Biomimetic Approach to Confer Redox Activity to Thin Chitosan Films." Advanced Functional Materials **20**(16): 2683-2694.

Kojic, N., M. J. Panzer, G. G. Leisk, W. K. Raja, M. Kojic and D. L. Kaplan (2012). "Ion Electrodiffusion Governs Silk Electrogelation." Soft Matter **8**(26): 6897-6905.

Krogman, K. C., J. L. Lowery, N. S. Zacharia, G. C. Rutledge and P. T. Hammond (2009). "Spraying Asymmetry into Functional Membranes Layer-by-Layer." Nature Materials **8**(6): 512-518.

Krylova, I. (2001). "Painting by Electrodeposition on the Eve of the 21st Century." Progress in Organic Coatings **42**(3-4): 119-131.

Kurzawa, C., A. Hengstenberg and W. Schuhmann (2002). "Immobilization Method for the Preparation of Biosensors Based on Ph Shift-Induced Deposition of Biomolecule-Containing Polymer Films." Analytical Chemistry **74**(2): 355-361.

Lefort, M., F. Boulmedais, L. Jierry, E. Gonthier, J.-C. Voegel, J. Hemmerlé, P. Lavalle, A. Ponche and P. Schaaf (2011). "Simultaneous Spray Coating of Interacting Species: General Rules Governing the Poly(Styrene Sulfonate)/Poly(Allylamine) System." Langmuir **27**(8): 4653-4660.

Leisk, G. G., T. J. Lo, T. Yucel, Q. Lu and D. L. Kaplan (2010). "Electrogelation for Protein Adhesives." Advanced Materials **22**(6): 711-715.

Li, B., B. Yu, W. T. Huck, W. Liu and F. Zhou (2013a). "Electrochemically Mediated Atom Transfer Radical Polymerization on Nonconducting Substrates: Controlled Brush Growth through Catalyst Diffusion." Journal of the American Chemical Society **135**(5): 1708-1710.

Li, B., B. Yu, W. T. Huck, F. Zhou and W. Liu (2012). "Electrochemically Induced Surface-Initiated Atom-Transfer Radical Polymerization." Angewandte Chemie, International Edition in English **51**(21): 5092-5095.

Li, B., B. Yu and F. Zhou (2013b). "In Situ Afm Investigation of Electrochemically Induced Surface-Initiated Atom-Transfer Radical Polymerization." Macromolecular Rapid Communications **34**(3): 246-250.

Li, F., Z. Wang, W. Chen and S. Zhang (2009). "A Simple Strategy for One-Step Construction of Bienzyme Biosensor by in-Situ Formation of Biocomposite Film through Electrodeposition." Biosensors and Bioelectronics **24**(10): 3030-3035.

Liang, R., H. Peng and J. Qiu (2008). "Fabrication, Characterization, and Application of Potentiometric Immunosensor Based on Biocompatible and Controllable Three-Dimensional Porous Chitosan Membranes." Journal of Colloid and Interface Science **320**(1): 125-131.

Liang, R. P., L. X. Fan, R. Wang and J. D. Qiu (2009). "One-Step Electrochemically Deposited Nanocomposite Film of Cs-Fc/Mwnts/God for Glucose Biosensor Application." Electroanalysis **21**(15): 1685-1691.

Liu, C. H., X. L. Guo, H. T. Cui and R. Yuan (2009). "An Amperometric Biosensor Fabricated from Electro-Co-Deposition of Sodium Alginate and Horseradish Peroxidase." Journal of Molecular Catalysis B-Enzymatic **60**(3-4): 151-156.

Liu, Y., Y. Cheng, H. C. Wu, E. Kim, R. V. Ulijn, G. W. Rubloff, W. E. Bentley and G. F. Payne (2011a). "Electroaddressing Agarose Using Fmoc-Phenylalanine as a Temporary Scaffold." Langmuir **27**(12): 7380-7384.

Liu, Y., K. J. Gaskell, Z. Cheng, L. L. Yu and G. F. Payne (2008). "Chitosan-Coated Electrodes for Bimodal Sensing: Selective Post-Electrode Film Reaction for Spectroelectrochemical Analysis." Langmuir **24**(14): 7223-7231.

Liu, Y., E. Kim, R. Ghodssi, G. W. Rubloff, J. N. Culver, W. E. Bentley and G. F. Payne (2010). "Biofabrication to Build the Biology-Device Interface." Biofabrication **2**(2): 022002.

Liu, Y., E. Kim, R. V. Ulijn, W. E. Bentley and G. F. Payne (2011b). "Reversible Electroaddressing of Self-Assembling Amino-Acid Conjugates." Advanced Functional Materials **21**(9): 1575-1580.

Lu, Q., Y. Huang, M. Li, B. Zuo, S. Lu, J. Wang, H. Zhu and D. L. Kaplan (2011). "Silk Fibroin Electrogelation Mechanisms." Acta biomaterialia **7**(6): 2394-2400.

Luo, X., A. T. Lewandowski, H. Yi, G. F. Payne, R. Ghodssi, W. E. Bentley and G. W. Rubloff (2008). "Programmable Assembly of a Metabolic Pathway Enzyme in a Pre-Packaged Reusable Biomems Device." Lab Chip **8**(3): 420-430.

Luo, X. L., J. J. Xu, Y. Du and H. Y. Chen (2004). "A Glucose Biosensor Based on Chitosan-Glucose Oxidase-Gold Nanoparticles Biocomposite Formed by One-Step Electrodeposition." Analytical Biochemistry **334**(2): 284-289.

Luo, X. L., J. J. Xu, Q. Zhang, G. J. Yang and H. Y. Chen (2005). "Electrochemically Deposited Chitosan Hydrogel for Horseradish Peroxidase Immobilization through Gold Nanoparticles Self-Assembly." Biosensors and Bioelectronics **21**(1): 190-196.

Ma, R., R. F. Epand and I. Zhitomirsky (2010). "Electrodeposition of Hyaluronic Acid and Hyaluronic Acid-Bovine Serum Albumin Films from Aqueous Solutions." Colloids and surfaces. B, Biointerfaces **77**(2): 279-285.

Mertz, D., J. Hemmerle, F. Boulmedais, J. C. Voegel, P. Lavalle and P. Schaaf (2007). "Polyelectrolyte Multilayer Films under Mechanical Stretch." Soft Matter **3**(11): 1413-1420.

Mertz, D., C. Vogt, J. Hemmerle, J. Mutterer, V. Ball, J. C. Voegel, P. Schaaf and P. Lavalle (2009). "Mechanotransductive Surfaces for Reversible Biocatalysis Activation." Nature Materials **8**(9): 731-735.

Ngounou, B., E. H. Aliyev, D. A. Guschin, Y. M. Sultanov, A. A. Efendiev and W. Schuhmann (2007). "Parallel Synthesis of Libraries of Anodic and Cathodic Functionalized Electrodeposition Paints as Immobilization Matrix for Amperometric Biosensors." Bioelectrochemistry **71**(1): 81-90.

Ngounou, B., S. Neugebauer, A. Frodl, S. Reiter and W. Schuhmann (2004). "Combinatorial Synthesis of a Library of Acrylic Acid-Based Polymers and Their Evaluation as Immobilisation Matrix for Amperometric Biosensors." Electrochimica Acta **49**(22-23): 3855-3863.

Nicosia, C., S. O. Krabbenborg, P. Chen and J. Huskens (2013). "Shape-Controlled Fabrication of Micron-Scale Surface Chemical Gradients Via Electrochemically Activated Copper(I) "Click" Chemistry." Journal of Materials Chemistry B **1**(40): 5417-5428.

Pang, X., T. Casagrande and I. Zhitomirsky (2009). "Electrophoretic Deposition of Hydroxyapatite-Casio3-Chitosan Composite Coatings." Journal of Colloid and Interface Science **330**(2): 323-329.

Pang, X. and I. Zhitomirsky (2005). "Electrodeposition of Composite Hydroxyapatite–Chitosan Films." Materials Chemistry and Physics **94**(2-3): 245-251.

Pang, X. and I. Zhitomirsky (2007). "Electrophoretic Deposition of Composite Hydroxyapatite-Chitosan Coatings." Materials Characterization **58**(4): 339-348.

Pang, X. and I. Zhitomirsky (2008). "Electrodeposition of Hydroxyapatite–Silver–Chitosan Nanocomposite Coatings." Surface and Coatings Technology **202**(16): 3815-3821.

Pishbin, F., A. Simchi, M. P. Ryan and A. R. Boccaccini (2011). "Electrophoretic Deposition of Chitosan/45s5 Bioglass® Composite Coatings for Orthopaedic Applications." Surface and Coatings Technology **205**(23-24): 5260-5268.

Qiu, J. D., R. P. Liang, R. Wang, L. X. Fan, Y. W. Chen and X. H. Xia (2009). "A Label-Free Amperometric Immunosensor Based on Biocompatible Conductive Redox Chitosan-Ferrocene/Gold Nanoparticles Matrix." Biosensors and Bioelectronics **25**(4): 852-857.

Reddy, K. R., F. Turcu, A. Schulte, A. M. Kayastha and W. Schuhmann (2005). "Fabrication of a Potentiometric/Amperometric Bifunctional Enzyme Microbiosensor." Analytical Chemistry **77**(15): 5063-5067.

Reiter, S., D. Ruhlig, B. Ngounou, S. Neugebauer, S. Janiak, A. Vilkanauskyte, T. Erichsen and W. Schuhmann (2004). "An Electrochemical Robotic System for the Optimization of Amperometric Glucose Biosensors Based on a Library of Cathodic Electrodeposition Paints." Macromolecular Rapid Communications **25**(1): 348-354.

Richert, L., A. J. Engler, D. E. Discher and C. Picart (2004). "Elasticity of Native and Cross-Linked Polyelectrolyte Multilayer Films." Biomacromolecules **5**(5): 1908-1916.

Rostovtsev, V. V., L. G. Green, V. V. Fokin and K. B. Sharpless (2002). "A Stepwise Huisgen Cycloaddition Process: Copper(I)-Catalyzed Regioselective "Ligation" of Azides and Terminal Alkynes." Angewandte Chemie International Edition **41**(14): 2596-2599.

Rydzek, G., T. Garnier, P. Schaaf, J.-C. Voegel, B. Senger, B. Frisch, Y. Haikel, C. Petit, G. Schlatter, L. Jierry and F. Boulmedais (2013). "Self-Construction of Supramolecular Polyrotaxane Films by an Electrotriggered Morphogen-Driven Process." Langmuir **29**(34): 10776-10784.

Rydzek, G., L. Jierry, A. Parat, J. S. Thomann, J.-C. Voegel, B. Senger, J. Hemmerlé, A. Ponche, B. Frisch, P. Schaaf and F. Boulmedais (2011a). "Electrochemically Triggered Assembly of Films: A One-Pot Morphogen-Driven Buildup." Angewandte Chemie-International Edition **50**(19): 4374-4377.

Rydzek, G., L. Jierry, A. Parat, J. S. Thomann, J. C. Voegel, B. Senger, J. Hemmerle, A. Ponche, B. Frisch, P. Schaaf and F. Boulmedais (2011b). "Electrochemically Triggered Assembly of Films: A One-Pot Morphogen-Driven Buildup." Angewandte Chemie, International Edition in English **50**(19): 4374-4377.

Rydzek, G., A. Parat, P. Polavarapu, C. Baehr, J. C. Voegel, J. Hemmerle, B. Senger, B. Frisch, P. Schaaf, L. Jierry and F. Boulmedais (2012a). "One-Pot Morphogen Driven Self-Constructing Films Based on Non-Covalent Host-Guest Interactions." Soft Matter **8**(2): 446-453.

Rydzek, G., P. Polavarapu, C. Rios, J. N. Tisserant, J. C. Voegel, B. Senger, P. Lavalle, B. Frisch, P. Schaaf, F. Boulmedais and L. Jierry (2012b). "Morphogen-Driven Self-Construction of Covalent Films Built from Polyelectrolytes and Homobifunctional Spacers: Buildup and Ph Response." Soft Matter **8**(40): 10336-10343.

Rydzek, G., J.-S. Thomann, N. Ben Ameur, L. Jierry, P. Mésini, C. Contal, J.-C. Voegel, B. Senger, P. Schaaf, B. Frisch and F. Boulmedais (2010). "Polymer Multilayer Films Obtained by Electrochemically Catalyzed Click-Chemistry." Langmuir **26**: 2816-2824.

Sassolas, A., L. J. Blum and B. D. Leca-Bouvier (2012). "Immobilization Strategies to Develop Enzymatic Biosensors." Biotechnology Advances **30**(3): 489-511.

Schaaf, P., J.-C. Voegel, L. Jierry and F. Boulmedais (2012). "Spray-Assisted Polyelectrolyte Multilayer Buildup: From Step-by-Step to Single-Step Polyelectrolyte Film Constructions." Advanced Materials **24**(8): 1001-1016.

Schlenoff, J. B., S. T. Dubas and T. Farhat (2000). "Sprayed Polyelectrolyte Multilayers." Langmuir **16**(26): 9968-9969.

Servoli, E., D. Maniglio, A. Motta and C. Migliaresi (2008). "Folding and Assembly of Fibroin Driven by an Ac Electric Field: Effects on Film Properties." Macromolecular bioscience **8**(9): 827-835.

Seyrek, E. and G. Decher (2012). 7.09 - Layer-by-Layer Assembly of Multifunctional Hybrid Materials and Nanoscale Devices. Polymer Science: A Comprehensive Reference. K. Matyjaszewski and M. Möller. Amsterdam, Elsevier**:** 159-185.

Shi, X. W., Y. Liu, A. T. Lewandowski, L. Q. Wu, H. C. Wu, R. Ghodssi, G. W. Rubloff, W. E. Bentley and G. F. Payne (2008). "Chitosan Biotinylation and Electrodeposition for Selective Protein Assembly." Macromolecular bioscience **8**(5): 451-457.

Shi, X. W., L. Qiu, Z. Nie, L. Xiao, G. F. Payne and Y. Du (2013). "Protein Addressing on Patterned Microchip by Coupling Chitosan Electrodeposition and 'Electro-Click' Chemistry." Biofabrication **5**(4): 041001.

Shi, X. W., C. Y. Tsao, X. H. Yang, Y. Liu, P. Dykstra, G. W. Rubloff, R. Ghodssi, W. E. Bentley and G. F. Payne (2009a). "Electroaddressing of Cell Populations by Co-Deposition with Calcium Alginate Hydrogels." Advanced Functional Materials **19**(13): 2074-2080.

Shi, X. W., X. H. Yang, K. J. Gaskell, Y. Liu, E. Kobatake, W. E. Bentley and G. F. Payne (2009b). "Reagentless Protein Assembly Triggered by Localized Electrical Signals." Advanced Materials **21**(9): 984-+.

Shida, N., Y. Ishiguro, M. Atobe, T. Fuchigami and S. Inagi (2012). "Electro-Click Modification of Conducting Polymer Surface Using Cu(I) Species Generated on a Bipolar Electrode in a Gradient Manner." Acs Macro Letters **1**(6): 656-659.

Simchi, A., F. Pishbin and A. R. Boccaccini (2009). "Electrophoretic Deposition of Chitosan." Materials Letters **63**(26): 2253-2256.

Sonogashira, K., Y. Tohda and N. Hagihara (1975). "A Convenient Synthesis of Acetylenes: Catalytic Substitutions of Acetylenic Hydrogen with Bromoalkenes, Iodoarenes and Bromopyridines." Tetrahedron Letters **16**(50): 4467-4470.

Sun, F., X. Pang and I. Zhitomirsky (2009). "Electrophoretic Deposition of Composite Hydroxyapatite–Chitosan–Heparin Coatings." Journal of Materials Processing Technology **209**(3): 1597-1606.

Tornøe, C. W., C. Christensen and M. Meldal (2002). "Peptidotriazoles on Solid Phase: [1,2,3]-Triazoles by Regiospecific Copper(I)-Catalyzed 1,3-Dipolar Cycloadditions of Terminal Alkynes to Azides." The Journal of Organic Chemistry **67**(9): 3057-3064.

Vilkanauskyte, A., T. Erichsen, L. Marcinkeviciene, V. Laurinavicius and W. Schuhmann (2002). "Reagentless Biosensors Based on Co-Entrapment of a Soluble Redox Polymer and an Enzyme within an Electrochemically Deposited Polymer Film." Biosensors & Bioelectronics **17**(11-12): 1025-1031.

Wang, X., H. Gu, F. Yin and Y. Tu (2009). "A Glucose Biosensor Based on Prussian Blue/Chitosan Hybrid Film." Biosensors and Bioelectronics **24**(5): 1527-1530.

Wong, I. Y., M. J. Footer and N. A. Melosh (2007). "Dynamic Control of Biomolecular Activity Using Electrical Interfaces." Soft Matter **3**(3): 267-274.

Wong, I. Y., M. J. Footer and N. A. Melosh (2008). "Electronically Activated Actin Protein Polymerization and Alignment." Journal of the American Chemical Society **130**(25): 7908-7915.

Wu, L. Q., A. P. Gadre, H. M. Yi, M. J. Kastantin, G. W. Rubloff, W. E. Bentley, G. F. Payne and R. Ghodssi (2002). "Voltage-Dependent Assembly of the Polysaccharide Chitosan onto an Electrode Surface." Langmuir **18**(22): 8620-8625.

Wu, L. Q., R. Ghodssi, Y. A. Elabd and G. F. Payne (2005a). "Biomimetic Pattern Transfer." Advanced Functional Materials **15**(2): 189-195.

Wu, L. Q., K. Lee, X. Wang, D. S. English, W. Losert and G. F. Payne (2005b). "Chitosan-Mediated and Spatially Selective Electrodeposition of Nanoscale Particles." Langmuir **21**(8): 3641-3646.

Wu, L. Q., M. K. McDermott, C. Zhu, R. Ghodssi and G. E. Payne (2006). "Mimicking Biological Phenol Reaction Cascades to Confer Mechanical Function." Advanced Functional Materials **16**(15): 1967-1974.

Wu, L. Q., H. M. Yi, S. Li, G. W. Rubloff, W. E. Bentley, R. Ghodssi and G. F. Payne (2003). "Spatially Selective Deposition of a Reactive Polysaccharide Layer onto a Patterned Template." Langmuir **19**(3): 519-524.

Xi, F., L. Liu, Q. Wu and X. Lin (2008). "One-Step Construction of Biosensor Based on Chitosan-Ionic Liquid-Horseradish Peroxidase Biocomposite Formed by Electrodeposition." Biosensors and Bioelectronics **24**(1): 29-34.

Yang, X., X. W. Shi, Y. Liu, W. E. Bentley and G. F. Payne (2009). "Orthogonal Enzymatic Reactions for the Assembly of Proteins at Electrode Addresses." Langmuir **25**(1): 338-344.

Yang, X. H., E. Kim, Y. Liu, X. W. Shi, G. W. Rubloff, R. Ghodssi, W. E. Bentley, Z. Pancer and G. F. Payne (2010). "In-Film Bioprocessing and Immunoanalysis with Electroaddressable Stimuli-Responsive Polysaccharides." Advanced Functional Materials **20**(10): 1645-1652.

Yi, H., S. Nisar, S. Y. Lee, M. A. Powers, W. E. Bentley, G. F. Payne, R. Ghodssi, G. W. Rubloff, M. T. Harris and J. N. Culver (2005a). "Patterned Assembly of Genetically Modified Viral Nanotemplates Via Nucleic Acid Hybridization." Nano Letters **5**(10): 1931-1936.

Yi, H., L. Q. Wu, R. Ghodssi, G. W. Rubloff, G. F. Payne and W. E. Bentley (2005b). "Signal-Directed Sequential Assembly of Biomolecules on Patterned Surfaces." Langmuir **21**(6): 2104-2107.

Yi, H. M., L. Q. Wu, W. E. Bentley, R. Ghodssi, G. W. Rubloff, J. N. Culver and G. F. Payne (2005c). "Biofabrication with Chitosan." Biomacromolecules **6**(6): 2881-2894.

Yi, H. M., L. Q. Wu, R. Ghodssi, G. W. Rubloff, G. F. Payne and W. E. Bentley (2004). "A Robust Technique for Assembly of Nucleic Acid Hybridization Chips Based on Electrochemically Templated Chitosan." Analytical Chemistry **76**(2): 365-372.

Zangmeister, R. A., J. J. Park, G. W. Rubloff and M. J. Tarlov (2006). "Electrochemical Study of Chitosan Films Deposited from Solution at Reducing Potentials." Electrochimica Acta **51**(25): 5324-5333.

Zeng, X., X. Li, L. Xing, X. Liu, S. Luo, W. Wei, B. Kong and Y. Li (2009). "Electrodeposition of Chitosan-Ionic Liquid-Glucose Oxidase Biocomposite onto Nano-Gold Electrode for Amperometric Glucose Sensing." Biosensors and Bioelectronics **24**(9): 2898-2903.

Zhitomirsky, D., J. A. Roether, A. R. Boccaccini and I. Zhitomirsky (2009). "Electrophoretic Deposition of Bioactive Glass/Polymer Composite Coatings with and without Ha Nanoparticle Inclusions for Biomedical Applications." Journal of Materials Processing Technology **209**(4): 1853-1860.

Zhitomirsky, I. (2002). "Cathodic Electrodeposition of Ceramic and Organoceramic Materials. Fundamental Aspects." Advances in Colloid and Interface Science **97**(1-3): 279-317.

CHAPTER 2: MATERIAL AND METHODS

2 MATERIAL AND METHODS.

CONTENTS

2.1 MATERIAL AND SAMPLE PREPARATION.

All the solutions were prepared using ultra-pure water with a resistivity of 18.2 MΩ.cm (Milli-Q-plus system, Millipore). Absolute ethanol at 99.5% (VWR) was used mixed to water in proportions specified for each case when the solution contained hydrophobic molecules.

2.1.1 Monomer, polymer, macromolecules and functional molecule solutions.

Commercial monomers. Commercial methacrylate monomers having different ethylene glycol chain lengths were used for polymer-brushes buildup. Oligo(ethylene glycol) methyl ether methacrylate (OEGMA) with a molecular weight of 475 and 300 g.mol^{-1} and 2-(2-methoxyethoxy)ethyl methacrylate (MeO_2MA) with a molecular weight of 188 g.mol^{-1} were purchased from Sigma Aldrich (ref: 447943, 447935, 447927). Their chemical structures are given in Figure 2.1.

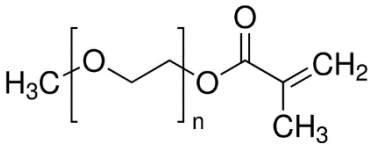

Figure 2.1 Molecular representation of OEGMA monomers with a molecular weight of 475 (n=8.5), 300 (n=3.5) and 188 g.mol^{-1} (n=2, MeO_2MA).

Commercial polymers. Branched poly(ethylene immine) (ref: P3143), poly(styrene sulfonate) (ref: 243051) and poly(allylamine hydrochloride) (ref: 283223) were purchased from Sigma Aldrich. Their chemical structures are given in Figure 2.2. PEI, PSS and PAH were solubilized at a concentration of 1 mg.ml^{-1} in an aqueous solution 150 mM $NaNO_3$. PEI, PSS and PAH have a respective pKa of 7-9, 0.5 and 8.5 (Hummel (2009)).

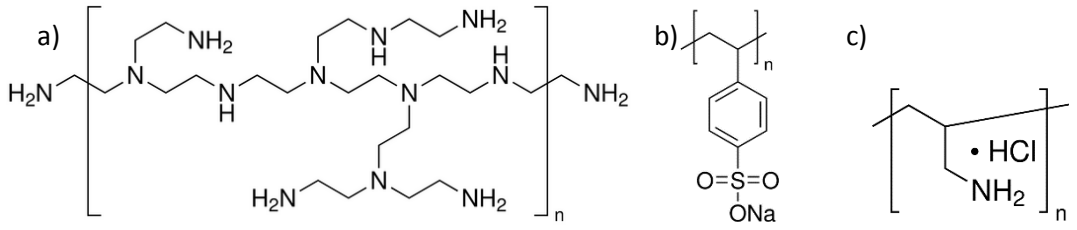

Figure 2.2 Molecular representations of branched poly(ethylene imine) (a), poly(styrene sulfonate) (b) and poly(allylamine hydrochloride) (c).

Functionalized polymers. Branched PEI was modified by bromo-isobutyramide functions at 15 % (determined by NMR). The synthesis was done by the team of Prof. J.F. Lutz (Figure 2.3a). The polymer is named PEI-Br in the rest of this thesis.

PAH was grafted with a stoichiometric amount of citraconic functions and has been synthesized by Dr. Tony Garnier (post-doctorant) following a method described by Lynn (Liu et al. 2008). It will be referred as *PAHc* in the following. PAH with a stoiechiometric amount of grafted dimethylmaleic functions (Figure 2.3c) has been synthesized following an original method developed by Dr. Tony Garnier. It will be referred as *PAHd* in the following.

Functionalized PSS with grafted rhodamine (PSS_{rho}) has been synthesized by Dr. Fouzia Boulmedais following a protocol described by Dähne et al (Dähne et al. 2001).

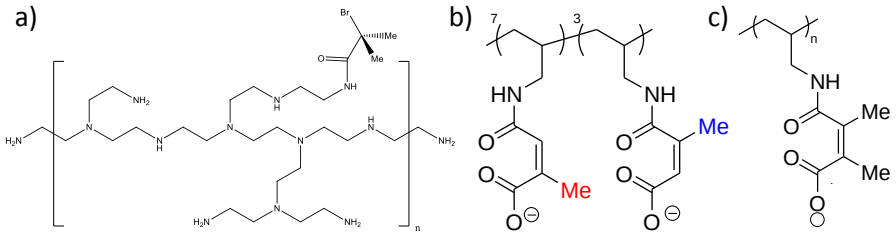

Figure 2.3 Molecular representation of poly(ethylene imine) bromo-isobutyramide (a), poly(allylamine hydrocholoride) citraconic (b) and poly(allylamine hydrochloride) dimethylmaleic (c).

Macromolecules. Phosphatase alkaline (AP, ref: P-4002) with an isoelectric point between 4.4 and 5.8 as well as pig liver esterase (PLE, ref: E3019) with an isoelectric point between 4.8 and 5.8 were purchased from Sigma Aldrich.

Functionalized Macromolecules. Phosphatase alkaline grafted with fluorescein isothiocyanate at 1 % was synthesized by Dr. Loïc Jierry (maître de conference) following an original procedure.

Low molecular weight molecules. Tris(2-pyridylmethyl)amine (TPMA, ref: 723134), hydroquinone (ref: H17902) para-nitrophenylphosphate (PNP, ref: N7653) and tetrabutylammonium bromide (TBAB, ref : 193119) were purchased from Sigma Aldrich. They were used without further treatment or purification.

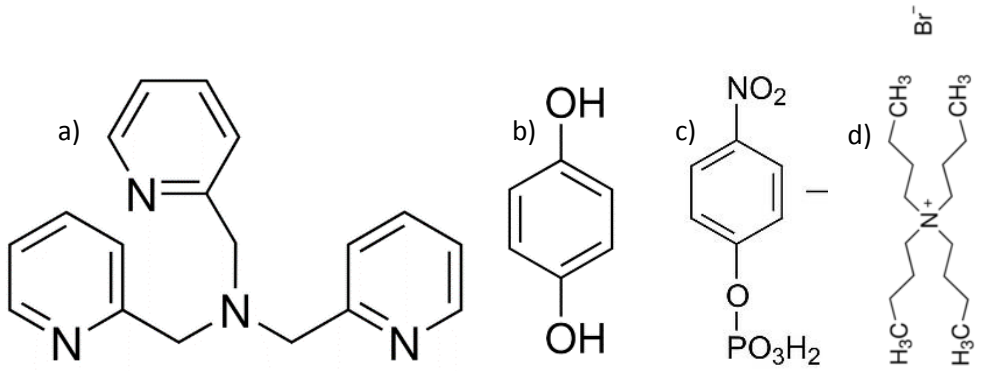

Figure 2.4 Molecular representation of Tris(2-pyridylmethyl)amine (a), hydroquinone(b), para-nitrophenylphosphate(c) and tetrabutylammonium bromide (d).

2.2 CHARACTERIZATION AND ANALYSIS METHODS.

2.2.1 Electrochemical methods.

Different electrochemical methods were used during this PhD: cyclic voltammetry (CV), chronopotentiometry, chronoamperometry and chronoelectrogravimetry.

2.2.1.1 Three-electrode electrochemical setup.

The quartz crystal microbalance described later in section 2.2.2 has been coupled to an electrochemical modulus. The realized setup is a classical three electrode electrochemical circuit containing a working electrode (WE), a reference electrode (RE) and a counter electrode (CE). Figure 2.5 schematically shows a three electrode setup with the current flowing between the WE and the CE while the potential difference (*pdiff*) is measured or applied between the WE and the RE.

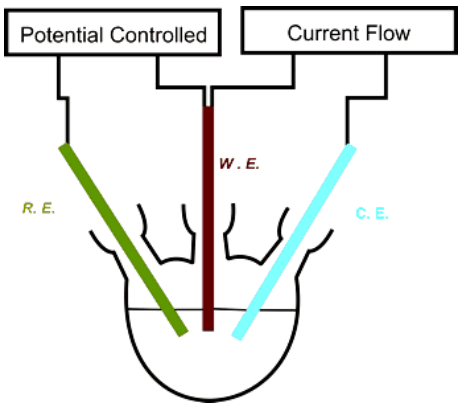

Figure 2.5 Schematic representation of a three electrode electrochemical cell: the working electrode (WE), the reference electrode (RE) and the counter electrode (CE) are immersed in a solution. The current flows between the WE and the CE while the potential is measured or controlled between the WE and the RE.

The working electrode is made of a quartz crystal coated with two conducting gold layers. Only the top layer of the crystal is in contact with the solution containing the electroactive species thus making it the working electrode.

The reference electrode is an electrode made of a redox couple with a stable and known potential. In our case, it is a silver chloride rigid electrode based on the *Ag/AgCl* couple. The *pdiff* is applied or measured between this electrode and the WE. It is often referred to as a potential applied at the working electrode but it is actually a *pdiff* applied between the WE and the RE. The chemical composition of the RE can vary, thus varying its potential. In order to compare the *pdiff* applied or measured with different REs, it exists an absolute RE based on the H^+/H_2 couple with a redox potential fixed at 0. The standard potential of the *Ag/AgCl* electrode is 0.280 V at 25°C with respect to the H^+/H_2 electrode.

The counter electrode is made of platinum. Its role is to collect the current flowing in the electrochemical cell. The chemical nature of this electrode is very important. As a matter of fact, when a *pdiff* is applied between the WE and the RE, the real *pdiff* is slightly inferior to the set value. This phenomena, called ohmic voltage drop, is due to the solution resistance toward the current flow. The real *pdiff* is then given by:

$$pdiff_{real} = pdiff_{set\ value} - E_{ohmic\ voltage\ drop} = pdiff_{set\ value} - \rho * d * I$$

Where ρ is the solution resistivity, d the distance between the WE and the RE and I the current intensity.

Since the intensity is in of order of 10^{-6} A, that the distance is of the order of 10^{-3} m and the resistivity is roughly 10^2 Ω.m, the current I flowing between the WE and the RE is negligible. This then renders the ohmic voltage drop also negligible.

2.2.1.2 Cyclic Voltammetry.

Cyclic voltammetry (CV) is an electrochemical method where a potential difference (*pdiff*) is applied over a potential range between a working electrode (WE) and a reference electrode (RE) while measuring the current intensity *I* flowing in the electrochemical cell between the WE and the counter electrode (CE). When a current appears in the circuit, it is characteristic of an electrochemical reaction (oxidation or reduction) in the vicinity of an electrode.

During a cyclic voltammetry experiment, each scanning cycle proceeds in two steps: first, the potential difference (*pdiff*) is increased from an initial potential E_i to a final potential E_f (oxidation), then, the

pdiff is decreased from E_f to E_i (reduction). This signal is triangular over time hence its denomination as cyclic (Figure 2.6).

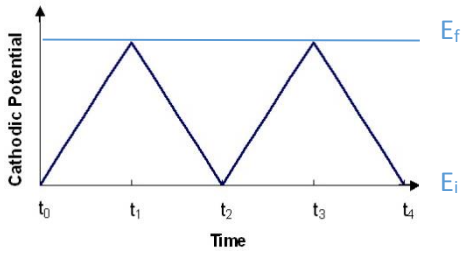

Figure 2.6 Triangular variation of the applied potential difference over time for a cyclic voltammetry experiment. The first part of the first scanning cycle, i.e. the oxidation corresponding to the progressive increase of the pdiff from E_i to E_f happens between t_0 and t_1. Once the pdiff reaches its maximum value E_f, the second part of the first cycle consists in decreasing the pdiff from E_f to E_i between t_1 and t_2 in order to reduce the electroactive compound.

The scanning speed on this potential range is defined as:

$$v = \frac{dE}{dt}$$

The initial potential, the final potential and the scanning speed are fixed and the current *i* is measured.

A simple redox system can be described as follows:

$$x * Ox + ne^{-} = y * Red$$

where *Ox* and *Red* respectively represents the oxidizing and reducing species, *x* and *y* are stoichiometric numbers and *n* is the number of exchanged electrons.

The current measured in the electrochemical cell corresponds to the oxidation or reduction of the electroactive species in solution and its intensity depends on the working electrode surface area and on the electroactive species concentration. Therefore, for a given surface area, the current intensity can be used to determine the concentration of the electroactive species.

In order to obtain a physical measurement independent of the WE surface area, the current density *J* in $A.m^{-2}$ is almost always used. However, in our case, the WE surface area is constant thus the current intensity can be directly used.

A typical *i(V)* curve for a cyclic voltammetry experiment for a reversible electroactive compound is given in figure 7. Conventionally in Europe, this voltamperogram is plotted according to the following rules: the *pdiff* goes from the negative to the positive values (from left to right) and the reductive currents are represented on the bottom of the graph while the oxidative currents are represented on the top.

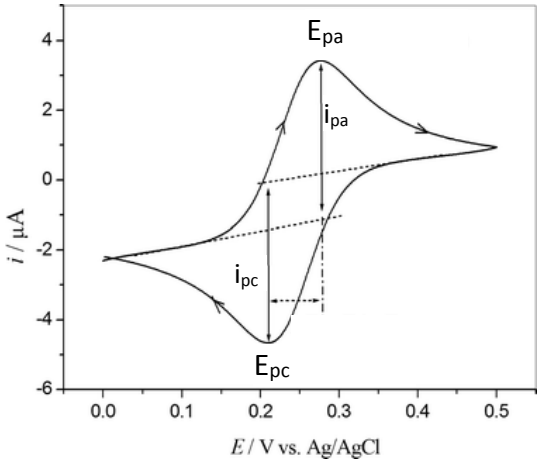

Figure 2.7 Typical voltamperogram of a reversible system displaying one oxidation peak E_{pa} of intensity i_{pa} and one reduction peak E_{pc} of intensity i_{pc}.

The potential difference ranges from an initial minimum value E_i to a maximum final value E_f. For the reversible redox reaction given above, two intensity peaks appear: the first one at a potential E_{pa} with an intensity i_{pa} corresponds to the oxidation of the electroactive compound and the second one at a potential E_{pc} with an intensity i_{pc} corresponds to the reduction reaction. The "half-wave" redox potential characteristic of a reversible system is given by the algebraic mean of E_{pa} and E_{pc}:

$$E_{1/2} = \frac{E_{pa} + E_{pc}}{2}$$

The electrochemical equilibrium between the oxidizing *[Ox]* and reducing *[Red]* species depends on the *pdiff* applied and is given by the Nernst equation. For the redox reaction given above, the Nernst equation will be written:

$$E = E_0 + \frac{RT}{nF} ln\left(\frac{[Ox]^x}{[Red]^y}\right)$$

With E the applied *pdiff* in V, E_0 the standard potential characteristic of the system in V, R the perfect gas constant, T the temperature in K, n the number of exchanged electrons, F the Faraday constant in $C.mol^{-1}$, *[Ox]* and *[Red]* the respective concentrations of the oxidizing and reducing species.

The oxidation reaction corresponds to an electronic transfer of the electroactive compound in the vicinity of the electrode surface. The current intensity decrease observed in Figure 2.7 beyond the maximum peak E_{pa} potential is due to a diffusion limitation of the reducer: it is consumed much faster than it diffuses toward the electrode. Thus, when the potential exceeds E_{pa}, its concentration at the interface gets closer to 0 hence the current i_{pa} decreases whereas the reaction is more favoured. The same mechanism happens in the second half cycle with the oxidizing specie and the intensity peak i_{pc}.

The voltamperogram allows the qualitative observation of the electronic transfer reversibility: it can be irreversible, quasi reversible or reversible. In the case of a slow or one direction electronic transfer, i.e. oxidation and reduction peaks of very different intensities or absence of one peak, the system is called irreversible. When the two peaks are observed but the potential separating these two peaks is larger than 0.2 V, then the system is also called irreversible.

Asymmetric peaks with a potential difference between these two peaks larger than RT/nF is characteristic of a quasi-reversible system.

When the oxidation and reduction peaks are symmetric and that the electronic transfer is fast, the system is called reversible (Figure 2.7).

2.2.1.3 Capacitive and faradic currents.

The current intensity measured in an electrochemical cell is the sum of two phenomena: the capacitive current and the faradic current with their respective intensities i_c and i_f.

The capacitive current comes from a molecular organisation of the solvent at the electrode/solution interface. According to the "electronic double-layer" model (also called Gouy-Chapman-Stern model) the ions close to the electrode surface organize themselves in order to compensate the electrode surface charge.

A first dense layer, called Stern layer, composed of desolvated ions of opposite charge with respect to the electrode surface and with a low ionic mobility screens the electrode surface charges. This screening drastically decreases the electrode surface potential and behaves like a resistance.

Beyond this dense layer, we find a diffuse layer of a few nanometers composed of ions. This layer contains more ions of opposite charge with respect to the electrode surface charge than the rest of the solution far from the electrode. These ions feel less the surface potential than the ones in the Stern layer. The heterogeneous ion composition hence decreases as we go further from the electrode until we reach a homogeneous ions composition. This layer possesses an electric charge capacity and thus behaves like a capacitor. Figure 2.8 schematically represents this electronic double layer model.

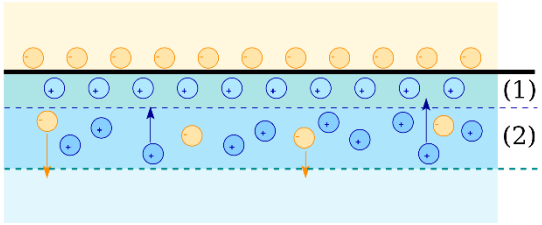

Figure 2.8: Schematic representation of the electronic double layer model: 1) Stern layer of desolvated ions behaving like a resistance and 2) Gouy-Chapman layer of heterogeneous ion composition behaving like a capacitor.

The surface/double layer system behaves like a classical Resistance Capacitor (RC) circuit. This explains the presence of a current intensity i_c when a *pdiff* is applied onto an electrochemical cell without electroactive species.

The faradic current comes from an effective electronic transfer between the electrode and an electroactive compound in solution. This current therefore implies the existence of an electrochemical reaction. To happen, an electronic transfer has to take place. This implies that the electroactive compounds diffuse to the WE and adsorb onto it. The diffusion of the electroactive compound towards the WE is thus of primary importance since the currents results from a competition between the consumption of the electroactive species at the WE/solution interface and their renewal by diffusion. Once the electronic transfer has happened, the oxidized or reduced compounds desorb from the WE surface and diffuse into the solution. The mathematical description of the faradic current leads to the determination of the electrochemical reaction kinetic for a given *pdiff* but its expression, formalized by Butler and Volmer, can be complex (Miomandre 2011).

In our setup, the capacitive current measured is of the order of tens of nanoAmperes while the faradic current is of the order of hundreds of microAmperes due to the high concentration of electroactive species. Therefore, the total intensity *i* of the electrochemical cell can be written as:

$$i = i_c + i_f \approx i_f$$

Only the faradic contribution is considered since the majority of the current comes from the electrochemical reactions of the electroactive species.

2.2.2 Quartz Crystal Microbalance with Dissipation coupled to an electrochemical modulus (EC-QCM-D).

The quartz crystal microbalance (QCM) is a technique developed in the early 60th by G. Sauerbrey. This technique is based on the quartz piezoelectric properties, i.e. the capacity of a quartz to deform when submitted to an electrical field or to polarize when applying a mechanical strain (King Jr 1964).

When an electrical potential is applied between the two gold layers that sandwich the quartz disc, the quartz crystal deforms following a pure shearing movement in the horizontal plane (Figure 2.9).

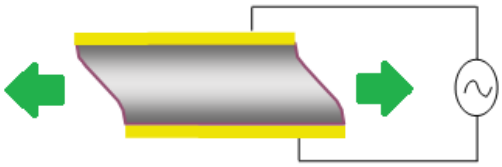

Figure 2.9: Schematic representation of a sandwiched quartz crystal submitted to an electrical field and vibrating in the horizontal plane by a pure shearing movement.

Such a quartz crystal can be considered as an harmonic oscillator that possesses a resonance frequency f_r given by the equation:

$$f_r = \frac{\omega_r}{2\pi} = \frac{1}{2\pi}\sqrt{\frac{k}{M}}$$

where ω_r is the resonance angular frequency of the oscillator, k its stiffness constant in $N.m^{-1}$ and M its mass in kg. In the case of a slight mass deposition m with $m<<M$ on the top of the crystal surface, the resonance frequency of the oscillator changes and becomes:

$$\Delta f = f - f_r = -f_r \frac{m}{2M}$$

The frequency shift is then given by:

$$\frac{\Delta f}{f_r} = -\frac{m}{C}$$

where C is the characteristic crystal constant defined by:

$$C = \frac{2M}{f_r}$$

Figure 2.10 schematically represents the frequency shift of a quartz crystal during the adsorption of a rigid or soft layer that can be measured by QCM.

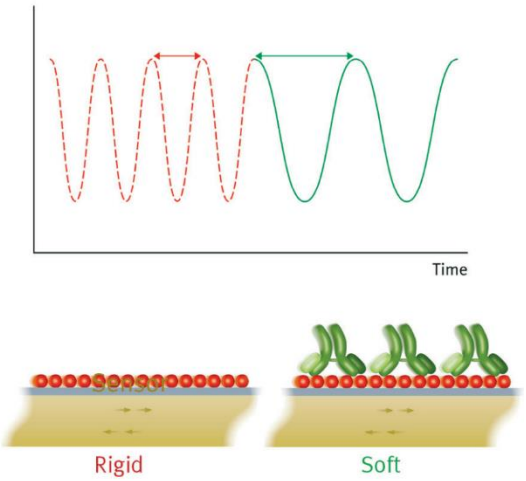

Figure 2.10: Schematic representation of the QCM-D quartz crystal frequency shift for the adsorption of a rigid and soft layer.

The QCM-D allows the determination of a viscous dissipation factor D which correspond to the sum of all the losses in the system. This parameter is defined by the proportion of dissipated energy at each oscillation with respect to the total stored energy:

$$D = \frac{1}{\pi f \tau} = \frac{E_{dissipated\ at\ each\ oscillation}}{2\pi E_{stored}}$$

This dissipation factor is measured by exciting the quartz crystal at its fundamental frequency and the odd harmonics and then by measuring the relaxation time τ. This relaxation time depends on the energy stored in the crystal, in the deposit and in the medium in contact with the crystal surface (Figure 2.11).

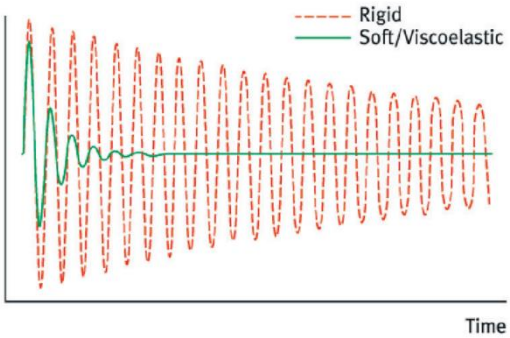

Figure 2.11: Schematic representation of the dissipation factor D variation in the case of a rigid and visco-elastic coating. The damping observed for a rigid film is low while the damping corresponding to the adsorption of a visco-elasctic layer is high due to the dissipative nature of the visco-elastic film towards the acoustic wave generated by the resonator.

The frequency shift Δf measured by QCM can be used to determine the deposited mass per area unit with a resolution inferior to 1 ng.cm^{-2}.

It is also possible to measure the frequency shifts of the odd harmonics during the experiment with:

$$m = -C\frac{\Delta f_n}{n}$$

where *n* is the number of the considered harmonic. This equation, named the Sauerbrey equation, can be applied for uniform and rigid layers in air. It can also be applied in aqueous systems if $\frac{\Delta f_n}{n}$ is independent of n. However, it cannot be applied for vicous layers when this last relation does not hold.

It exists a penetration depth of the acoustic wave generated by the vibrating oscillator given by:

$$\delta = \sqrt{\frac{\eta}{\pi f \rho}}$$

where δ is the penetration depth, η is the shear viscosity and ρ is the density of the adsorbed layer.

If the film buildup exceeds this penetration depth, the signal saturates and the EC-QCM-D stops recording the construction. As seen from the equation above, the penetration depth is related to the inverse square root of the frequency. This means that higher frequencies, i.e. 3rd, 5th or 7th overtones, scans less deeply into the construction and saturate faster for massive buildup.

The *D* factor gives an indication of the visco-elastic character of a coating. If it is superior to a few tens, the viscous modulus of the deposit cannot be neglected and the Sauerbrey relation is not valid anymore. In this case, two different models can be employed: the Voigt-Voinova (Voinova et al. 1999) or the Maxwell model. These models are not detailed here since they weren't used during this work.

2.2.2.1 Coupling of the QCM-D with an electrochemical modulus: EC-QCM-D.

The coatings on top of the QCM-D crystals, i.e. in contact with the solution, can be either conducting or insulating. When this coating is conducting, the crystals can be used as a WE in an electrochemistry setup.

The crystal surface is then used both as the substrate for the buildup and as a WE. The two major conducting coatings available are gold or indium tin oxide (ITO). These two coatings both present advantages and disadvantages: the crystals covered with ITO are transparent and support a *pdiff* going from -0.5 to 2 V whereas the gold ones are opaque and support a *pdiff* ranging from –2 V to 0.8 V.

Furthermore, the ITO coated crystal surfaces exhibit an AFM topography with large grain size (Figure 2.12b, Rms= 2.7 nm) whereas the gold ones have a topography with small grain size (Figure 2.12a, Rms= 0.9 nm).

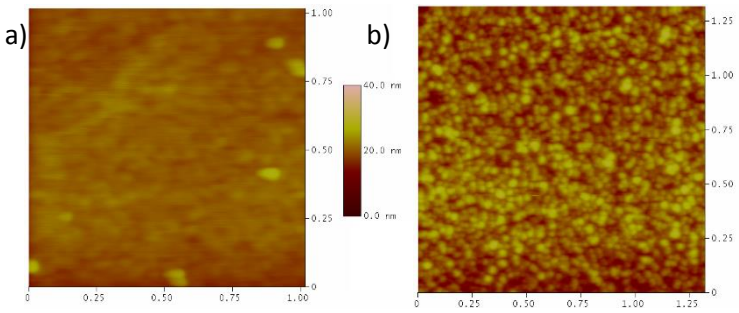

Figure 2.12: AFM surface topographies of a gold coated quartz crystal with thin grain size (a) and of an indium tin oxide coated quartz crystal with large grain size (b).

Gold coated crystals were used during this thesis. In the electrochemical three-electrode setup, an *Ag/AgCl* electrode was used as the RE and a platinum electrode was used as the CE. Figure 2.13 schematically represents the EC-QCM-D electrochemical cell.

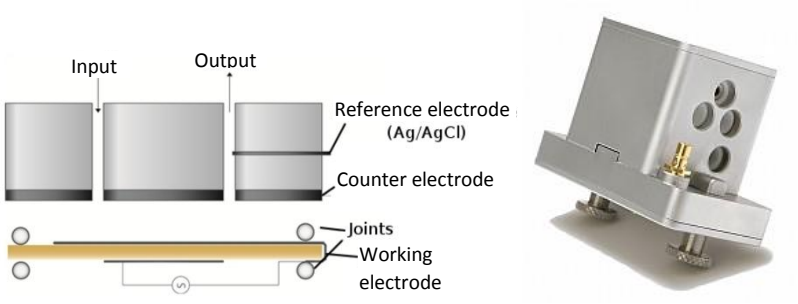

Figure 2.13: Schematic representation of the three electrode EC-QCM-D electrochemical cell (a) Picture of the three electrode EC-QCM-D electrochemical cell (b).

The interest of coupling the QCM-D to an electrochemical modulus lies in the fact that we can both measure the frequency shift of the quartz crystal and its dissipation factor while measuring or applying a *pdiff* or a current. The *pdiff* is measured between the WE and the RE while the current is measured between the WE and the CE.

The frequency shift quantitatively indicates if a mass deposition is taking place and the dissipation factor D relates it to its visco-elastic character.

The data analysis gives the mass of product deposited on the substrate by the electrochemical reaction.

2.2.2.2 EC-QCM-D working principle.

The instrument used is the Q-Sense E1 model (Q-Sense AB, Göteborg, Sweden). It is equipped with a QEM 401 electrochemical modulus and with a CHI 660E (CH Instrument, Austin, Texas) potentiostat/galvanostat. The apparatus is composed of a Peltier thermostated cell and includes a

three-electrode electrochemical setup. The electrochemical cell is connected on one hand to a control electronic interface controlled by a software (QSoft) which measures the frequencies shift and the dissipation factors and on the other hand to a potentiostat/galvanostat monitored by the CHI software.

The quartz crystal, used as a sensor, is excited by a sinusoidal tension generator. The excitation frequency corresponds to the fundamental and odd harmonic resonance frequencies and is applied for a few microseconds. At each excitation stop, the crystal oscillates freely at the fundamental and harmonic frequencies thus inducing the apparition of electric oscillations. These are then collected and treated by the QSoft software in order to obtain the frequency shifts and the dissipation factors of the quartz crystal.

2.2.2.3 Experimental protocol.

The QCM-D used in this thesis uses crystal discs with a thickness of 300 µm and coated by two conducting gold layers (Figure 2.14).

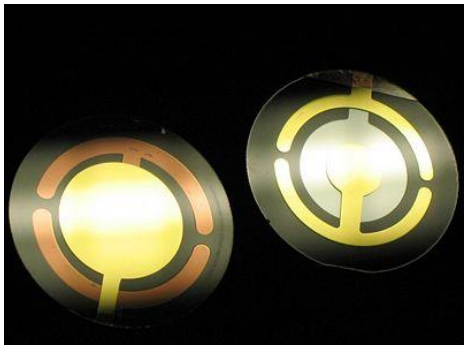

Figure 2.14: Schematic representation of a QCM-D quartz crystal sandwiched by two gold layers. The larger gold electrode on the left is the one in contact with the solution. The gold electrode displayed on the right is in contact with the electronic card controlling the EC-QCM-D.

The quartz crystals used are coated with a thin gold layer of 100 nm (QSX 301 type, Q-Sense). They possess a fundamental resonance frequency f_1 at 5 MHz as well as odd harmonics at 15, 25, 35 and 45 MHz respectively noted f_3, f_5, f_7 and f_9 in the rest of this manuscript. The crystals are treated by UV ozone during 15 minutes to make them hydrophilic before each experiment.

A cyclic voltammetry is then applied between 0 and 600 mV with a scan rate of 50 mV/s during 5 cycles in an aqueous solution of 150 mM $NaNO_3$. The capacitive current hence measured allows to plot the bare crystal voltamperogram. Figure 2.15 shows an example of the capacitive current on a bare crystal.

This voltamperogram should not display any peaks because this would mean that an electrochemical reaction is taking place in the vicinity of the WE and thus that it is polluted. If this is the case, it is

possible to decontaminate the crystal by applying a cyclic voltammetry between -0.5 and 0.7 V in the presence of 0.6M sulphuric acid H_2SO_4 while applying a flux (1 ml/min). If the capacitive current does not reach more than 1 µA, the WE is not resistive and can be used for an experiment.

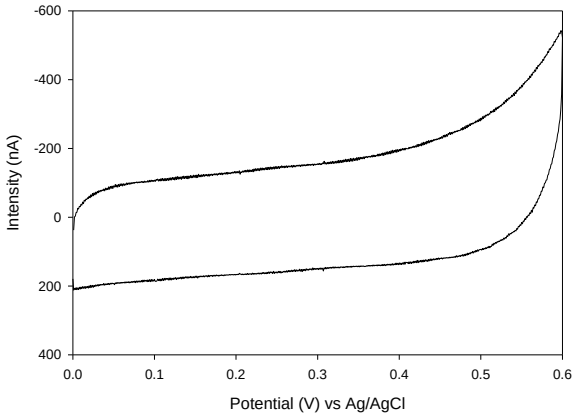

Figure 2.15: Example of a bare quartz crystal voltamperogram which does not display any oxidation or reduction peak.

In order to ensure that the potentials measured during the experiments are correct, the RE is tested. An aqueous solution of 10 mg/ml of tetrapotassium (II) hexacyanoferrate (K_4FeCN_6) at pH=7 prepared in 150 mM sodium nitrate $NaNO_3$ is injected in the electrochemical cell. A cyclic voltammetry between 0 and 600 mV at 50 mV/s is applied for 5 cycles. The obtained voltamperogram should display two peaks corresponding to the oxidation and reduction of the electrochemical probe (K_4FeCN_6). Figure 2.16 shows the obtained voltamperogram.

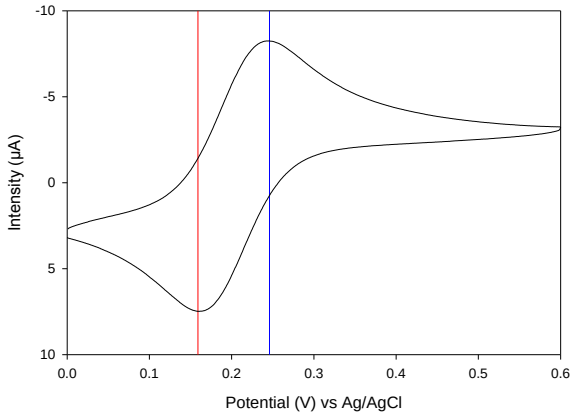

Figure 2.16: Voltamperogram of K_4FeCN_6 at 10 mg/ml in 150 mM $NaNO_3$ on QCM gold coated crystals. One oxidation and reduction peak are respectively observed at 250 and 160 mV.

These characteristic peaks should be situated at 160 and 250 mV to ensure that the RE is well calibrated. If these two peaks are shifted, i.e. separated by more than 100 mV or located in a lower or

higher potential range, the RE is unbalanced. If this is the case, it is necessary to clean it and to balance it. The electrode is first immersed in a sulphuric acid solution at 0.6 M during 20 min and then rinsed to dissolve the possible organic polluting species. After that, it is necessary to re-establish the equilibrium between the Ag^{+} silver ions in excess and the metallic silver by proceeding to an electrochemical setup. The goal of this step is to form again metallic silver and the silver chloride by applying a *pdiff* of -2 V between the *Ag/AgCl* electrode and the platinum one during few cycles of 15 seconds in presence of an aqueous solution of potassium chloride (KCl) at 3M until a stabilisation of the measured current is observed. The setup is the following: the *Ag/AgCl* electrode is connected to the "working electrode" output of the potentiostat while the platinum electrode is connected to the "reference electrode" and "counter electrode" output of the potentiostat.

Once it is confirmed that the two electrodes aren't contaminated, the electrochemical setup can be used for the experiment.

The internal temperature is then thermostated at 22°C by the mean of the QCM-D software. Prior to the injection of the polymer solutions, a measurement of the frequency shifts is taken during at least 15 min until stabilisation of the signal in contact with the buffer solution. This serves as a reference or baseline before any polymer adsorption. Once the baseline is done, a first cationic layer is adsorbed on the gold surface to promote the coating buildup. The monomers –or polymers- solution containing the functional molecules are then injected in the cell. Once the signal stabilizes, the electrochemical stimulus is applied. The mass and the visco-elastic properties of the molecular assembly is characterized in real time by the QCM-D.

2.2.3 Atomic Force Microscopy (AFM).

Developed in the early 80's by Binnig, Quate and Guerber to overcome the limitation of the scanning tunnelling microscope to conducting samples, the atomic force microscope (AFM) is a close field microscopy technique. This technique is based on the interactions between a thin tip and the surface of the sample to analyse.

The apparatus is constituted of a piezoelectric sample holder and of a thin tip fixed at the extremity of a lever of known stiffness constant k_c (cantilever) on top of which reflects a laser beam detected by a four quadrant photodiode. The sample is placed on a magnetized piezoelectric, called piezo tube, able to displace itself in the three dimension (x,y,z). Once the tip interacts with the surface, the cantilever deflects, hence changing the optical path of the laser and thus the position of the laser spot on the four quadrant photodiode. The spot displacement is transduced by a change in the electrical

tension proportional to the tip height variation. Figure 2.17 schematically shows the working principle of an AFM.

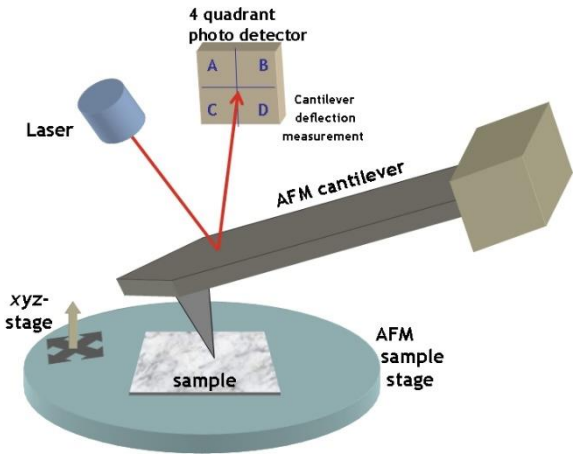

Figure 2.17: Schematic representation of an atomic force microscope: the sample is placed on a magnetized piezotube able to displace itself in the three dimensions (x,y,z). A laser beam is reflected on top of a thin tip attached to a lever of constant stiffness, also called cantilever, and is detected by a four quadrant detector. The cantilever is approached to the sample surface until it interacts with it and deflects. This deflection changes the optical path of the laser beam which is transduced by a change in the electrical tension detected by the photo detector proportionally to the tip deflection.

The force *F* exerted between the tip and the sample can be related to the vertical deflection *d* following the Hooke law:

$$F = k_c . d$$

The apparatus resolution is of the order of a tens of nanometer in the sample displacement plane (x,y) and of the order of the nanometer range on the z axis. When the tip approaches the surface, several interactions happen between the tip and the sample (e.g: Van der Waals, capillarity, electrostatic, chemical potential, solvation forces, etc…). These interactions are attractive at first and when the tip gets closer to the surface, they become repulsive. The force curve with respect to the distance between the tip and the sample then takes the form of a Lennard-Jones potential (Figure 2.18).

2.2.3.1 Contact mode and dynamic modes.

The AFM can be used in several modes (non-contact, intermittent contact, contact and force modulation) depending on the interaction –and hence the distance- between the tip and the sample. The choice of the mode is made by the experimenter depending on the sample type and interaction force tip-sample wanted. Figure 2.18 represents the several modes of the AFM with respect to the distance *d* between the tip and the sample.

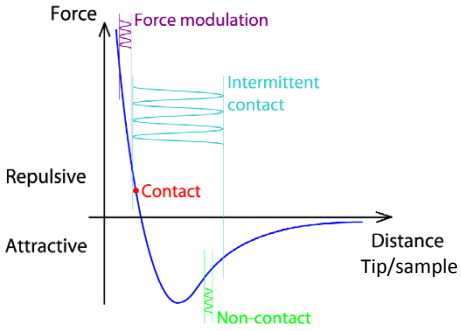

Figure 2.18: Schematic representation of the AFM modes with respect to the distance between the tip and the sample.

The non-contact mode is based on the attractive interactions between the tip and the surface. In this case, the tip is oscillating close to the surface without having a physical contact with it. This mode has the advantage not to destroy the sample by applying a stronger force than necessary. It is however the most difficult mode to use because the interaction tip-sample is weak and can be easily lost while imaging.

The intermittent contact mode, also called tapping, is one of the most widely used. It consists in oscillating the tip close to the surface. The lower point of this oscillation makes contact with the sample surface through a repulsive interaction. The lateral forces exerted on the cantilever are much lower than in contact mode considering the small amount of tip-sample contact time. This mode is essentially used to obtain high resolution on fragile sample.

In contact mode, the cantilever is in physical contact with the surface of the sample to analyse. In this mode, two possibilities exist: one called at “constant height” where the surface is scanned in the plane without changing the height of the cantilever (*d* varies) and one at “constant force” where the force between the sample and the tip is maintained constant (*d* constant). The second case is the most common one because imaging at constant height implies that the vertical deflection of the cantilever varies while scanning. This can result in damaging the sample and/or the tip when the sample surface is rough. In constant force imaging, the tip-sample distance is maintained constant which allows the tip to follow the surface topography while avoiding a partial destruction of the sample. This mode is particularly easy to use and is adapted to imaging rigid and robust samples.

The force modulation mode is a dynamic form of the contact mode and consist in oscillating the tip in contact with the sample. Unlike in the intermittent contact mode where the tip is in physical contact with the sample surface only at the lower point of its oscillating amplitude, in the force modulation mode the tip is constantly in physical contact with the surface during all its oscillation amplitude.

Figure 2.19 schematically represents these different modes.

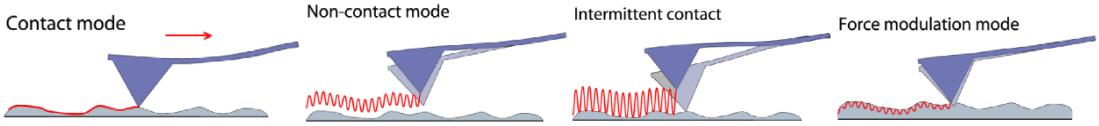

Figure 2.19 Schematic representation of the contact and dynamic modes of the AFM.

During this work, a Veeco Multimode Nanoscope IIIA microscope from Digital Instrument (Santa Barbara, USA) was used. All the images were taken in contact mode with silicon nitride Si_3N_4 cantilevers possessing a curvature radius of 20 to 40 nm and a stiffness constant of k_c= *0.6 N.m*$^{-1}$. The AFM images intend to show the surface state (homogeneity, roughness) of the coatings and their thickness by imaging the sample after scratching.

2.2.4 X-ray Photoelectron spectroscopy (XPS).

X-ray photoelectron spectroscopy (XPS) is an analytical technique which was developed in the 60's by Turner, Price and Siegbahn. Theoretical basics of XPS relies on the photoelectric effect discovered in 1906 by Einstein. A monochromatic source of X-rays with an energy *hv* is used to excite the atom's core electrons of the sample. The ejected electrons have a kinetic energy T given by:

$$T = h\nu - E_L - W$$

With T the kinetic energy of the emitted electron, E_L the corresponding binding energy and W the electron extraction work in the vacuum (tabulated value).

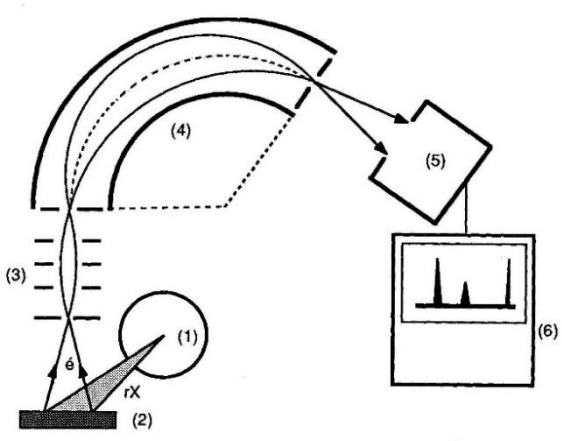

Figure 2.20: Schematic representation of the X-ray photospectroscopy: an x-ray source (1) illuminates the sample (2) and ejects core electrons which are focused by an electronic focusing system (3). The ejected electrons are then classified depending on their kinetic energies by the spectrometer (4) and detected by the electron detector (5) to give the spectrum (6).

The emitted electrons can be classified depending on their kinetic energy T with respect to the incoming energy *hv* (Figure 2.20). This gives access to the corresponding binding energy E_L for each electron. Since all the atomic orbital energies are classified and specific for each element (ex: N1s: 400 eV, C1s: 285 eV, O1s: 540 eV), it is possible to do an elementary analysis of the sample. However, since the emitted electrons are core electrons, this does not gives access to the oxidation states.

Given the weak free mean path of the incident and emitted rays, the whole measure must be done in a high vacuum of 10^{-2} torr for the irradiating chamber and 10^{-5} torr for the kinetic energy analyser. The penetration depth for organic samples is estimated to be of the order of 9 nm. XPS hence gives an insight of the chemical composition of the sample surface.

For this work, Thermo VG Scientific spectrometer equipped with an Al K_α (hv= 1486.6 eV) x-ray source at 225 W was used with a source/analyzer angle of 90°. The analysis is done in two times. A first low resolution spectrum is done with an energy of 50 eV in order to give a general atomic composition of the sample. Then, to distinguish the different component, high resolution spectrum based on atomic transition are performed with an energy of 20 eV. Spectra are represented as a function of the number of photoelectrons detected for a given binding energy. The signal is dependent on the number of analysed atoms. Data are treated with the Avantage V.2.26 and CasaXPS software.

2.2.5 Fluorescence microscopy.

The fluorescence process is the ability of a molecule to absorb a photon and to reemit another photon at a higher wavelength. When the fluorophore in a ground state (S_0) is submitted to a light excitation of energy hv_1, the fluorescent molecule goes to an excited state (S_1). At room temperature, the internal conversion leads to a partial loss of the absorbed energy by vibrational relaxation and the molecule is in an excited state at a lower energy (T_1). The relaxation of the molecule to its ground state (S_0) is associated to a photon emission at a lower energy hv_2 than the excitation one hv_1, i.e. at a higher wavelength (Stokes shift). Figure 2.21 schematically represent the fluorescence phenomenon (Jablonski diagram).

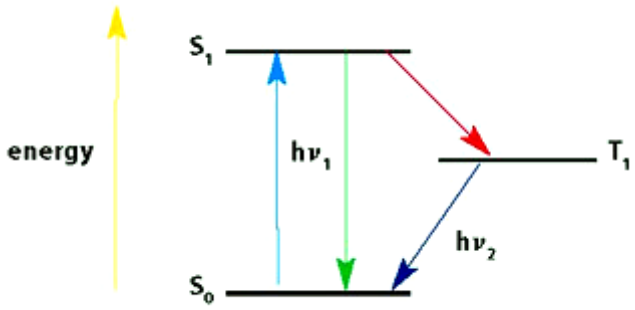

Figure 2.21: Jablonski diagram. The fluorescent molecule initially in its ground state S_0 absorb an incoming photon of energy hv_1 and goes to the excited state S_1. During relaxation, the molecule first lose energy by internal conversion due to vibrations and molecular chocks and reach a lower energy state T_1 and then undergoes an electronic transition from the excited T_1 state to its ground state. This transition from T_1 to S_0 release a photon with a lower energy than the excitation one, i.e. with a higher wavelength.

In fluorescence microscopy, a polychromatic light source is filtered through an excitation filter to provide only the excitation wavelength of the fluorophore. The monochromatic beam is directed towards the sample by means of a dichroic mirror and the beam is focalised through the objective. The specimen then gets excited by the excitation beam and produces the fluorescence photons at higher wavelength. The emitted fluorescence optical pathway goes through the objective first and passes the dichroic mirror to be filtered before it reaches the ocular and/or detector. Figure 2.22 schematically represents a fluorescence microscope.

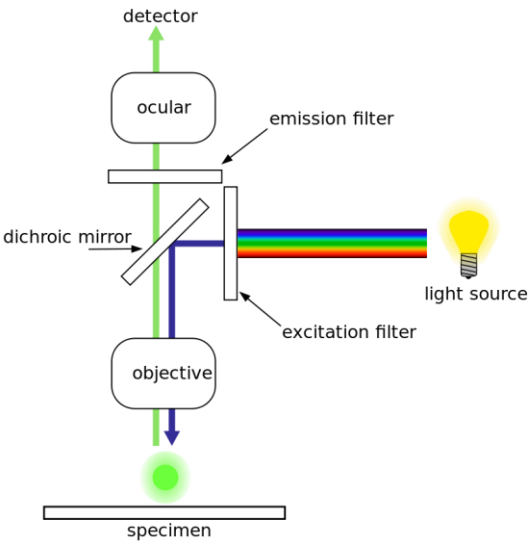

Figure 2.22 Schematic representation of a fluorescence microscope. The polychromatic light source is filtered through the excitation to provide a monochromatic light source corresponding to the excitation wavelength of the specimen. The excitation beam is directed towards the specimen by the mean of a dichroic mirror and is focalised by the objective. The excited specimen then produces fluorescence photons that passes through the objective and the dichroic mirror. The emitted fluorescence beam is then filtered by the emission filter until it reaches the ocular and/or detector.

For this work, an inverted Nikon Microphot-FXA (Japan) epi-fluorescence microscope equipped with a mercury lamp was used. The pictures were taken with a digital camera at a magnification of 10 and 40 times. The fluorescence images were colorized and analysed using the ImageJ software to remove background noise, enhance contrast and insert scale bars.

REFERENCES

Dähne, L., S. Leporatti, E. Donath and H. Möhwald (2001). "Fabrication of Micro Reaction Cages with Tailored Properties." Journal of the American Chemical Society **123**(23): 5431-5436.

Hummel, P. J. (2009). Single-Walled Carbon Nanotube Device Fabrication Using Spin Coating of Dispersions, ProQuest.

King Jr, W. H. (1964). "Piezoelectric Sorption Detector." Analytical Chemistry **36**(9): 1735-1739.

Liu, X. H., J. T. Zhang and D. M. Lynn (2008). "Polyelectrolyte Multilayers Fabricated from 'Charge-Shifting' Anionic Polymers: A New Approach to Controlled Film Disruption and the Release of Cationic Agents from Surfaces." Soft Matter **4**(8): 1688-1695.

Miomandre, F. (2011). Electrochimie Des Concepts Aux Applications. Paris, Dunod.

Voinova, M. V., M. Rodahl, M. Jonson and B. Kasemo (1999). "Viscoelastic Acoustic Response of Layered Polymer Films at Fluid-Solid Interfaces: Continuum Mechanics Approach." Physica Scripta **59**(5): 391-396.

CHAPTER 3: ELECTROCHEMICAL SURFACE INITIATED ATOM TRANSFER RADICAL POLYMERIZATION (ESI-ATRP)

3 ELECTROCHEMICAL SURFACE INITIATED ATOM TRANSFER RADICAL POLYMERIZATION (ESI-ATRP).

CONTENTS

Chapter 3: Electrochemical Surface Initiated Atom Transfer Radical Polymerization (eSI-ATRP)

3.1 GENERALITIES ON ATOM TRANSFER RADICAL POLYMERIZATION (ATRP) IN SOLUTION.

To palliate the problem of the low molecular weights and poor polydispersity index of polymers obtained by Free Radical Polymerization (FRP), a new approach consisting of controlling the radical polymerization emerged in the 90's. Control radical polymerization (CRP) techniques permit to obtain polymers of well-defined weights, structures and polydispersities. The three main CRP techniques are the Nitroxide Mediated Polymerization (NMP)(Hawker et al. 2001, Nicolas et al. 2013), the Reversible Addition-Fragmentation chain-Transfer (RAFT)(Chiefari et al. 1998) and the Atom Transfer Radical Polymerization (ATRP)(Kato et al. 1995, Matyjaszewski et al. 1995, Wang et al. 1995).

Among them, ATRP outstands due to its robustness and its tolerance towards many functional group (Matyjaszewski et al. 2001, Matyjaszewski 2011). ATRP is defined as a control or "living" radical polymerization because the main reason for the polymerization reaction to stop is due to a total conversion of the monomers, i.e. an absence of reactive species, and not to the termination of all the growing chains as it is the case for FRP. Thus, the adding of monomers would restart the polymerization reaction hence its denomination as "living" polymerization.

3.1.1 Classical ATRP (ATRP).

ATRP is a technique that was co-discovered by Matyjaszewski and Sawamoto in 1995 (Kato et al. 1995, Wang et al. 1995). It relies on the redox reaction between an initiator with a radically transferable atom or group and a catalyst complex comprising a transition metal in a lower oxidation state. The reaction is based on an equilibrium between a "dormant state" in which the transferable atom or group is on the initiator (no radicals) so that no polymerization occurs and a "living state" in which the transferable atom or group is on the complex thus creating the radical and polymerizing. The transition metal complex acts as a catalyst for the system to alternate between the "dormant" and the "living" state.

The reaction in which the transferable atom or group is taken from the initiator to the transition metal complex is called the "activation" reaction. Once the system undergoes this reaction, it creates a radical and the polymerization goes on. In ATRP, this radical is rapidly neutralized through the reaction on which the transferable atom or group is given back from the transition metal complex to the initiator. This reaction is called the "deactivation" reaction.

Figure 3.1 shows an ATRP process on which the initiator containing the transferable atom or group (R-X) reacts with the transition metal complex in a lower oxidation state (Mt^n/L, often Cu(I)Br) through

the activation reaction (k_{act}). The transferable atom or group (X, often Br) is transferred on the transition metal complex at a higher oxidation state ($Mt^{n+1}X/L$) thus creating the radicals (R°) that polymerize (k_p) with the monomers (M). The termination reactions (k_t) involving two radicals which couple (R-R) are greatly reduced due to the fact that most of the polymers are in the "dormant" state (R-X).

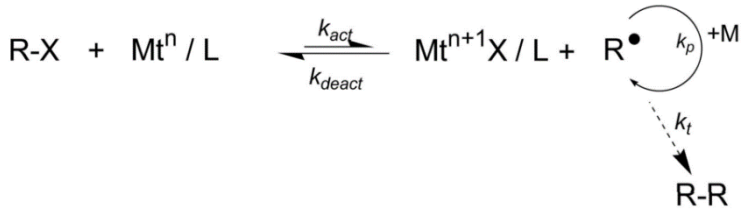

Figure 3.1 ATRP chemical pathway: the transferable atom or group (X) contained in the ATRP initiator (R-X) is transferred to the transition metal complex at a lower oxidation state (Mt^n/L) through the activation reaction (k_{act}). The radical is formed (R°) that polymerizes (k_p) with the monomers (M). The system is in the "living" state where the polymerization occurs. The oxidized transition metal complex containing the transferable atom or group ($Mt^{n+1}X/L$) reduces by transferring back the transferable atom or group (X) to the radical (R°) through the deactivation reaction (k_{deact}). This deactivation reaction is greatly favoured compared to the activation reaction ($k_{act}<<k_{deact}$) thus maintaining most of the polymer chains in the "dormant" state. The direct effect of this equilibrium is to reduce considerably the termination (k_t) reaction on which two radicals couples (R-R) (Matyjaszewski et al. 2006).

The whole ATRP process is controlled by the equilibrium between the activation and deactivation reactions (Kamigaito et al. 2001). The deactivation reaction must be favoured, i.e. $k_{act}<<k_{deact}$, so that most of the polymer chains are in the "dormant" state. In that case, the amount of radicals present in the solution is sufficiently low so that the termination reactions are almost suppressed and concerns only of the order of 1-10 % of the chains (Matyjaszewski 2011). The rate of polymerization for an ATRP process is given by:

$$R_p = k_p K_{eq}[M][RX]_0 \frac{[Cu^+]}{[Cu^{2+}]}$$

With R_p the rate of polymerization, k_p the propagation rate constant of polymerization, K_{eq} ($=k_{act}/k_{deact}$) the equilibrium constant, [M] the monomer concentration, [Cu^+] and [Cu^{2+}] the copper concentrations in the lower and higher oxidation state, respectively (de Vries et al. 2001).

From this equation, it appears that the polymerization rate is dependent on the ratio between the Cu(I) and the Cu(II) and not on their absolute concentration. For instance, if the concentration of copper (I) is too high compared to the concentration of copper (II), it means that most of the chains are in the living state (k_{act} favoured). This would then lead to many termination reactions between the

radicals and to the loss of the reaction control as in FRP. It is therefore of primary importance that the system contains more copper (II) than copper (I).

Investigation of the ATRP kinetic shows that there is a constant concentration of active radicals in the polymerization and a first-order kinetic with respect to the monomers. However, since the termination reactions are still present in low proportions, the concentration of copper (II) increases with time and a deviation from linearity is observed. Such kinetic behaviour is characterized by a typical linear variation of monomer conversion with time in semi-logarithmic coordinates. Figure 3.2 shows the monomer conversion over time in linear and semi-logarithmic coordinate, i.e. the variation in time of the monomer concentration $[M]_t$ with respect to the initial concentration of monomers $[M]_0$ ($[M]_0/[M]_t$).

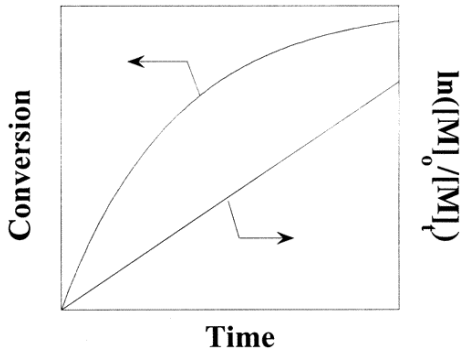

Figure 3.2 Schematic representation of the dependence of conversion on time in linear and semi-logarithmic coordinates. The monomer conversion is given by the initial concentration of monomers $[M]_0$ over the varying concentration of monomers during the polymerization $[M]_t$. Such graph is representative of a first order kinetic (Matyjaszewski et al. 2001).

The versatility of the technique and its tolerance toward many functional groups lead to the fabrication of polymers with well-defined topologies, composition and functionality. Figure 3.3 schematically shows the different compositions, topologies and functionalities that can be obtained by an ATRP process (Matyjaszewski et al. 2009). The compositions includes homo, block (Pitsikalis et al. 1998, Mecerreyes et al. 1999, Hadjichristidis et al. 2001, Davis et al. 2002, Lutz et al. 2003c), grafted (Pitsikalis et al. 1998, Börner et al. 2002), random (Davis et al. 2002), periodic (Lutz et al. 2003a, Lutz et al. 2003b) and gradient (Matyjaszewski et al. 2000) polymers. The topology can be varied to obtain linear, star (Matyjaszewski 2003, Li et al. 2004), brush (Beers et al. 1998, Pyun et al. 2003, Luzinov et al. 2004), (hyper)branched (Gaynor et al. 1996, Matyjaszewski et al. 1997a, Matyjaszewski et al. 1997b, Matyjaszewski et al. 1997c, Matyjaszewski et al. 1998b) and network polymers. The functionality of the formed polymers can be finely tuned to obtain side, end, site-specific functional polymers as well as telechelic and multifunctional polymers.

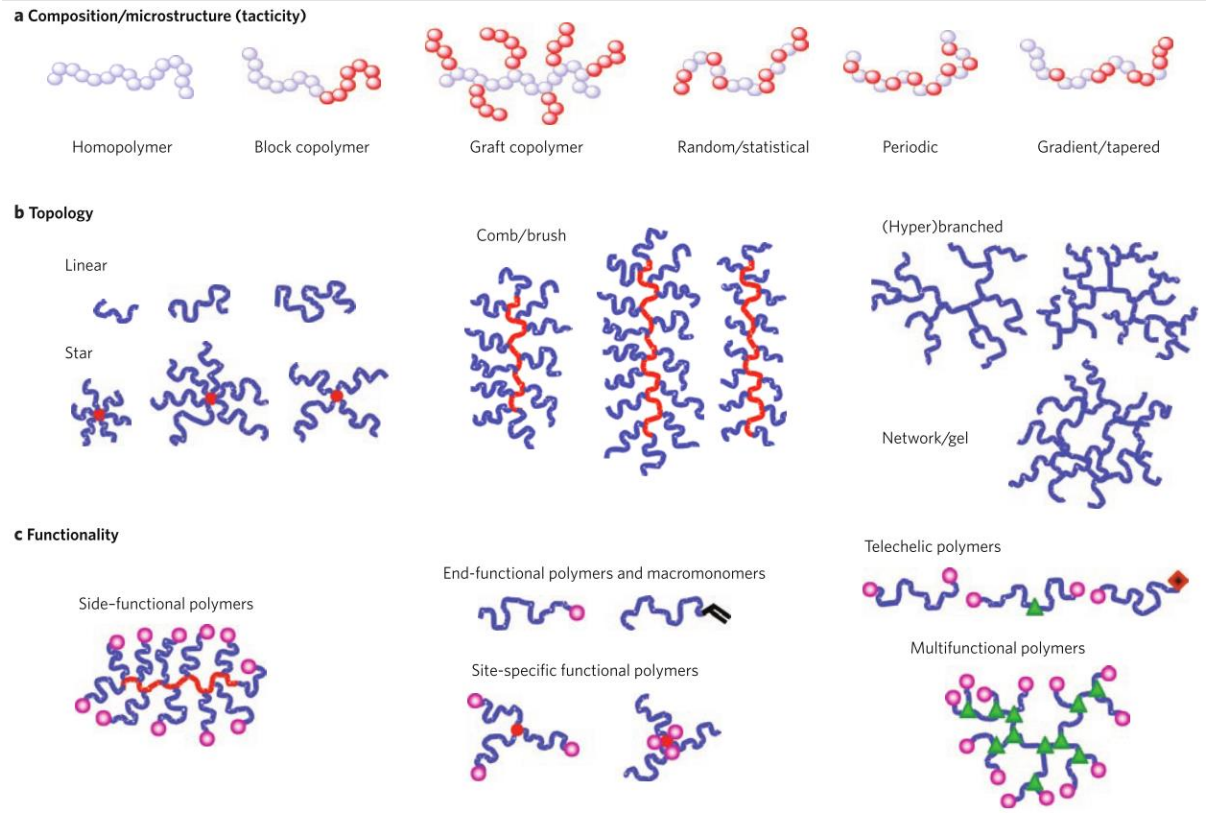

Figure 3.3 Schematic representation of the various polymer compositions, topologies and functionalities that can be obtained by ATRP. The composition includes homo, block, graft, random, periodic and gradient polymers. The topology can be tuned to be linear, star shaped, brush shaped, (hyper)branched or a network. The polymers can be multifunctional, telechelic or the functionality can be located on the side, at the end or on a specific site of the chain (Matyjaszewski et al. 2009).

These complex architectures allow for the formation of stimuli responsive polymers such as pH sensitive (Mao et al. 2005) or thermo-responsive ones (Liu et al. 2005, Lutz et al. 2006, Lutz 2008, Lutz 2011).

The high functionality of polymers obtained by ATRP can be of interest, for instance, in the biomaterial field to form polymer bioconjugates, drug delivery systems, diagnostic and imaging platforms, tissue engineering hydrogels and bioactive surfaces (Siegwart et al. 2012).

The ATRP process uses four essential components: a molecule with at least one transferable atom or group (R-X), a transition metal compound undergoing redox reactions (Mt^n), a ligand that complexes with the transition metal compound (L) to modify its solubility and activity and one or more radically (co)polymerizable monomers (M). Due to language difference, the process involving these four components has also been denominated as living radical polymerization mediated by transition metal complexes (LRP-MTM), metal catalysed living radical polymerization (MC-LRP), copper mediated living radical polymerization (CM-LRP), single electron transfer living radical polymerization (SET-LRP) and

outer sphere electron transfer metal catalysed polymerization (OSET-MCP). All these variations in the nomenclature require these same four components to work.

The transition metal complexes involved in the ATRP process are usually copper (I) but other complexes have also been used to successfully performed the reaction, e.g. nickel, molybdenum, chromium, rhenium, ruthenium, iron, rhodium, palladium (Matyjaszewski et al. 2001). In a classical ATRP process, a copper (I) salt is introduced at its lower oxidation state in a high concentration equivalent to the initiator concentration, typically around 1000 ppm (Matyjaszewski et al. 1998a). This causes a major issue since the transition metal complex can be easily oxidized to a higher oxidation state if oxidizing species such as the oxygen contained in air are present in the setup. The reaction must therefore be conducted under inert atmosphere which causes a complex handling of the polymerization. Such a high catalyst concentration also reduces industrial application due to catalyst cost and the need for its removal in the final solution.

3.1.2 Electrochemical ATRP (*e*ATRP).

One of the latest development in the field of ATRP polymerization which overcome these limitations relies on the use of electrochemistry instead of organic or inorganic reducing species to generate the ATRP catalyst from the transition metal complex at a higher oxidation state (Bortolamei et al. 2011, Magenau et al. 2011).

Figure 3.4 schematically shows the eATRP process on which a cathodic current is applied on the solution containing the oxidized transition metal catalyst (Cu^{II}-Br_2/Me_6TREN) to reduce it (Cu^{I}-Br/Me_6TREN). The ATRP catalyst formed (Cu^{I}Br/Me_6TREN) reacts with the ATRP initiator (P_n-X) to form the persistent radical (P_n°) that polymerizes (k_p) with the monomers (M) and the classical ATRP process takes place. Application of an anodic current oxidizes the ATRP catalyst and forces the system to stay in the dormant state.

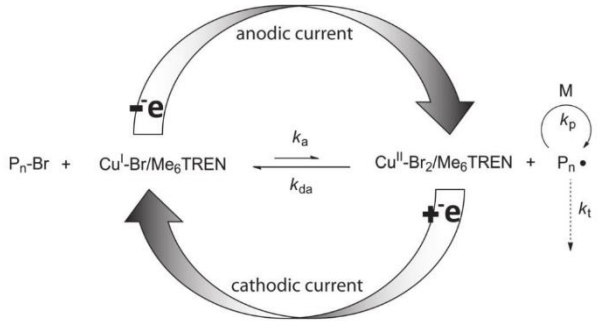

Figure 3.4 Schematic representation of eATRP: A cathodic current is applied on the oxidized transition metal complex (Cu^{II}-Br_2/Me_6TREN) to reduce it. The formed ATRP catalyst (Cu^I-Br/Me_6TREN) reacts with the ATRP initiator (P_n-Br) through the activation reaction (k_a). The persistent radical (P_n°) is formed that polymerize (k_p) with the monomers (M) and the classical ATRP process takes place. Application of an anodic current oxidize the transition metal complex forcing the system to stay in the dormant state (Magenau et al. 2011).

The eATRP was successfully conducted both in organic and aqueous media with a few ppm of copper. (Bortolamei et al. 2011, Magenau et al. 2011, Lou et al. 2012) (Matyjaszewski 2012).

In aqueous eATRP, the copper (II) complex was introduced in the same concentration than the ATRP initiator containing the transferable atom. The transition metal ligand was carefully chosen to avoid the copper (I) disproportionation in water (cf. 3.1.3) and the monomers were chosen to be soluble in water. Copper cyclic voltammetry investigation revealed that the copper (I) formed quickly reacted with the initiator leading to a high polymerization rate and thus a poor control of the reaction. Analysis of the reaction rate with respect to the potential difference applied in the electrochemical cell confirmed that the reaction could be controlled by applying a potential corresponding to a slow and steady formation of copper (I). In that case, a linearity of the first-order kinetic plot (cf. Figure 3.2) was observed confirming the control of the $[Cu^{2+}]/[Cu^{+}]$ ratio and thus of the ATRP process. Adding a large excess of halide ions in the solution to promote the deactivator, i.e. the $X\text{-}Cu^{II}L^{+}$, formation also increased the ATRP process control leading to lower polydispersities.

Such a technique presents several advantages compared to the classical ATRP reaction: the transition metal complex is introduced in its higher oxidation state at a lower concentration and the setup can be realized in presence of air. Indeed, the application of the reduction potential will reduce the transition metal complex and form the ATRP catalyst in situ. This catalyst will react first with oxygen from air and scavenge it completely. Once the setup is free of air and other oxidizing agents, the continuously regenerated ATRP catalyst will start the ATRP process. The continuous regeneration of the transition metal complex at lower oxidation state allows for its introduction in low quantities thus avoiding the expensive and time-costly catalyst removal step.

3.1.3 The special case of ATRP in aqueous solvent.

The use of ATRP in water represents a considerable interest since it is the cheapest and more environmental friendly solvent with a high thermal capacity. It is then an attractive medium for exothermic radical copolymerization and "green" ATRP (Tsarevsky et al. 2007c). Early works relied on aqueous heterogeneous media such as suspensions, dispersions, emulsions, miniemulsions and microemulsions to conduct the ATRP process (Qiu et al. 2001, Cunningham 2002, Sawamoto et al. 2002). Indeed, water is one of the worst solvent in which an ATRP process can be conducted since several complex equilibriums compete with ATRP (Tsarevsky et al. 2007b).

Figure 3.5 schematically represents an ATRP process in an aqueous solvent: the classical ATRP process where the activator ($Cu^{I}L_m$) reacts with the ATRP initiator (R-X) through the activation first step (k_{act}) to form the persistent radical (R°) is in presence of side reactions. Water can cause:

- In green: disproportionation (K^*_{disp}) of the activator ($Cu^{I}L_m$) to form copper (II) complexes ($Cu^{II}L_m$) and metallic copper (Cu^0) which releases the ligands (m L).
- In red: hydrolysis of the initiator or dormant chain (R-X) with water (H_2O)
- In blue: dissociation of the halide ligand (K_X) from the copper (II) based deactivator ($Cu^{II}L_mX$).
- In yellow: complexation of the dissociated complex ($K_{Cu,aq}$) or halide ($K_{X,aq,j}$) with the solvent or polar monomer.

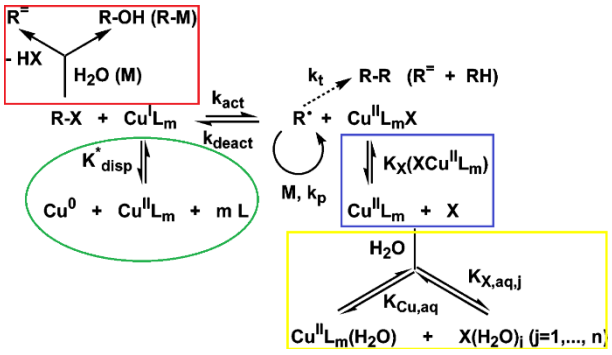

Figure 3.5 Schematic representation of an aqueous ATRP experiment. The classical ATRP process where the activator ($Cu^{I}L_m$) reacts with the ATRP initiator (R-X) through the activation reaction (k_{act}) to form the persistent radical (R°) that polymerize (k_p) with the monomers (M) happens in the presence of side reaction. These side reaction includes the disproportionation (K^*_{disp}) of the activator ($Cu^{I}L_m$) into higher oxidation state complex ($Cu^{II}L_m$) and zerovalent metal (Cu^0) releasing the ligand (m L) (in green); the hydrolysis of the initiator or dormant chain (R-X) (in red); the dissociation (K_X) of the halide ligand (X) from the copper (II) based deactivator ($Cu^{II}L_mX$) (in blue) and the subsequent complexation of the dissociated complex ($K_{Cu,aq}$) and halide ($K_{X,aq,j}$) with the solvent (H_2O) (Tsarevsky et al. 2007c).

The hydrolysis of the initiator or dormant chain and the dissociation of the halide from the transition metal complex greatly increase the polymerization rate (R_p) due to better solvation of the copper-based ATRP catalyst and to the partial dissociation of the deactivator ($XCu^{II}L_m$). This favouring of the activation reaction due to the modification of the [Cu(I)]/[Cu(II)] ratio increases the concentration of active radicals and thus the termination reactions (k_t). The ATRP process in water provides then a poor or a total loss of control of the polymerization.

The choice of the ligand in aqueous ATRP is a crucial point since it should both present a high activity towards the activation step and decrease catalyst disproportionation. Stability constant of the copper (II) and copper (I) complexes with the chosen ligand are respectively noted β^{II} and β^{I}. Both β^{II} and β^{I} should be large to prevent the catalyst deactivation through competitive coordination and a high β^{II}/β^{I} ratio is then needed for high catalytic activity. On the other hand, the ligand significantly affects the disproportionation equilibrium of copper (I) (without ligand = K_{disp}) according to the equation:

$$K_{disp}^{*} \approx \frac{\beta^{II}}{(\beta^{I})^{2}[L]} K_{disp}$$

Therefore, for ligand forming 1:1 complexes with copper ions, the activity of the catalyst is proportional to the β^{II}/β^{I} ratio whereas the tendency of the copper (I) to disproportionate in aqueous solvent is proportional to the $\beta^{II}/(\beta^{I})^{2}[L]$ ratio (Tsarevsky et al. 2007a, Tsarevsky et al. 2007b). Disproportionation equilibrium constant of non-complexed copper (I) in water can be as large as $K_{disp}=10^{6}$.

Thus, a map can be constructed to select a ligand for aqueous ATRP that forms an active complex yet remains stable towards disproportionation. Figure 3.6 shows various copper (I) ligands with their respective activity and tendency to disproportionate copper (I) in water. Higher β^{II}/β^{I} ratio (higher ordinate) describe higher activities whereas lower $\beta^{II}/(\beta^{I})^{2}[L]$ ratio (lower abscissa) describe greater stabilisation of copper (I) toward disproportionation. Suitable copper (I) ligands to conduct ATRP in water are thus in the top left corner of this graph.

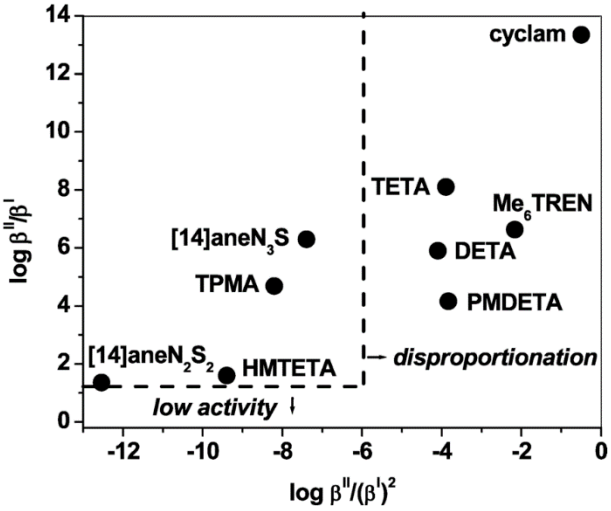

Figure 3.6 Effect of several copper (I) ligand on the activity and stabilization of copper (I) in aqueous solvent. Higher β^{II}/β^{I} ratio (higher ordinate) describe higher activities whereas lower $\beta^{II}/(\beta^{I})^2[L]$ ratio (lower abscissa) describe greater stabilisation of copper (I) toward disproportionation. Suited ligand to conduct ATRP experiment in water are located on the top left corner of the graph (dashed line) (Tsarevsky et al. 2007a).

By carefully considering the side reactions described above and the choice of the copper (I) ligand in aqueous solvent, it is possible to conduct ATRP experiments in water with a good control of the process (Qiu et al. 2001, Robinson et al. 2001, Cunningham 2002, Perrier et al. 2002, Sawamoto et al. 2002, Tsarevsky et al. 2004, Tsarevsky et al. 2006, Tsarevsky et al. 2007a, Tsarevsky et al. 2007b, Mueller et al. 2008, Braunecker et al. 2009, Millard et al. 2009, Averick et al. 2012, Konkolewicz et al. 2012, Simakova et al. 2012, Cao et al. 2013).

3.2 SURFACE INITIATED-ATRP (SI-ATRP).

3.2.1 The "grafting from" approach.

Initiating an ATRP process from surfaces represents a real interest for surface functionalization with stimuli responsive polymer materials (Stuart et al. 2010). Indeed, surface initiated ATRP (SI-ATRP) allows the buildup of high density grafted polymer brushes with well-defined compositions, topologies and functionalities (Barbey et al. 2009, Lee et al. 2010).

Unlike the classical "grafting to" approach on which already formed polymers are grafted to the surfaces, SI-ATRP allows the polymers to be "grafted from" the surfaces. Figure 3.7 schematically represents the difference between the "grafting to" and the "grafting from" approach (Edmondson et al. 2009). The "grafting to" approach (on top) consists in grafting an already formed polymer onto the surface. Such grafting method gives a low grafting density since the polymer chains adopt a

"mushroom" conformation on the surface. Moreover, the grafting can be inhomogeneous due to steric interactions between the chains. The "grating from" approach relies on the deposition of an ATRP initiator layer on the surface prior to the polymer brushes buildup. The ATRP initiator layer is usually formed of either a self-assembled monolayer (SAM) of small molecules containing the initiator (middle) or by depositing a polymeric macroinitiator on the surface (bottom). The polymer brushes are then constructed by an ATRP process involving the SAM or macroinitator thus giving a high density of grafted polymers with well-defined composition, structure and properties.

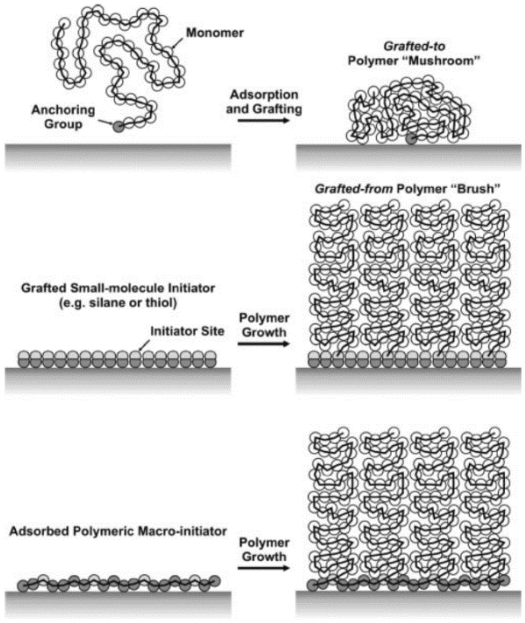

Figure 3.7 Schematic representation of the grafting to and grafting from approach. The grafting to approach (top) relies on the grafting of formed polymers on the surface. These polymer chains adopt a "mushroom" conformation thus leading to low density and possibly inhomogeneous grafting due to steric interactions. The grafting from approach uses an ATRP initiator layer that is deposited prior to the brushes buildup. The ATRP initiator layer can be deposited by the mean of a small molecule SAM bearing the initiator (middle) or by the adsorption of a polymeric macroinitiator (bottom). The polymer brushes are then polymerized from the surface by an ATRP process thus leading to the formation of a dense polymer layer with well-defined structure and properties (Edmondson et al. 2009).

In SI-ATRP, a layer of ATRP initiator is deposited on the surface and the substrate is put into contact with the monomer solution containing the transition metal complex thus allowing the ATRP process to start. Figure 3.8 schematically shows an SI-ATRP process in which an ATRP initiator (red diamonds) is deposited on a substrate (in yellow). In presence of the ATRP activator and monomers (blue circles), the ATRP process is initiated and the polymer brushes start polymerizing. As in an ATRP process, the chain end is successively activated (reaction 1) to form the persistent radical (red dot) that polymerizes (reaction 2) and then deactivates (reaction 3). The activation and deactivation is made through the respective transfer and back transfer of the atom or group (X) onto the transition metal catalyst.

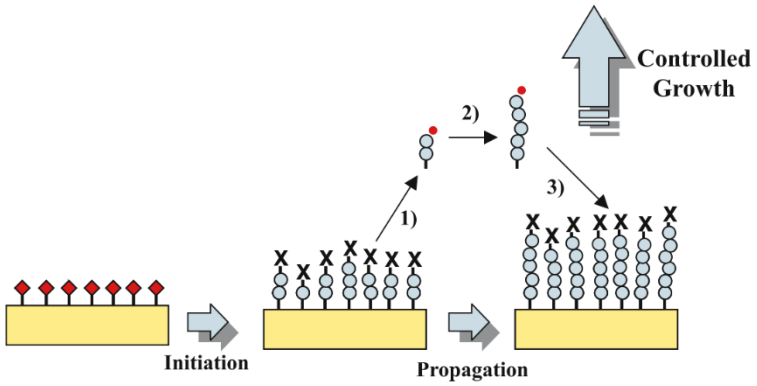

Figure 3.8 Schematic representation of a SI-ATRP concept. An ATRP initiator layer (red diamonds) is deposited on top of the surface (yellow rectangle). In presence of the monomers (blue circles) and ATRP activator, the ATRP process is initiated. As in a classical ATRP process, the chain end is successively activated (reaction 1) to form the propagating radical (red dot) that polymerize (reaction 2) and then deactivated (reaction 3). The activation and deactivation respectively occurs by the transfer and back transfer of the atom or group (X) onto the transition metal catalyst (Tsujii et al. 2006).

Among the ATRP initiator layers that can be deposited on a surface, polyelectrolytic macroinitiators represent a great interest since they can be easily adsorbed by electrostatic interactions onto the surface (Edmondson et al. 2007). Furthermore, the initiator density on the surface can be enhanced by depositing various layers of polyelectrolytes macroinitiators in a layer-by-layer construction (Edmondson et al. 2008).

The conformation of molecular brushes built by SI-ATRP is particularly interesting since it is governed by side chains separated by a distance much smaller than their unperturbed dimensions. This then leads to significant monomer congestion and entropically unfavourable extension of both the backbone and side chains.

The polymeric brush layer can thus be used to form stimuli responsive surfaces such as temperature, pH, ionic strength, magnetic, solvent, light or mechanically responsive ones (Yahiro et al. 2007, Chen et al. 2010, Lee et al. 2010). The mechanisms and driving forces for the conformational variation in response to external stimuli are unique for molecular brushes since they can be restricted to a single molecule.

Surface properties such as its wettability, biocompatibility, chemical and mechanical stability can also be modified by the SI-ATRP buildup of polymeric brushes (Barbey et al. 2009, Król et al. 2014).

3.2.2 Structures of SI-ATRP brushes.

The polymer brushes built by SI-ATRP can adopt complex architectures. Figure 3.9 shows the different brushes structures and compositions that can be obtained by SI-ATRP: block copolymers, random

copolymers, cross-linked polymers, free standing polymers, hyperbranched polymers, highly branched polymers, Y-shaped binary mixed polymers, standard binary mixed polymers, molecular weight gradient polymers, grafting density gradient polymers and chemical composition gradient polymers.

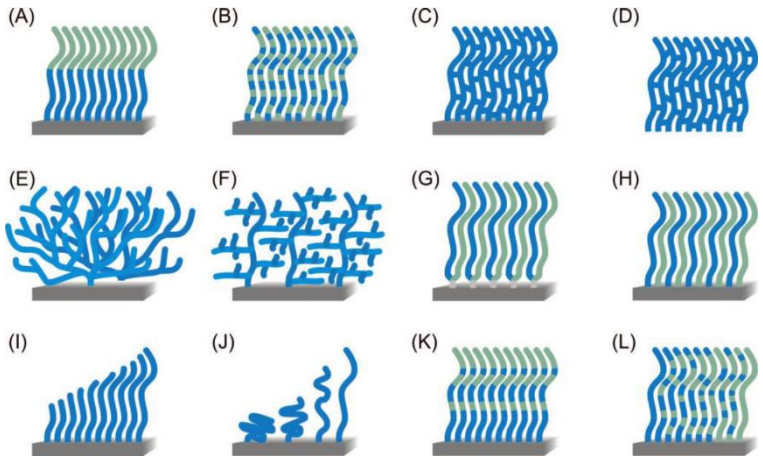

Figure 3.9 Overview of different polymer brushes architecture obtained by SI-ATRP: block copolymer brushes (a), random copolymer brushes (b), cross-linked polymer brushes (c), free-standing polymer brushes (d), hyperbranched polymer brushes (e), highly branched polymer brushes (f), Y-shaped binary mixed polymer brushes (g), standard binary mixed polymer brushes (h), molecular weight gradient polymer brushes (i), grafting density gradient polymer brushes (j), chemical composition gradient polymer brushes (k, l) (Barbey et al. 2009).

All these complex architectures show the versatility of the ATRP process on surfaces and highlight the interest of the "grafting from" method compared to the "grafting to" approach where such structures were impossible to obtain.

3.2.3 Surface topology and applications.

The SI-ATRP process can be initiated from surfaces with various topologies including flat surfaces and spherical particles on which the ATRP initiator is deposited. Figure 3.10 schematically represents the buildup of polymer brushes from flat (left) and spherical (right) surfaces.

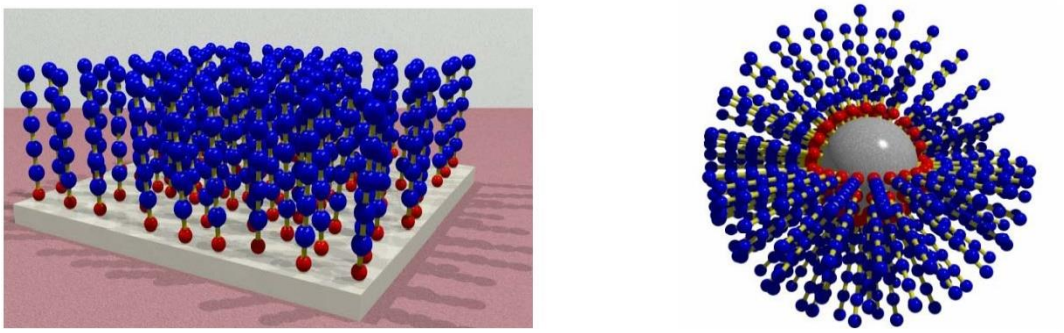

Figure 3.10 Polymer brushes buildup by SI-ATRP from flat (left) and spherical (right) surfaces.

On spherical surfaces, SI-ATRP can be performed to buildup polymer brushes on organic or inorganic particles. In the case of organic particles, such coating can be used for example to modify their hydrophobicity (Jonsson et al. 2009).

In the case of inorganic particles, SI-ATRP brushes form hybrid materials with inorganic core and organic shell (Matyjaszewski et al. 2009). The inorganic core may be chosen for its interesting magnetic, optical, electric, mechanical or catalytic properties (Pyun et al. 2001). A synergy of both the organic shell and inorganic core allows the creation of hybrid materials with predefined structures and performances with notable applications in biohybrid polymer capsules (van Dongen et al. 2009).

The inorganic core can also be dissolved once the SI-ATRP polymer shell has been formed and then serve as a template to obtain organic hollow spheres (Mandal et al. 2000). In that sense, inorganic dissolvable framework have also been used to create porous polymer structures with high specific areas which can be used as gas storage, separation material, encapsulation agent for controlled drug release, catalyst, catalyst support, sensor, precursor for nanostructured carbon material, biomolecular immobilization and cell scaffold, low dielectric constant material, photonic band gap material, filtration/separation membrane, proton exchange membrane, template for structure replication, mask for nanopatterning or lithography, packing material in chromatography, electrode material for energy storage, antireflecting coatings and many other applications (Wu et al. 2012).

On flat surfaces, SI-ATRP has been performed to build polymer brushes on several different inorganic substrates such as silicon wafer, gold, silica (Kamigaito et al. 2001). The tailored surface properties permit to obtain, among others, stimuli responsive (Lee et al. 2010), bioactive (Xu et al. 2009), antifouling, antibacterial (Król et al. 2014), cell adhesive, protein binding (Barbey et al. 2009), transductive and environmental sensing surfaces(Chen et al. 2010).

The polymer brushes buildup can be spatially controlled by patterning the ATRP initiator deposition on the substrate. Various patterning methods such as micro-contact imprinting or photolithography have been described to control the ATRP initiator deposition and thus spatially control the polymer brushes buildup. This approach presents an interest in providing locally different properties such as stimuli responsiveness on the inorganic substrate (Barbey et al. 2009, Olivier et al. 2012).

3.3 SCOPE OF THE STUDY.

As mentioned in the chapter 1, competitive papers were published on the first project of my PhD, namely, the control chain buildup localized on the surface through an electrochemical Surface

Initiated Atom Transfer Radical Polymerization (*e*SI-ATRP). In this project, the electrochemical stimulus would allow obtaining an ATRP catalyst gradient, namely copper (I) complexes, from a surface containing an ATRP polymeric macroinitiator. In presence of monomers, polymer brushes buildup by ATRP will be triggered. The obtained brushes should possess a well-defined structure and polydispersity with potential applications in the field of biomaterials (Badi et al. 2009, Barbey et al. 2009, Stuart et al. 2010, Siegwart et al. 2012). Figure 3.11 schematically shows the original goal of the project, namely developing *e*SI-ATRP.

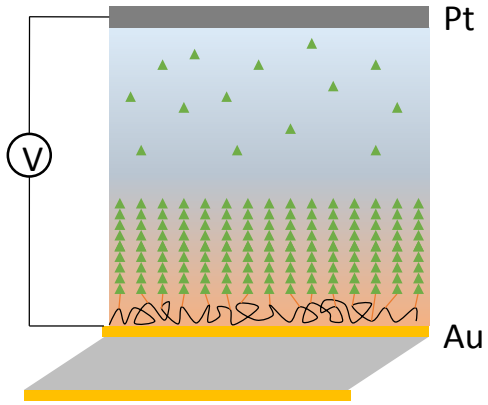

Figure 3.11 Schematic representation of the eSI-ATRP: polymer brushes are obtained by ATRP on a conducting substrate on which a polymeric macro-initiator is adsorbed. The reaction is meant possible by the catalyst gradient electrochemically generated from the surface (morphogen). Triangles represent the monomers and the Cu(I) gradient is represented by the orange gradient.

The materials used during our experiments will be presented in section 3.4 as well as the experimental parameters. Section 3.5.1 present the electrochemical analysis of three copper (II) salts to determine the best suited one for conducting eSI-ATRP. We will demonstrate the surface localized polymerization of a methacrylate monomer by applying a cyclic voltammetry (3.5.1.4).

The control experiments are presented in the section 3.5.2 while the influence of various parameters on the buildup were investigated in section 3.5.3. In the last section 3.6 we will conclude over this project. Finally, section 3.7 will describe the competitive works on eSI-ATRP.

3.4 MATERIALS.

3.4.1 Choice of the monomers.

To perform ATRP in water, the choice of the monomers is of primary importance since most of them are not water soluble. Oligo(ethyleneglycol) methacrylates (OEGMAs) were chosen as model monomers since they are both water soluble and well described in the literature (Lutz et al. 2006, Badi et al. 2009, Bortolamei et al. 2011). Figure 3.12 shows the chemical structure of the three OEGMAs monomers used.

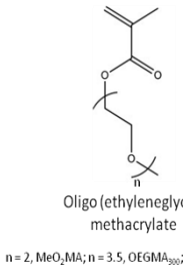

Figure 3.12 Chemical representation of the monomers used; oligo(ethyleneglycol) methacrylates with different poly(ethylene glycol) side chains of weight 188 (n=2, MeO_2MA), 300 (n=3.5, $OEGMA_{300}$) and 475 g.mol^{-1} (n=8.5, $OEGMA_{475}$).

3.4.2 Choice of the initiator.

The variety of ATRP initiators is quite wide in the literature and one has to carefully determine the adequate initiator before conducting a polymerization experiment. The choice of the initiator depends on the solvent used and on its activity. Figure 3.13 shows a non-exhaustive list of initiators with their respective activity, i.e. their influence on the ATRP process kinetic (R_p), at 35 °C in acetonitrile.

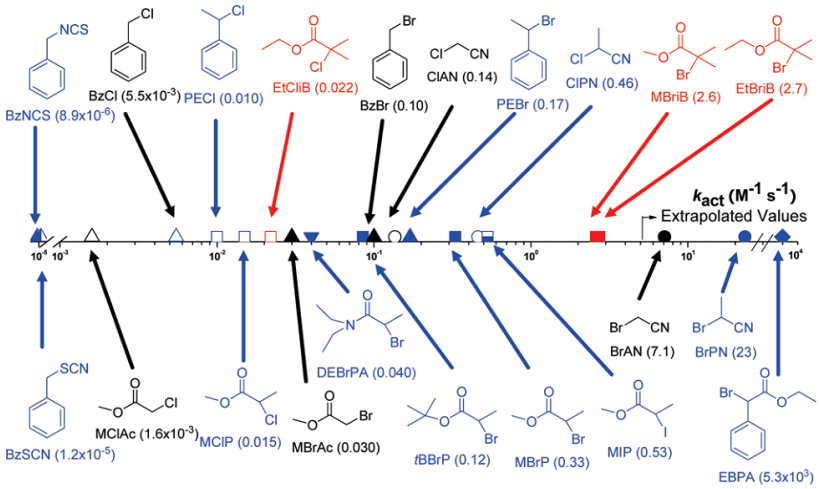

Figure 3.13 Table of the common initiators used in ATRP with their respective activity in acetonitrile at 35°C (Tang et al. 2007).

From Figure 3.13 one can notice that tertiary bromoesters are more active than secondary and primary ones. This general rule also applies in aqueous solvent. The choice of a tertiary bromoester was then logical since its strong activity would increase the overall ATRP kinetics.

In the case of SI-ATRP, it is possible to graft the initiator onto a polymer or a polyelectrolyte and thus to form a macro-initiator (Edmondson et al. 2007, Edmondson et al. 2008, Edmondson et al. 2009).The macro-initiator presented in Figure 3.14 was used in our experiments (synthesis: Dr. Loïc Jierry).

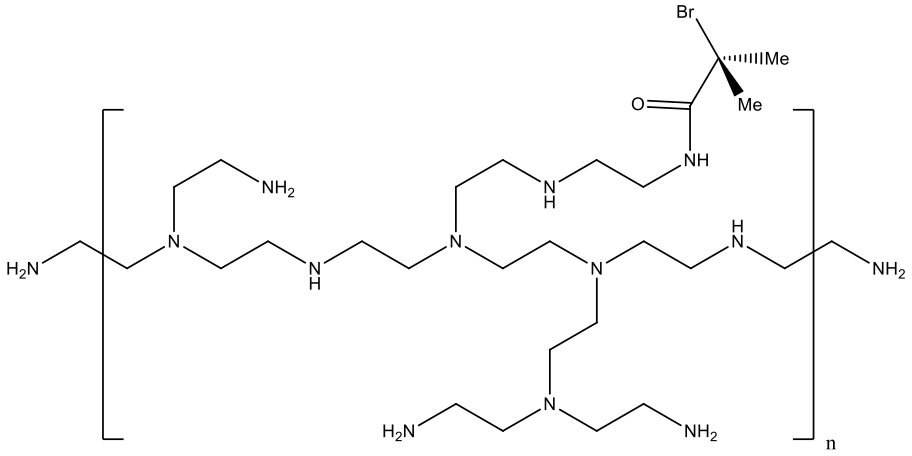

Figure 3.14 Chemical structure of the used initiator: poly(ethylene imine) with grafted bromoisobutyramide (PEI-Br), 20% of grafting determined by ^{1}H NMR.

PEI was chosen to immobilize the ATRP initiator since it is a positively charged polyelectrolyte that can be adsorbed on the gold working electrode surface by electrostatic interaction.

PEI-Br solutions were prepared at a concentration of 1 mg/ml in a solution of 150 mM $NaNO_3$/ EtOH (9:1) at room temperature without adjusting the pH. This solution was filtered through a 0.2 µm pore filter.

3.4.3 Choice of the ligand and copper salt.

Similarly to the initiators, many copper ligands can be used for ATRP. The choice is determined by the solvent and by the chemical function of the monomer used. The section 3.1.3 discussed the influence of the copper ligand towards the activity of the transition metal complex with respect to its ability to reduce disproportionation in aqueous solvent. Figure 3.15 shows some of the common ATRP ligands with their activities at 35°C in acetonitrile.

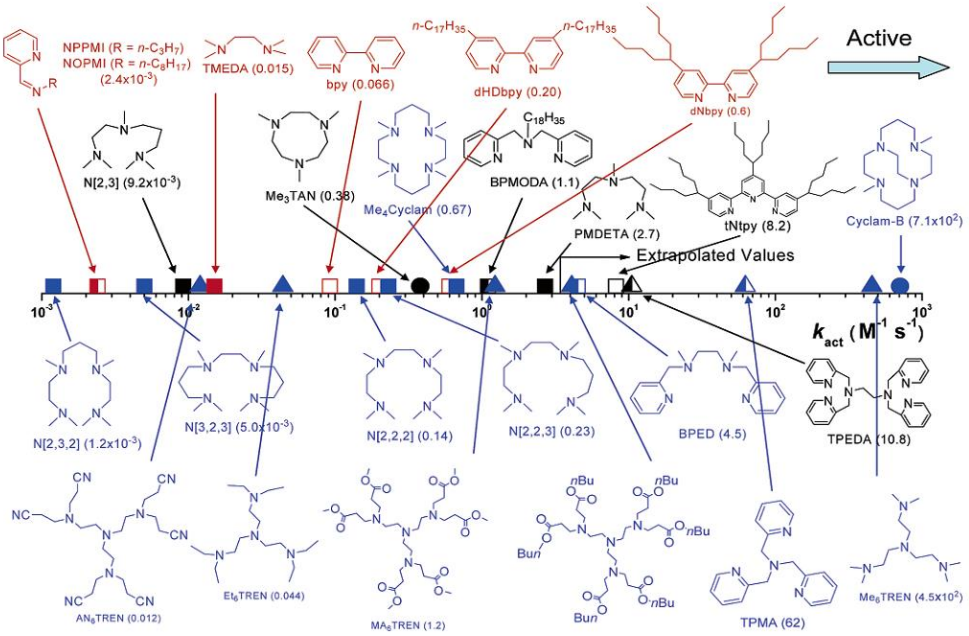

Figure 3.15 Common ligands used in ATRP with their respective activities at 35°C in acetonitrile.(Tang et al. 2006)

From the literature, the tris(2-pyridylmethyl)amine (TPMA) ligand was selected since it is commercially available and known to be water soluble, with a high activity, a low disproportionation constant in water and is suitable to conduct ATRP experiments on methacrylates (Bortolamei et al. 2011). The ligand has always been introduced at the same concentration than the copper salts.

Three copper salts were studied: $CuSO_4.5\ H_2O$, $Cu(CF_3SO_3)_2$ and $CuBr_2$.

The solutions were prepared at a concentration of 20 mM with a pH of 3.5 for cyclic voltammetry experiments in presence of the TPMA ligand at 20 mM (3.5.1.1). For polymerization experiments, the concentration was fixed at 1.6 mM and the pH was adjusted at 3.5.

3.4.4 Summary of the parameters.

Table 1 summarize the monomers, copper salts and ligand used in our eSI-ATRP experiments.

		Concentration (CV experiments)	Concentration (buildup experiments)
Monomers	$OEGMA_{475}$	--	(40 % in vol.)
Copper salts	$CuSO_4.5\ H_2O$, $Cu(CF_3SO_3)_2$ and $CuBr_2$	20 mM	1.6 mM
Ligand	TPMA	20 mM	1.6 mM

Table 1 Summary of the experimental parameters used for CV and eSI-ATRP experiments.

3.5 RESULTS AND DISCUSSION.

3.5.1 Build-up protocol.

3.5.1.1 Electrochemical study of the copper salts.

As mentioned in the section 3.1.1, the ATRP kinetics is controlled by the Cu(I)L/X-Cu(II)L ratio, i.e. the activator/deactivator ratio. To be able to control the eSI-ATRP, the electrochemical properties of the Cu(II) salts were studied in the presence of the TPMA ligand.

To determine the potential range at which the Cu(I) complex is formed, several electrochemistry experiments were performed on different copper salts in presence of the TPMA ligand ($CuSO_4.5\ H_2O$, $Cu(CF_3SO_3)_2$ and $CuBr_2$). The idea was to both determine the potential at which Cu(I) complex forms and also to choose the most suited copper salt with respect to its solubility and its electrochemical response.

In electrochemistry, Cu(I) catalyst can be generated at high concentrations on the surface of the working electrode, i.e. at the surface on which we would like to build the polymer brushes. But, when one takes a look at the ATRP process (Figure 3.1), it appears that the deactivation reaction involving the Cu(II) ions must be favored compared to the activation reaction involving Cu(I). This means that it is necessary to find a way to favor the Cu(II) deactivator complex over Cu(I) complex at this interface in order to slow down the polymerization reaction and therefore allow a better control of the polymer-brush growth.

3.5.1.1.1 Copper (II) Bromide: $CuBr_2$.

Copper (II) bromide seems to be an appropriate copper salt candidate for *e*SI-ATRP since the presence of bromide in this salt will indirectly favor the deactivation reaction in the ATRP process by favoring the formation of the deactivator ($X\text{-}Cu^{II}L$). As mentioned earlier in section 3.1.3, the overall ATRP kinetic is much higher in water than in other solvent due to side reactions resulting in a loss of the polymerization control. Among these side reactions, the dissociation of the halide from the deactivator ($X\text{-}Cu^{II}L$) cause a shift in the Cu(I)L/X-Cu(II)L ratio thus contributing to the loss of polymerization control. The introduction of bromide in the solution should favour the formation of the deactivator thus maintaining a high deactivator concentration and a low Cu(I)L/X-Cu(II)L ratio resulting in an increase of the reaction control.

Figure 3.16 shows the CV measurement of $CuBr_2$ obtained with the TPMA ligand. The CV was done between -600 mV and +300 mV at 10 mV/s on an aqueous $CuBr_2$ solution at 20 mM, pH = 3.5 with TPMA at the same concentration.

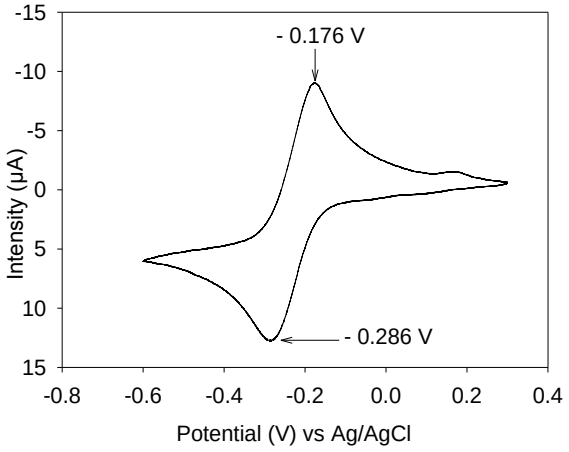

Figure 3.16 Measurement of a $CuBr_2$ cyclic voltammogram at 20 mM in presence of TPMA at 20 mM, pH = 3.5. The cyclic voltammogram shows an oxidation and reduction peak at respectively -0.176 and -0.286 V vs Ag/AgCl.

This cyclic voltammogram is quite simple in the presence of the TPMA ligand: only one oxidation and one reduction peaks at respectively -0.176 V and -0.286 V vs Ag/AgCl are observed. The reduction peak at -0.286 V can be attributed to the reduction of Cu(II) into Cu(0) while the oxidation peak at -0.176 V can be attributed to the oxidation of Cu(0) to Cu(II).

However, even if $CuBr_2$ appears to be a good copper salt candidate for eSI-ATRP, copper (I) bromide is not well soluble in water (Li et al. 2008). This is a major issue since it is the catalyst of the ATRP process.

Therefore, EC-QCM-D experiments were conducted by applying a ramp of reducing potentials from 0 to -350 mV by steps of 50 mV during five minutes on a $CuBr_2$ solution containing the TPMA ligand each at 1.6 mM followed by the application of +600 mV (Figure 3.17). The purpose of these experiments was to check if a mass deposit occurs on the working electrode when applying the reducing potentials and if this deposit can be dissolved by applying the oxidizing potential.

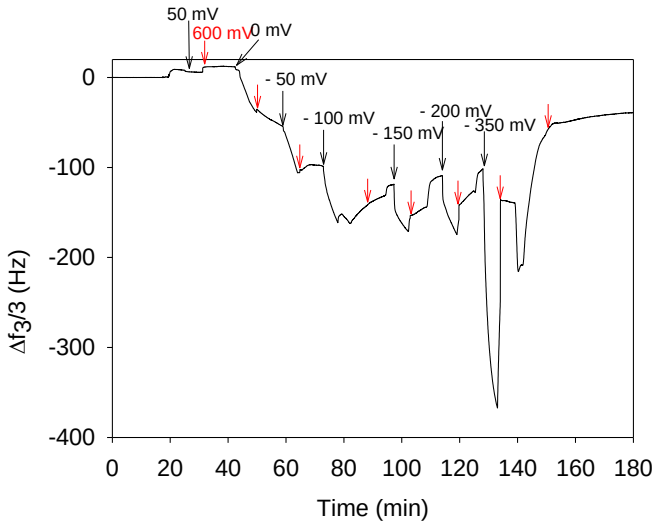

Figure 3.17 EC-QCM-D data for the application of a reducing potential varying from 0 to -350 mV with 50 mV steps during 5 minutes on an aqueous $CuBr_2$ solution with the TPMA ligand both at 1.6 mM. Each reducing potential is followed by an oxidizing potential step at +600 mV during 1 minute (red arrows).

The EC-QCM-D signal in Figure 3.17 shows that we have indeed a mass deposit for all the applied potentials below 50 mV. It also shows that we are not able to dissolve this deposit by applying +600 mV. If the mass deposited came from the formation of metallic copper, it would be dissolved by the application of the oxidizing potential (Rydzek et al. 2010a). It is thus reasonable to attribute this mass deposition to the formation of insoluble Cu(I)Br on the working electrode.

This is a problem since the precipitation of this salt would occur during or instead of the polymerization on the gold working electrode, thus generating a signal in the EC-QCM response that would not come from any polymerization on the surface. Moreover, since the nucleation of these crystals would occur on the gold surface, they may also screen the ATRP initiator and block the buildup of the polymer brushes.

3.5.1.1.2 Copper (II) trifluoromethanesulfonate: $Cu(CF_3SO_3)_2$.

Copper (II) triflate represents a potential candidate for eSI-ATRP. Figure 3.18 shows a cyclic voltammogram from -0.6 to 0.3 V at 10 mV/s of aqueous copper (II) triflate at 20 mM, pH= 3.5 with TPMA at the same concentration.

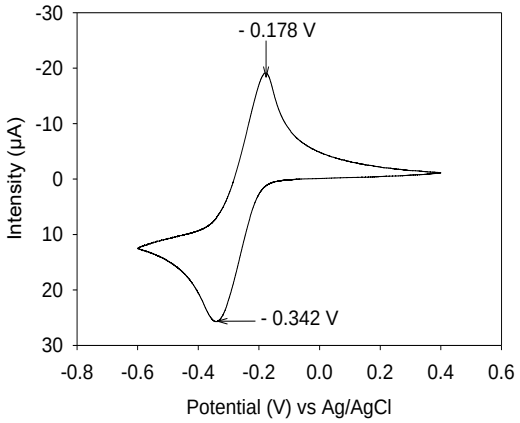

Figure 3.18 Cyclic voltammogram from -0.6 to 0.3 V at 10 mV/s of aqueous copper (II) triflate at 20 mM, pH= 3.5, in the presence of TPMA.

The copper (II) triflate cyclic voltammogram in the presence of TPMA shown in Figure 3.18 presents the advantage of being fairly simple with only one oxidation and one reduction peak at respectively -0.178 and -0.342 V. These peaks can be attributed to the change of Cu(0) to Cu(II) back and forth. This salt can therefore be used for eSI-ATRP experiments.

3.5.1.1.3 Copper (II) sulfate: $CuSO_4$.

Copper (II) sulfate is a salt well described in the literature for electrochemical experiments. Its cyclic voltammogram presents one oxidation and one reduction peak corresponding respectively to the oxidation of Cu(0) to Cu(II) and to the reduction of Cu(II) to Cu(0).

Figure 3.19 shows the cyclic voltammogram from -0.6 to 0.3 V at 10 mV/s of aqueous copper (II) sulfate at 20 mM, pH= 3.5 in the presence of the TPMA ligand at the same concentration.

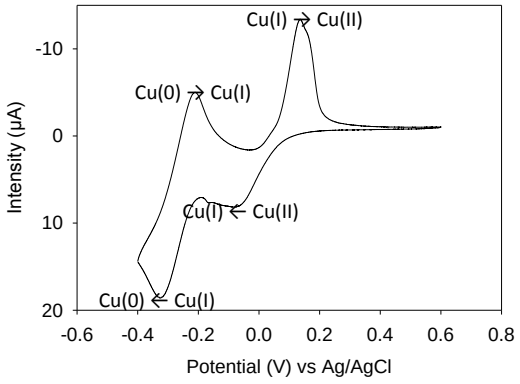

Figure 3.19 Cyclic voltammogram from -0.6 to 0.3 V at 10 mV/s of $CuSO_4$ at 20 mM, pH= 3.5 in the presence of the TPMA ligand at the same concentration.

The copper (II) sulfate CV in the presence of TPMA exhibits an unexpected behavior since it displays two additional peaks compared to the CV of copper (II) bromide and copper (II) triflate in the same conditions. The two additional peaks are attributed to the stabilization of copper (I) by the ligand, i.e. to the reduction of Cu(II) to Cu(I) and to the oxidation of Cu(0) to Cu(I).

Furthermore, it is known from previous studies that copper sulfate do not form insoluble mass deposits on the electrode (Rydzek et al. 2010b). This, combined to the fact that Cu(I) is strongly stabilized by the TPMA ligand with $CuSO_4$ makes it the best choice for conducting eSI-ATRP experiments.

3.5.1.1.4 Conclusion on the copper salts.

From theses electrochemical studies, it appears that both copper (II) triflate and copper (II) sulfate with TPMA can be good candidates for eSI-ATRP since they do not form insoluble Cu(I)Br salt during the cyclic voltammetry. Copper (II) sulfate has the advantage of displaying two more peaks in its CVs attributed to the stabilization of the Cu(I) by the TPMA ligand. This confirms that this copper salt form stable copper (I) complex with a low tendency to disproportionation thus making it the best candidate to perform eSI-ATRP experiments.

3.5.1.2 Effect of the monomer solution viscosity on the QCM measurement.

The EC-QCM-D is a very sensitive technique towards changes of viscosity. Therefore, it is important to discriminate apparent mass deposition due to a change of the viscosity or to a reversible adsorbtion of the monomers from the medium contacting the electrode in comparison to an actual polymerization. Considering that $OEGMA_{475}$ is a viscous monomer due to its hydrated PEG side chains, it is important to check the EC-QCM-D response towards its presence.

Figure 3.20 shows the EC-QCM-D response when an aqueous solution containing $OEGMA_{475}$ (40 % in volume), copper (II) sulfate and TPMA ligand at 1.6 mM each was introduced into the cell and washed away with a buffer.

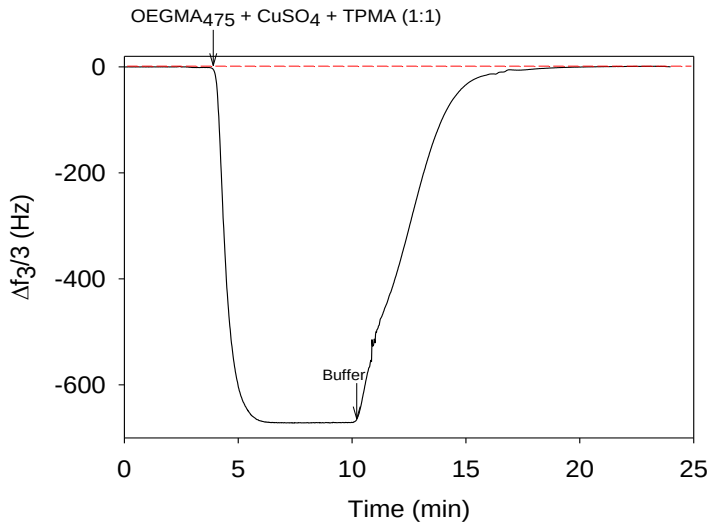

Figure 3.20 Introduction of an aqueous solution containing $OEGMA_{475}$ (40 % in volume,) $CuSO_4$ and TPMA at 1.6 mM into the EC-QCM-D cell and washing with a buffer.

The introduction of the monomer solution into the EC-QCM-D cell leads to a baseline shift of several hundred of Hertz. When the buffer solution is introduced, the frequency signal increases to the baseline. Therefore, it is clear that this apparent mass deposition is only due to the viscosity of the monomer solution or to a reversible adsorption of the monomers onto the electrode.

3.5.1.3 Determination of the applied potential for an eSI-ATRP experiment.

The range of potential at which copper (I) will be formed must be determined in order to polymerize $OEGMA_{475}$. Thus, potential cycles between -350 and +600 mV (vs Ag/AgCl, 10 mV/s) were applied on an aqueous solution containing $OEGMA_{475}$ at 40 % in volume, copper (II) sulfate and TPMA at 1.6 mM, pH= 3.5.

In Figure 3.21, the EC-QCM-D and potential signals of this experiment were superimposed so that the frequency shift corresponding to a mass deposition could be related to a precise potential.

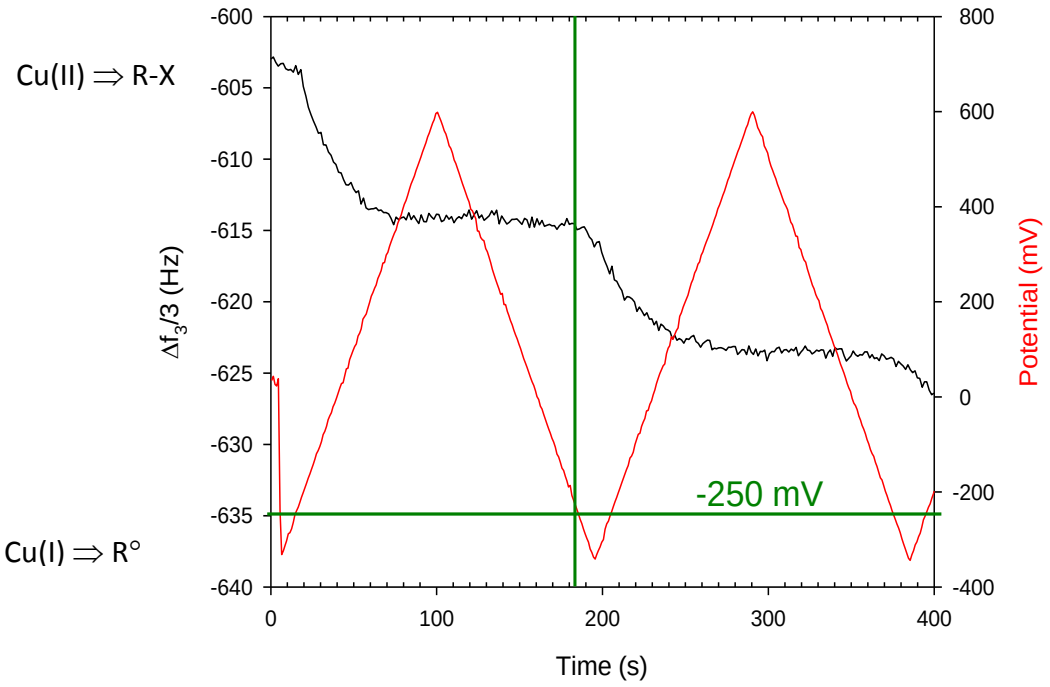

Figure 3.21 Superposition of the EC-QCM-D and potentiostat signal for a cyclic voltammetry ranging from -350 to 600 mV at 10 mV/s applied on an aqueous solution of $OEGMA_{475}$ (40 % in volume) containing $CuSO_4$ and TPMA at 1.6 mM each. The mass deposition seen on the EC-QCM-D corresponds to a potential of -250 mV approximately (green lines).

The mass deposition observed on this experiment is attributed to the polymerization of the $OEGMA_{475}$ monomers (cf. 3.5.2.2) and starts at a potential around -250 mV (green lines). Since this polymerization can only happen in the presence of copper (I), one can conclude that the potential applied at the working electrode must be inferior or equal to -250 mV to form the copper (I) catalyst and to start the polymerization process which is in agreement with the cyclic voltammogram obtained (Figure 3.19).

3.5.1.4 Cyclic voltammetry polymerizations.

An aqueous solution of $OEGMA_{475}$ monomers (40% in volume) containing copper (II) sulfate (1.6 mM), TPMA (1.6 mM) and a bromide salt (TBAB at 0.8 mM, cf. section 3.5.3.1) at pH 3.5 was polymerized two different times by applying a CV between -250 mV to 600 mV at a scan rate of 50 mV/s (Figure 3.22). The CV experiments presents the advantage of forming the Cu(I) catalyst only during a short period of time since the applied potential is in the copper (I) formation range only during a part of the cycle. The potential window for the formation of copper (I) is roughly between 0 and -0.25 V (cf. Figure 3.19), i.e. much narrow than the potential window applied during the whole cycle (between -0.25 and +0.6 V). If we consider that the CV half cycle is in a total potential range of 850 mV and that this half cycle takes 850/50 = 17 s to complete, the applied potential is in the copper (I) formation window only

during 250/50 = 5 s. That means that for a half cycle that takes 17 second to complete, the polymerization will only be performed when the copper (I) catalyst is present, i.e. during 5 seconds. In the rest of the half cycle the copper is at a higher oxidation state and the reaction cannot start.

Considering the ATRP process, this roughly means that the system will be in the "living state" only during 5 s of the half cycle whereas it will be in the "dormant state" 12 s. This favoring of the "dormant state" is the condition needed to slow down the ATRP process and control the polymerization. This means that the application of CV must lead to a slow reaction kinetic with an expected good control over the brush polydispersity.

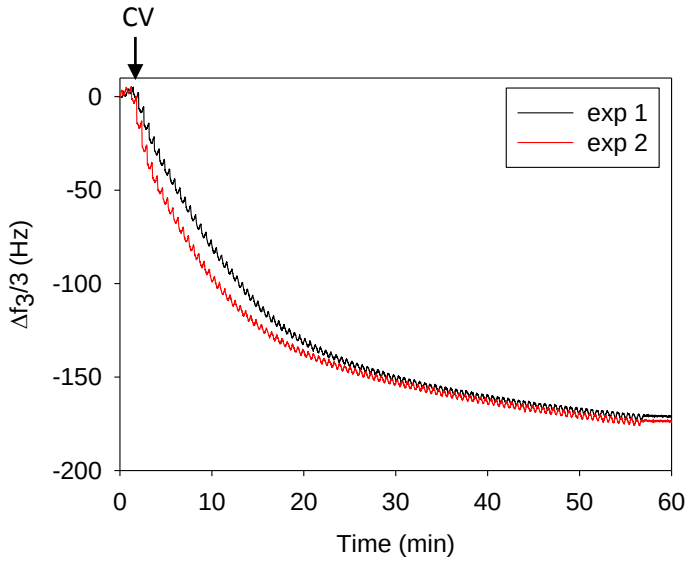

Figure 3.22 Two polymerizations (exp 1 & 2) by application of a CV between -250 and 600 mV at 50 mV/s during 1h on an aqueous $OEGMA_{475}$ solution (40% in volume) containing $CuSO_4$ (1.6 mM), TPMA (1.6 mM) and TBAB (0.8 mM), pH= 3.5 .

These polymerizations do not exhibit a strong adsorption at the beginning of the electrochemical stimulus. The reaction is fairly slow, continuous and reproducible during one hour.

Therefore, since the polymerization is slow and continuous during at least an hour, it may be reasonable to assume that we are working in ATRP conditions.

The polymer brushes obtained by application of a CV between -250 mV to 600 mV at 50 mV/s during 1h on an aqueous solution of $OEGMA_{475}$ (40% in volume) containing $CuSO_4$ (1.6 mM), TPMA (1.6 mM) and TBAB (0.8 mM) at pH 3.5 were analyzed by AFM in contact mode (Figure 3.23).

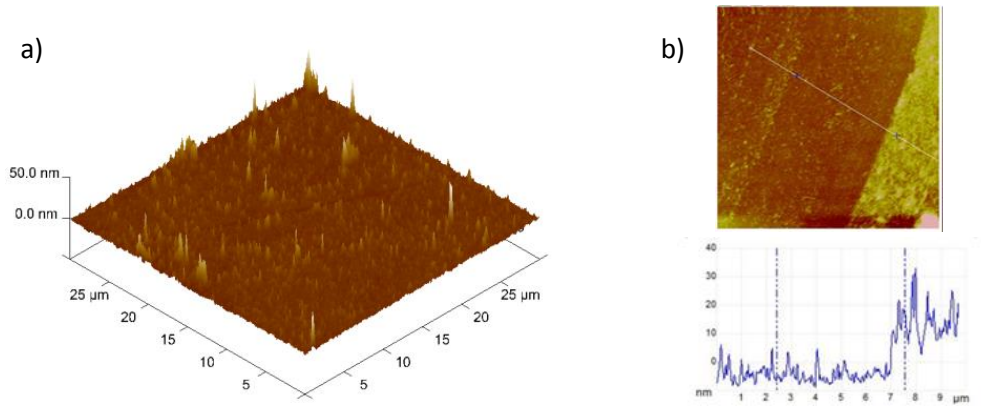

*Figure 3.23 AFM in liquid conditions of the brushes built by application of a CV between -250 and 600 mV at 50 mV/s during 1h on an aqueous solution of $OEGMA_{475}$ (40% in volume) containing $CuSO_4$ (1.6 mM), TPMA (1.6 mM) and TBAB (0.8 mM), pH 3.5.A topography of the surface is realized on 30 µm * 30 µm and gives a roughness of 3 ± 0.8 nm (a). A profilometric measurement of the brushes gives a thickness of ca. 20 nm (b).*

AFM images were performed in contact mode to get access to the topographies of the films. The brushes obtained after a construction time of one hour are thin (ca. 20 nm) and smooth with a roughness of 3 ± 0.8 nm. The low roughness of the brushes obtained suggest that they are quite monodisperse. In that case, they represent an argument toward the possibility of an ATRP process.

A control experiment was performed by replacing the $OEGMA_{475}$ monomers by a non polymerizable PEG_{400} to check whether the mass deposition observed came from a Cu(0) deposition or from the polymerization of the $OEGMA_{475}$ monomers (3.5.2.1).

3.5.2 Control experiments.

3.5.2.1 Cyclic voltammetry on non polymerizable PEG_{400}.

In order to verify that the construction observed in Figure 3.22 were not related to a Cu(0) deposition on the working electrode, the same experiment was performed by replacing the $OEGMA_{475}$ monomers by a non polymerizable PEG_{400} solution.

A CV from -250 mV to 600 mV at 50 mV/s was then applied during one hour on an aqueous PEG_{400} solution (40 % in volume) containing $CuSO_4$ (1.6 mM), TPMA (1.6 mM) and TBAB (0.8 mM) at pH 3.5 (Figure 3.24).

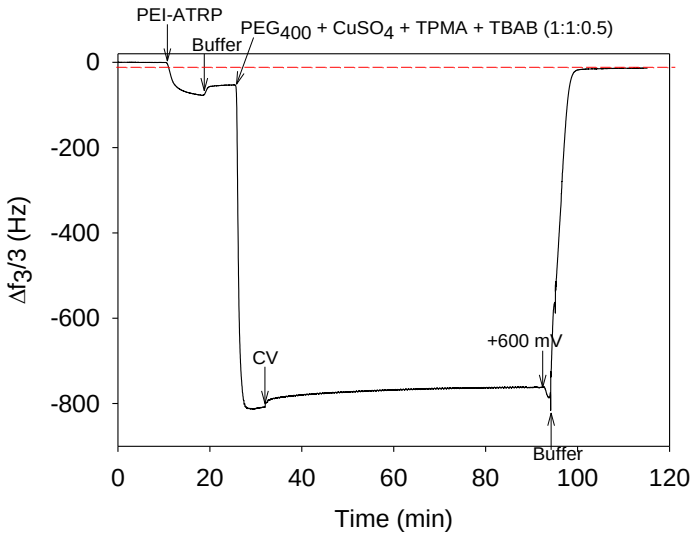

Figure 3.24 Control experiment: EC-QCM-D data for the application of a CV from -250 to +600 mV at 50 mV/s during one hour on an aqueous PEG_{400} solution (40 % in volume) containing $CuSO_4$ (1.6 mM), TPMA (1.6 mM) and TBAB (0.8 mM) at pH 3.5.

A slight increase in the frequency shift is observed during the application of the CV indicating that the macro-initiator is slightly desorbing from the working electrode. No buildup is observed for the non polymerizable PEG_{400} suggesting that the buildup previously obtained with the $OEGMA_{475}$ monomers corresponds indeed to pOEGMA brushes.

3.5.2.2 Anti-fouling properties of the pOEGMA$_{475}$ brushes.

In order to confirm that the mass deposited on the WE during the application of the CV in section 3.5.1.4 came from the formation of pOEGMA brushes, the antifouling properties of these brushes were tested. Indeed, the PEG lateral chains grafted onto the $OEGMA_{475}$ are well known for their anti-fouling properties toward proteins.

A bovine serum albumin solution at 1 mg/ml was put into contact with the precursor layer of macro-initiator (PEI-Br) and with the brushes obtained by eSI-ATRP after one hour of construction. Figure 3.25 shows the frequency shift of the EC-QCM-D corresponding to the adsorption of albumin.

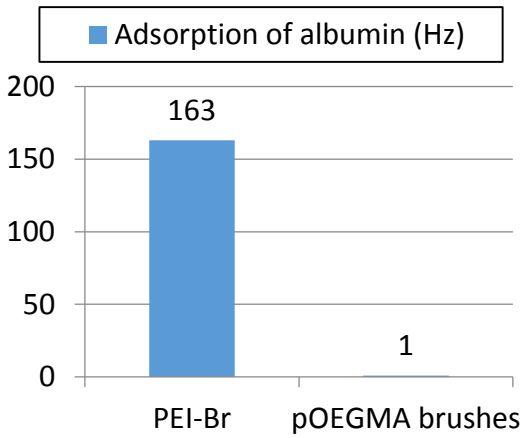

Figure 3.25 EC-QCM-D response towards the adsorbtion of albumin: test of the anti-fouling properties of the brushes built by eSI-ATRP during one hour.

Figure 3.25 shows that the albumin strongly adsorb onto the PEI-Br whereas no adsorption is observed on the brushes built during one hour by eSI-ATRP. This result confirms that the mass deposited on the working electrodes during the application of the CV correspond to the buildup of $pOEGMA_{475}$ brushes.

3.5.3 Influence of the build-up parameters.

3.5.3.1 Influence of a bromide salt.

As described in the section 3.1.1, the ATRP kinetic is controlled by the activator/deactivator ration, i.e. the Cu(I)L/X-Cu(II)L ratio. This ratio must be low in order to provide a slow polymerization kinetic and a good control of the ATRP process. However, it was discussed in the section 3.1.3 that the halide ion can be dissociated from the transition metal complex when one perform an ATRP process in water. This side reaction decreases of the deactivator concentration which leads to a faster polymerization kinetics and a lower control of the ATRP process. The halide ion dissociation from the transition metal complex is then a reaction that must be unfavored in order to keep a good control of the process. The introduction of a bromide salt in the media, e.g. tetra-n-butylammonium bromide (TBAB), represents a possible way to decrease the deactivator dissociation in water.

The influence of the TBAB salt on the polymerization kinetics was investigated by varying its concentration in the monomer solution. The polymerizations were performed by applying a CV between -250 mV to 600 mV at 50 mV/s during one hour on an aqueous solution of $OEGMA_{475}$ (40% in volume) containing $CuSO_4$ (1.6 mM), TPMA (1.6 mM) and TBAB at different concentrations varying from 0 to 1.6 mM at pH 3.5 (Figure 3.26).

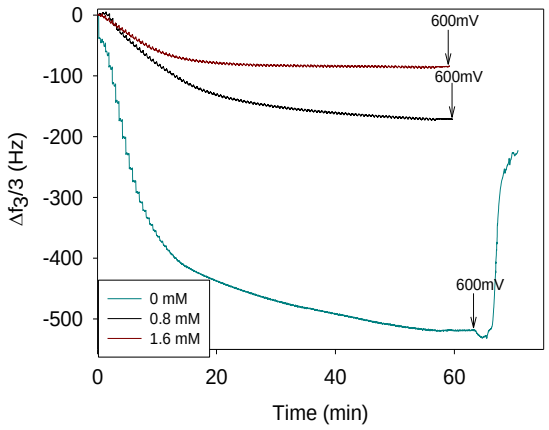

Figure 3.26 Influence of the TBAB concentration in the monomer solution on the buildup kinetics. Polymerization by applying a CV between -250 and 600 mV at 50 mV/s during one hour on an aqueous $OEGMA_{475}$ monomer solution (40% in volume) containing $CuSO_4$ (1.6 mM), TPMA (1.6 mM) and TBAB in a concentration of 0; 0.8 and 1.6 mM, pH= 3.5.

Figure 3.26 shows that the introduction of TBAB greatly changes the kinetic of the polymerization reaction. When this salt is not present, a strong polymerization is observed in the first minutes with a deposition of Cu(0) that can be desorbed by applying an oxidation potential of + 600 mV. The polymerization reaction is fast in the first 15 minutes of the CV thus showing that the reaction is poorly controlled. On the other hand, by increasing the concentration of TBAB the polymerization kinetic is reduced. When this salt is present, no Cu(0) deposition is observed since no change of frequency is observed when applying a oxidation potential of + 600 mV. Furthermore, the kinetic reduction observed is expected since the bromide salt should favor the deactivator (X-Cu(II)L) formation and thus maintain a low Cu(I)L/X-Cu(II)L needed for a controlled ATRP process. It is then clear that TBAB is needed to obtain reaction kinetics similar to ATRP and to avoid Cu(0) formation.

3.5.3.2 Influence of the CV Scan rate.

The influence of the CV scan rate was investigated as well. Polymerization processes were conducted by applying a CV between -250 and 600 mV at a scan rate varying from 10 to 100 mV/s on an aqueous solution of $OEGMA_{475}$ (40 % in volume) containing $CuSO_4$ (1.6 mM), TPMA (1.6 mM) and TBAB (0.8 mM) (Figure 3.27).

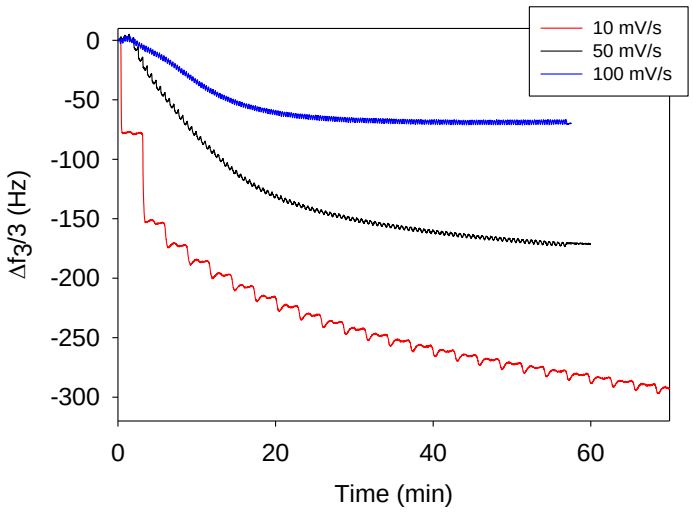

Figure 3.27 Polymerization kinetic for the application of a CV between -250 and 600 mV at a scan rate of 10, 50 and 100 mV/s on an aqueous solution of $OEGMA_{475}$ (40% in volume), $CuSO_4$ (1.6 mM), TPMA (1.6 mM) and TBAB (0.8 mM), pH= 3.5.

One observes that the scan rate has a strong influence on the polymerization of $OEGMA_{475}$. The frequency shift of the construction at 10 mV/s shows a continuous polymerization during at least 70 minutes and a total mass deposited higher than for 50 mV/s. The polymerization at 100 mV/s shows a slower kinetics than for 50 mV/s and for 10 mV/s. Moreover at 100 mV/s, the construction seems to stop after 20 minutes.

From these observations, it is clear that the slower the scan rate of the CV, the higher is the mass deposition and the quicker is the kinetic. Such result can be explained by the fact that in a slow CV the varying potential stays longer in the window of potential corresponding to the formation of copper (I). As discussed earlier, the varying potential applied during the CV stays 5 seconds (per half cycle) in the potential window corresponding to the copper (I) formation when scanning at 50 mV/s. However, this time is reduced to 2.5 seconds when scanning at 100 mV/s whereas it is increased to 25 seconds when scanning at 10 mV/s.

A sample polymerized by applying a CV between -250 and 600 mV/s at 10 mV/s during one hour on an aqueous solution of $OEGMA_{475}$ (40% in volume) containing $CuSO_4$ (1.6 mM), TPMA (1.6 mM) and TBAB (0.8 mM) at pH 3.5, was analyzed by AFM in contact mode to determine its topography (Figure 3.28).

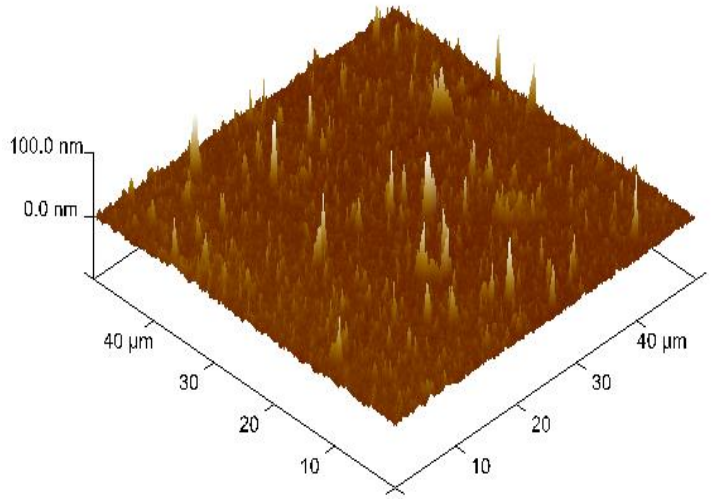

*Figure 3.28 Topography of the film constructed by a CV between -250 and 600 mV at 10 mV/s on an aqueous solution of $OEGMA_{475}$ (40 % in volume) containing $CuSO_4$ (1.6 mM), TPMA (1.6 mM) and TBAB (0.8 mM) at pH= 3.5; surface of 50 µm * 50 µm.*

The AFM image show that the film covers homogeneously the working electrode. The film thickness is around 20 nm with a low roughness of 5.9 nm. The films constructed at 10 mV/s is slightly rougher than for a construction at 50 mV/s (Rq= 3 ± 0.8 nm) (Figure 3.23).

3.6 CONCLUSION

In this chapter, a new strategy for morphogen buildup of polymers in one-pot was highlighted. The eSI-ATRP mechanism presents the advantage of being fast and allows brushes buildup with a density high enough for the surface to prevent albumin adsorption.

Electrochemical experiments were conducted on different copper salts in presence of the TPMA ligand. The cyclic voltammetry of $CuBr_2$ in presence of a ligand leads to the formation of an insoluble CuBr salt. Both the cyclic voltammogram of $Cu(CF_3SO_3)_2$ and $CuSO_4$ were simple and didn't form insoluble salts. The cyclic voltammogram of $CuSO_4$ in presence of ligand had the advantage of showing peaks corresponding to the formation of Cu(I). The copper (II) sulfate was then chosen for all the experiments.

To obtain the eSI-ATRP, cyclic voltammetry was applied on $OEGMA_{475}$ monomer solutions that lead to a slow and continuous buildup corresponding to a smooth thin film.

Control experiments showed that the deposited mass observed during the buildups most probably came from the polymerization of $OEGMA_{475}$ and that the pOEGMA brushes possessed the expected antifouling properties towards proteins.

The influence of a bromide salt (TBAB) was studied to decrease the polymerization kinetic and to improve the control of the brushes buildup. The reduction of the kinetic was attributed to the favoring of the deactivator (X-Cu(II)L) formation. This maintained a low Cu(I)L/X-Cu(II)L ratio needed to obtain the ATRP kinetic.

The last parameter studied was the cyclic voltammetry scan rate. From the QCM results, we saw that the kinetic was correlated to the scan rate and the quicker we scanned, the slower was the kinetic.

In conclusion, eSI-ATRP experiments were successfully performed by applying cyclic voltammetry on an $OEGMA_{475}$ solution containing a bromide salt. The kinetic observed was in accordance to ATRP kinetic and the AFM analysis displayed smooth thin films that homogeneously covers the gold crystal working electrode. Unfortunately, competitive papers were published in the meantime of this study (Li et al. 2012, Li et al. 2013a, Li et al. 2013b) (section 3.7). We thus stopped further investigation.

3.7 COMPETITIVE PUBLICATIONS ON ELECTROCHEMICAL SURFACE INITIATED-ATRP (ESI-ATRP).

One year after the beginning of my thesis, competitive papers on SI-ATRP triggered by electrochemistry were published (Li et al. 2012, Hosseiny et al. 2013, Li et al. 2013a, Li et al. 2013b, Yan et al. 2013).

In the first paper published in 2012, two alkane thiol, one bearing the ATRP initiator, were deposited on a gold electrode to form a self-assembled monolayer (SAM). An aqueous solution containing monomers, copper (II) chloride ($Cu^{II}Cl_2$) with a bipyridine (bpy) ligand and a supporting chlorinated electrolyte was brought into contact with the SAM coated working electrode. Application of a suited potential lead to the buildup of polymer brushes by eSI-ATRP (Figure 3.29).

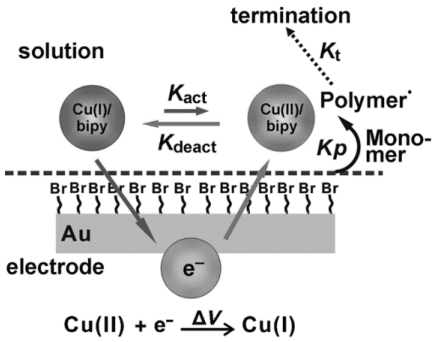

Figure 3.29 Schematic representation of polymer brushes buildup by eSI-ATRP. A gold working electrode covered with a SAM containing an ATRP initiator is brought into contact with an aqueous solution containing monomers, copper (II) chloride with the bipyridine ligand. A fixed potential is applied at the interface reducing the copper (II) complex into copper (I) thus forming the ATRP catalyst. The classical ATRP process then takes place leading to the formation of brushes (Li et al. 2012).

One can note that these experimental parameters are somewhat similar to ours since their system possess: an ATRP initiator layer (a SAM instead of our polyelectrolyte macroinitiator), a transition metal catalyst with a ligand in a solution containing halide ions to favour the deactivator formation.

The authors showed that the ratio between the thiol molecule containing the ATRP initiator and the alkane thiol molecule was of primary importance for the formation of a conducting SAM. Indeed, the alkane thiol molecule was needed to serve as charge-transfer pathway for the reduction of copper (II) to copper (I) since the other thiol molecule containing the ATRP initiator formed an insulating layer and therefore did not allow electron transfer needed for the reduction of copper (II) into copper (I).

The authors showed that brushes grow, leading to a smooth homogeneous films around 140 nm in 2 hours even in the presence of soluble dioxygen (coming from air) and then the construction stopped. The oxygen was supposed to be scavenged by the copper (I) complexes continuously formed at the

working electrode. As in eATRP, it was found that the $[Cu^{I}]/[Cu^{II}]$ ratio and thus the ATRP kinetic could be controlled by tuning the applied potential. Furthermore, the monomer solution could be reused several times on different gold covered electrodes to buildup the polymer brushes. Several monomer solutions could also be used alternately to construct homo or block copolymers on patterned electrode. It is the diffusion of Cu(I) from the electrode towards the solution that allows the construction. This buildup can thus be denoted as a **morphogen buildup**.

In 2013, the technique was further investigated by performing the eSI-ATRP process in presence of an atomic force microscope. The polymer brushes buildup on a patterned substrate could be followed in real time by atomic force microscopy to investigate the buildup kinetic. Figure 3.30 schematically shows the setup on which the patterned gold working electrode bearing the initiator is immersed in the aqueous monomer solution containing the copper (II) complex and chlorinated electrolyte. The application of a suited potential reduce the copper (II) complex thus forming the ATRP catalyst and triggering the polymer brushes buildup that are imaged in situ by an AFM.

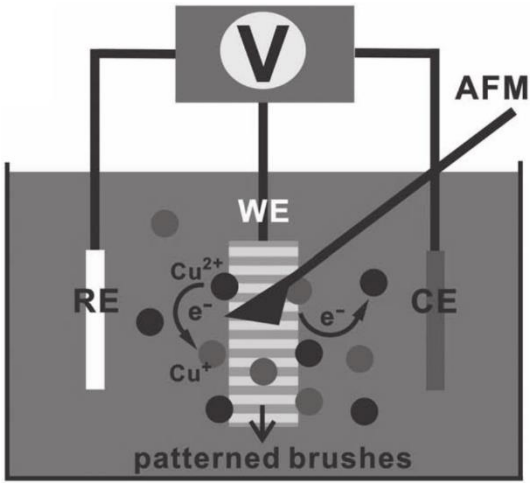

Figure 3.30 Schematic representation of the polymer brushes buildup: a patterned working electrode is immersed in an aqueous solution containing the monomers, the copper (II) complex and the chlorinated electrolyte. Application of a suited potential forms the ATRP catalyst thus triggering the brushes buildup which is imaged in real time by AFM. RE: reference electrode, WE: working electrode, CE: counter electrode (Li et al. 2013b).

The versatility of the method was demonstrated by the polymerization of several monomers and by controlling the electrochemical stimulus to start or stop the buildup.

A buildup kinetic difference was observed between the different types of monomers. These differences were attributed to the complex interactions between charged monomers, propagation halide terminus and catalyst complex. To investigate further this phenomenon, counter ions were

introduced in the solution to screen the charges of the monomers. It was found out that the polymer growth could be increased up to five orders of magnitude depending on the counter ion.

The latest development of the technique is based on the buildup of polymer brushes by eSI-ATRP on non-conducting substrates such as silicon wafers. In this approach, the copper (I) complex catalyst is generated from copper (II) complexes at a working electrode and then diffuses to the non-conducting surface on which is deposited the ATRP initiator. The ATRP process then starts on the silicon wafer substrate. The distance between the working electrode and the silicon wafer controls the $[Cu^{I}]/[Cu^{II}]$ ratio and the presence of a tilt permits the construction of gradient polymers (Figure 3.31).

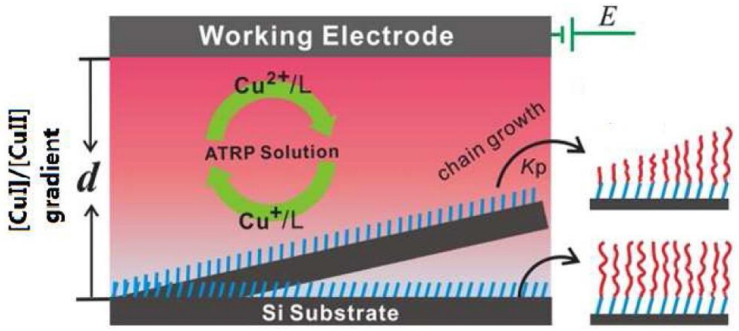

Figure 3.31 Schematic representation of eSI-ATRP on a non-conducting substrate: an ATRP initiator is deposited on a silicon wafer located at a distance d from the working electrode. When the fixed potential is applied on the aqueous monomer solution containing the copper (II) complex and chlorinated electrolyte, the ATRP catalyst is generated that diffuses to the Si-wafer and the ATRP process takes place. The presence of a tilt between the working electrode and the Si-wafer allows the buildup of gradient polymer brushes (Li et al. 2013a).

In the previous methods described above, the copper (I) catalyst was generated at the interface where the brushes buildup took place. This caused a major problem since the copper (I) concentration at the interface was high and it was then difficult to control the deactivator/activator ratio. Indeed, the complementary $X\text{-}Cu^{II}/L$ deactivator has the opposite distribution than the Cu^{I} activating species. The modification of the setup described in the Figure 3.31 allows a better control of the deactivator/activator ratio by tuning both the applied potential and the gap between the silicon wafer and the working electrode.

In this case, linear buildup was observed up to 5h for a thickness of 300 nm unlike in the previous experiments on conducting substrates where the growth levelled up at 140 nm after 30 minutes. This phenomena was attributed to the low concentration of deactivator species in the previous experiments and thus to a low control and high amount of termination reactions. Polymers brushes were successfully built on patterned surfaces with this approach.

This last technique significantly improved the control of eSI-ATRP buildup experiment in aqueous media by a better modulation of the activator/deactivator ratio. Furthermore, the brushes were built on inexpensive substrate and the formation of gradient polymer was straight forward to obtain just by changing the sample conformation.

REFERENCES

Averick, S., A. Simakova, S. Park, D. Konkolewicz, A. J. D. Magenau, R. A. Mehl and K. Matyjaszewski (2012). "Atrp under Biologically Relevant Conditions: Grafting from a Protein." Acs Macro Letters **1**(1): 6-10.

Badi, N. and J. F. Lutz (2009). "Peg-Based Thermogels: Applicability in Physiological Media." J Control Release **140**(3): 224-229.

Barbey, R., L. Lavanant, D. Paripovic, N. Schuwer, C. Sugnaux, S. Tugulu and H. A. Klok (2009). "Polymer Brushes Via Surface-Initiated Controlled Radical Polymerization: Synthesis, Characterization, Properties, and Applications." Chemical Reviews **109**(11): 5437-5527.

Beers, K. L., S. G. Gaynor, K. Matyjaszewski, S. S. Sheiko and M. Moller (1998). "The Synthesis of Densely Grafted Copolymers by Atom Transfer Radical Polymerization." Macromolecules **31**(26): 9413-9415.

Börner, H. G. and K. Matyjaszewski (2002). "Graft Copolymers by Atom Transfer Polymerization." Macromolecular Symposia **177**(1): 1-16.

Bortolamei, N., A. A. Isse, A. J. Magenau, A. Gennaro and K. Matyjaszewski (2011). "Controlled Aqueous Atom Transfer Radical Polymerization with Electrochemical Generation of the Active Catalyst." Angewandte Chemie, International Edition in English **50**(48): 11391-11394.

Braunecker, W. A., N. V. Tsarevsky, A. Gennaro and K. Matyjaszewski (2009). "Thermodynamic Components of the Atom Transfer Radical Polymerization Equilibrium: Quantifying Solvent Effects." Macromolecules **42**(17): 6348-6360.

Cao, J., L. Zhang, X. Jiang, C. Tian, X. Zhao, Q. Ke, X. Pan, Z. Cheng and X. Zhu (2013). "Facile Iron-Mediated Dispersant-Free Suspension Polymerization of Methyl Methacrylate Via Reverse Atrp in Water." Macromolecular Rapid Communications **34**(22): 1747-1754.

Chen, T., R. Ferris, J. M. Zhang, R. Ducker and S. Zauscher (2010). "Stimulus-Responsive Polymer Brushes on Surfaces: Transduction Mechanisms and Applications." Progress in Polymer Science **35**(1-2): 94-112.

Chiefari, J., Y. K. Chong, F. Ercole, J. Krstina, J. Jeffery, T. P. T. Le, R. T. A. Mayadunne, G. F. Meijs, C. L. Moad, G. Moad, E. Rizzardo and S. H. Thang (1998). "Living Free-Radical Polymerization by Reversible Addition−Fragmentation Chain Transfer: The Raft Process." Macromolecules **31**(16): 5559-5562.

Cunningham, M. F. (2002). "Living/Controlled Radical Polymerizations in Dispersed Phase Systems." Progress in Polymer Science **27**(6): 1039-1067.

Davis, K. and K. Matyjaszewski (2002). Statistical, Gradient, Block, and Graft Copolymers by Controlled/Living Radical Polymerizations. Statistical, Gradient, Block and Graft Copolymers by Controlled/Living Radical Polymerizations, Springer Berlin Heidelberg. **159:** 1-13.

de Vries, A., B. Klumperman, D. de Wet-Roos and R. D. Sanderson (2001). "The Effect of Reducing Monosaccharides on the Atom Transfer Radical Polymerization of Butyl Methacrylate." Macromolecular Chemistry and Physics **202**(9): 1645-1648.

Edmondson, S. and S. P. Armes (2009). "Synthesis of Surface-Initiated Polymer Brushes Using Macro-Initiators." Polymer International **58**(3): 307-316.

Edmondson, S., C. D. Vo, S. P. Armes and G. F. Unali (2007). "Surface Polymerization from Planar Surfaces by Atom Transfer Radical Polymerization Using Polyelectrolytic Macroinitiators." Macromolecules **40**(15): 5271-5278.

Edmondson, S., C. D. Vo, S. P. Armes, G. F. Unali and M. P. Weir (2008). "Layer-by-Layer Deposition of Polyelectrolyte Macroinitiators for Enhanced Initiator Density in Surface-Initiated Atrp." Langmuir **24**(14): 7208-7215.

Gaynor, S. G., S. Edelman and K. Matyjaszewski (1996). "Synthesis of Branched and Hyperbranched Polystyrenes." Macromolecules **29**(3): 1079-1081.

Hadjichristidis, N., M. Pitsikalis, S. Pispas and H. Iatrou (2001). "Polymers with Complex Architecture by Living Anionic Polymerization." Chemical Reviews **101**(12): 3747-3792.

Hawker, C. J., A. W. Bosman and E. Harth (2001). "New Polymer Synthesis by Nitroxide Mediated Living Radical Polymerizations." Chemical Reviews **101**(12): 3661-3688.

Hosseiny, S. S. and P. van Rijn (2013). "Surface Initiated Polymerizations Via E-Atrp in Pure Water." Polymers **5**(4): 1229-1240.

Jonsson, M., D. Nystrom, O. Nordin and E. Malmstrom (2009). "Surface Modification of Thermally Expandable Microspheres by Grafting Poly(Glycidyl Methacrylate) Using Arget Atrp." European Polymer Journal **45**(8): 2374-2382.

Kamigaito, M., T. Ando and M. Sawamoto (2001). "Metal-Catalyzed Living Radical Polymerization." Chemical Reviews **101**(12): 3689-3746.

Kato, M., M. Kamigaito, M. Sawamoto and T. Higashimura (1995). "Polymerization of Methyl-Methacrylate with the Carbon-Tetrachloride Dichlorotris(Triphenylphosphine)Ruthenium(Ii) Methylaluminum Bis(2,6-Di-Tert-Butylphenoxide) Initiating System - Possibility of Living Radical Polymerization." Macromolecules **28**(5): 1721-1723.

Konkolewicz, D., A. J. D. Magenau, S. E. Averick, A. Simakova, H. K. He and K. Matyjaszewski (2012). "Icar Atrp with Ppm Cu Catalyst in Water." Macromolecules **45**(11): 4461-4468.

Król, P. and P. Chmielarz (2014). "Recent Advances in Atrp Methods in Relation to the Synthesis of Copolymer Coating Materials." Progress in Organic Coatings **77**(5): 913-948.

Lee, H. I., J. Pietrasik, S. S. Sheiko and K. Matyjaszewski (2010). "Stimuli-Responsive Molecular Brushes." Progress in Polymer Science **35**(1-2): 24-44.

Li, B., B. Yu, W. T. Huck, W. Liu and F. Zhou (2013a). "Electrochemically Mediated Atom Transfer Radical Polymerization on Nonconducting Substrates: Controlled Brush Growth through Catalyst Diffusion." Journal of the American Chemical Society **135**(5): 1708-1710.

Li, B., B. Yu, W. T. Huck, F. Zhou and W. Liu (2012). "Electrochemically Induced Surface-Initiated Atom-Transfer Radical Polymerization." Angewandte Chemie, International Edition in English **51**(21): 5092-5095.

Li, B., B. Yu and F. Zhou (2013b). "In Situ Afm Investigation of Electrochemically Induced Surface-Initiated Atom-Transfer Radical Polymerization." Macromolecular Rapid Communications **34**(3): 246-250.

Li, H., R. Liu, H. L. Kang, Y. F. Zheng and Z. D. Xu (2008). "Growth and Characterization of Highly Oriented Cubr Thin Films through Room Temperature Electrochemical Route." Electrochimica Acta **54**(2): 242-246.

Li, M., N. M. Jahed, K. Min and K. Matyjaszewski (2004). "Preparation of Linear and Star-Shaped Block Copolymers by Atrp Using Simultaneous Reverse and Normal Initiation Process in Bulk and Miniemulsion." Macromolecules **37**(7): 2434-2441.

Liu, G. and G. Zhang (2005). "Collapse and Swelling of Thermally Sensitive Poly(N-Isopropylacrylamide) Brushes Monitored with a Quartz Crystal Microbalance." Journal of Physical Chemistry B **109**(2): 743-747.

Lou, Q. and D. A. Shipp (2012). "Recent Developments in Atom Transfer Radical Polymerization (Atrp): Methods to Reduce Metal Catalyst Concentrations." Journal of Chemical Physics and Physical Chemistry **13**(14): 3257-3261.

Lutz, J.-F., T. Pakula and K. Matyjaszewski (2003a). Synthesis and Properties of Copolymers with Tailored Sequence Distribution by Controlled/Living Radical Polymerization. Advances in Controlled/Living Radical Polymerization, American Chemical Society. **854:** 268-282.

Lutz, J. F. (2008). "Polymerization of Oligo(Ethylene Glycol) (Meth)Acrylates: Toward New Generations of Smart Biocompatible Materials." Journal of Polymer Science Part a-Polymer Chemistry **46**(11): 3459-3470.

Lutz, J. F. (2011). "Thermo-Switchable Materials Prepared Using the Oegma-Platform." Advanced Materials **23**(19): 2237-2243.

Lutz, J. F., O. Akdemir and A. Hoth (2006). "Point by Point Comparison of Two Thermosensitive Polymers Exhibiting a Similar Lcst: Is the Age of Poly(Nipam) Over?" Journal of the American Chemical Society **128**(40): 13046-13047.

Lutz, J. F., B. Kirci and K. Matyjaszewski (2003b). "Synthesis of Well-Defined Alternating Copolymers by Controlled/Living Radical Polymerization in the Presence of Lewis Acids." Macromolecules **36**(9): 3136-3145.

Lutz, J. F., D. Neugebauer and K. Matyjaszewski (2003c). "Stereoblock Copolymers and Tacticity Control in Controlled/Living Radical Polymerization." Journal of the American Chemical Society **125**(23): 6986-6993.

Luzinov, I., S. Minko and V. V. Tsukruk (2004). "Adaptive and Responsive Surfaces through Controlled Reorganization of Interfacial Polymer Layers." Progress in Polymer Science **29**(7): 635-698.

Magenau, A. J., N. C. Strandwitz, A. Gennaro and K. Matyjaszewski (2011). "Electrochemically Mediated Atom Transfer Radical Polymerization." Science **332**(6025): 81-84.

Mandal, T. K., M. S. Fleming and D. R. Walt (2000). "Production of Hollow Polymeric Microspheres by Surface-Confined Living Radical Polymerization on Silica Templates." Chemistry of Materials **12**(11): 3481-3487.

Mao, B. W., L. H. Gan, Y. Y. Gan, K. C. Tam and O. K. Tan (2005). "Controlled One-Pot Synthesis of Ph-Sensitive Self-Assembled Diblock Copolymers and Their Aggregation Behavior." Polymer **46**(23): 10045-10055.

Matyjaszewski, K. (2003). "The Synthesis of Functional Star Copolymers as an Illustration of the Importance of Controlling Polymer Structures in the Design of New Materials." Polymer International **52**(10): 1559-1565.

Matyjaszewski, K. (2011). "State-of-the-Art of Controlled/Living Radical Polymerization." Abstracts of Papers of the American Chemical Society **242**.

Matyjaszewski, K. (2012). "Atom Transfer Radical Polymerization (Atrp): Current Status and Future Perspectives." Macromolecules **45**(10): 4015-4039.

Matyjaszewski, K., S. Gaynor, D. Greszta, D. Mardare and T. Shigemoto (1995). "Living and Controlled Radical Polymerization." Journal of Physical Organic Chemistry **8**(4): 306-315.

Matyjaszewski, K. and S. G. Gaynor (1997a). "Preparation of Hyperbranched Polyacrylates by Atom Transfer Radical Polymerization .3. Effect of Reaction Conditions on the Self-Condensing Vinyl Polymerization of 2-((2-Bromopropionyl)Oxy)Ethyl Acrylate." Macromolecules **30**(23): 7042-7049.

Matyjaszewski, K., S. G. Gaynor, A. Kulfan and M. Podwika (1997b). "Preparation of Hyperbranched Polyacrylates by Atom Transfer Radical Polymerization. 1. Acrylic Ab* Monomers in “Living” Radical Polymerizations." Macromolecules **30**(17): 5192-5194.

Matyjaszewski, K., S. G. Gaynor and A. H. E. Muller (1997c). "Preparation of Hyperbranched Polyacrylates by Atom Transfer Radical Polymerization .2. Kinetics and Mechanism of Chain Growth for the Self-Condensing Vinyl Polymerization of 2-((2-Bromopropionyl)Oxy)Ethyl Acrylate." Macromolecules **30**(23): 7034-7041.

Matyjaszewski, K., W. Jakubowski, K. Min, W. Tang, J. Huang, W. A. Braunecker and N. V. Tsarevsky (2006). "Diminishing Catalyst Concentration in Atom Transfer Radical Polymerization with Reducing Agents." Proceedings of the National Academy of Sciences of the United States of America **103**(42): 15309-15314.

Matyjaszewski, K. and A. Kajiwara (1998a). "Epr Study of Atom Transfer Radical Polymerization (Atrp) of Styrene." Macromolecules **31**(2): 548-550.

Matyjaszewski, K., J. Pyun and S. G. Gaynor (1998b). "Preparation of Hyperbranched Polyacrylates by Atom Transfer Radical Polymerization, 4 - the Use of Zero-Valent Copper." Macromolecular Rapid Communications **19**(12): 665-670.

Matyjaszewski, K. and N. V. Tsarevsky (2009). "Nanostructured Functional Materials Prepared by Atom Transfer Radical Polymerization." Nature Chemistry **1**(4): 276-288.

Matyjaszewski, K. and J. Xia (2001). "Atom Transfer Radical Polymerization." Chemical Reviews **101**(9): 2921-2990.

Matyjaszewski, K., M. J. Ziegler, S. V. Arehart, D. Greszta and T. Pakula (2000). "Gradient Copolymers by Atom Transfer Radical Copolymerization." Journal of Physical Organic Chemistry **13**(12): 775-786.

Mecerreyes, D., R. Jérôme and P. Dubois (1999). Novel Macromolecular Architectures Based on Aliphatic Polyesters: Relevance of the “Coordination-Insertion” Ring-Opening Polymerization. Macromolecular Architectures. J. Hilborn, P. Dubois, C. J. Hawker et al., Springer Berlin Heidelberg. **147:** 1-59.

Millard, P. E., N. C. Mougin, A. Boker and A. H. E. Muller (2009). "Controlling the Fast Atrp of N-Isopropylacrylamide in Water." Controlled/Living Radical Polymerization: Progress in Atrp **1023**: 127-137.

Mueller, A. H. E., P. E. Millard, N. C. Mougin and A. Boker (2008). "Poly 544-Fast Atrp of N-Isopropylacrylamide in Water and Its Application to Bioconjugates." Abstracts of Papers of the American Chemical Society **236**.

Nicolas, J., Y. Guillaneuf, C. Lefay, D. Bertin, D. Gigmes and B. Charleux (2013). "Nitroxide-Mediated Polymerization." Progress in Polymer Science **38**(1): 63-235.

Olivier, A., F. Meyer, J. M. Raquez, P. Damman and P. Dubois (2012). "Surface-Initiated Controlled Polymerization as a Convenient Method for Designing Functional Polymer Brushes: From Self-Assembled Monolayers to Patterned Surfaces." Progress in Polymer Science **37**(1): 157-181.

Perrier, S. and D. M. Haddleton (2002). "Effect of Water on Copper Mediated Living Radical Polymerization." Macromolecular Symposia **182**(1): 261-272.

Pitsikalis, M., S. Pispas, J. Mays and N. Hadjichristidis (1998). Nonlinear Block Copolymer Architectures. Blockcopolymers - Polyelectrolytes - Biodegradation. V. Bellon-Maurel, A. Calmon-Decriaud, V. Chandrasekhar et al., Springer Berlin Heidelberg. **135:** 1-137.

Pyun, J., T. Kowalewski and K. Matyjaszewski (2003). "Synthesis of Polymer Brushes Using Atom Transfer Radical Polymerization." Macromolecular Rapid Communications **24**(18): 1043-1059.

Pyun, J. and K. Matyjaszewski (2001). "Synthesis of Nanocomposite Organic/Inorganic Hybrid Materials Using Controlled/“Living” Radical Polymerization." Chemistry of Materials **13**(10): 3436-3448.

Qiu, J., B. Charleux and K. Matyjaszewski (2001). "Controlled/Living Radical Polymerization in Aqueous Media: Homogeneous and Heterogeneous Systems." Progress in Polymer Science **26**(10): 2083-2134.

Robinson, K. L., M. A. Khan, M. V. de Paz Báñez, X. S. Wang and S. P. Armes (2001). "Controlled Polymerization of 2-Hydroxyethyl Methacrylate by Atrp at Ambient Temperature." Macromolecules **34**(10): 3155-3158.

Rydzek, G., J. S. Thomann, N. Ben Ameur, L. Jierry, P. Mesini, A. Ponche, C. Contal, A. E. El Haitami, J. C. Voegel, B. Senger, P. Schaaf, B. Frisch and F. Boulmedais (2010a). "Polymer Multilayer Films Obtained by Electrochemically Catalyzed Click Chemistry." Langmuir **26**(4): 2816-2824.

Rydzek, G., J. S. Thomann, N. Ben Ameur, L. Jierry, P. Mesini, A. Ponche, C. Contal, A. E. El Haitami, J. C. Voegel, B. Senger, P. Schaaf, B. Frisch and F. Boulmedais (2010b). "Polymer Multilayer Films Obtained by Electrochemically Catalyzed Click Chemistry." Langmuir **26**(4): 2816-2824.

Sawamoto, M. and M. Kamigaito (2002). "Living Radical and Cationic Polymerizations in Water and Organic Media." Macromolecular Symposia **177**(1): 17-24.

Siegwart, D. J., J. K. Oh and K. Matyjaszewski (2012). "Atrp in the Design of Functional Materials for Biomedical Applications." Progress in Polymer Science **37**(1): 18-37.

Simakova, A., S. E. Averick, D. Konkolewicz and K. Matyjaszewski (2012). "Aqueous Arget Atrp." Macromolecules **45**(16): 6371-6379.

Stuart, M. A., W. T. Huck, J. Genzer, M. Muller, C. Ober, M. Stamm, G. B. Sukhorukov, I. Szleifer, V. V. Tsukruk, M. Urban, F. Winnik, S. Zauscher, I. Luzinov and S. Minko (2010). "Emerging Applications of Stimuli-Responsive Polymer Materials." Nature Materials **9**(2): 101-113.

Tang, W. and K. Matyjaszewski (2006). "Effect of Ligand Structure on Activation Rate Constants in Atrp." Macromolecules **39**(15): 4953-4959.

Tang, W. and K. Matyjaszewski (2007). "Effects of Initiator Structure on Activation Rate Constants in Atrp." Macromolecules **40**(6): 1858-1863.

Tsarevsky, N. V., W. A. Braunecker and K. Matyjaszewski (2007a). "Electron Transfer Reactions Relevant to Atom Transfer Radical Polymerization." Journal of Organometallic Chemistry **692**(15): 3212-3222.

Tsarevsky, N. V., W. A. Braunecker, A. Vacca, P. Gans and K. Matyjaszewski (2007b). "Competitive Equilibria in Atom Transfer Radical Polymerization." Macromolecular Symposia **248**(1): 60-70.

Tsarevsky, N. V. and K. Matyjaszewski (2006). "Environmentally Benign Atom Transfer Radical Polymerization: Towards “Green” Processes and Materials." Journal of Polymer Science Part A: Polymer Chemistry **44**(17): 5098-5112.

Tsarevsky, N. V. and K. Matyjaszewski (2007c). ""Green" Atom Transfer Radical Polymerization: From Process Design to Preparation of Well-Defined Environmentally Friendly Polymeric Materials." Chemical Reviews **107**(6): 2270-2299.

Tsarevsky, N. V., T. Pintauer and K. Matyjaszewski (2004). "Deactivation Efficiency and Degree of Control over Polymerization in Atrp in Protic Solvents." Macromolecules **37**(26): 9768-9778.

Tsujii, Y., K. Ohno, S. Yamamoto, A. Goto and T. Fukuda (2006). "Structure and Properties of High-Density Polymer Brushes Prepared by Surface-Initiated Living Radical Polymerization." Surface-Initiated Polymerization I **197**: 1-45.

van Dongen, S. F., H. P. de Hoog, R. J. Peters, M. Nallani, R. J. Nolte and J. C. van Hest (2009). "Biohybrid Polymer Capsules." Chemical Reviews **109**(11): 6212-6274.

Wang, J. S. and K. Matyjaszewski (1995). "Controlled Living Radical Polymerization - Atom-Transfer Radical Polymerization in the Presence of Transition-Metal Complexes." Journal of the American Chemical Society **117**(20): 5614-5615.

Wu, D., F. Xu, B. Sun, R. Fu, H. He and K. Matyjaszewski (2012). "Design and Preparation of Porous Polymers." Chemical Reviews **112**(7): 3959-4015.

Xu, F. J., K. G. Neoh and E. T. Kang (2009). "Bioactive Surfaces and Biomaterials Via Atom Transfer Radical Polymerization." Progress in Polymer Science **34**(8): 719-761.

Yahiro, C., M. Annaka, A. Kikuchi and T. Okano (2007). "Collapse and Swelling of Thermosensitive Poly(N-Isopropylacrylamide) Brushes Monitored by a Quartz Crystal Microbalance." Transactions of the Materials Research Society of Japan, Vol 32, No 3 **32**(3): 807-810.

Yan, J., B. Li, B. Yu, W. T. Huck, W. Liu and F. Zhou (2013). "Controlled Polymer-Brush Growth from Microliter Volumes Using Sacrificial-Anode Atom-Transfer Radical Polymerization." Angewandte Chemie, International Edition in English **52**(35): 9125-9129.

CHAPTER 4: ONE POT BUILDUP OF ELECTROSTATIC COHESIVE POLYANION / POLYCATION FILMS THROUGH A MORPHOGENIC APPROACH: RUBNER'S CHALLENGE IS OVERCOME.

4 One Pot Buildup of Electrostatic Cohesive Polyanion / Polycation Films Through a Morphogenic Approach: Rubner's Challenge is Overcome.

Contents

Chapter 4: One pot buildup of electrostatic cohesive polyanion/polycation films through a morphogenic approach: Rubner's challenge is overcome

4.1 ABSTRACT

All Polyelectrolyte multilayers are obtained by the alternate deposition of polyanions and polycations on a substrate. The Holy Grail would be to mix both constituents in solution and to have a film building up at the substrate through self-assembly. Based on the concept of morphogen driven self-construction of films, this challenge is addressed here by using a mixture of poly(styrene sulfonate) (PSS) and a charge shifting-polyelectrolyte, dimethylmaleic-modified poly(allylamine) (PAHd), which transforms into PAH under acidic conditions. By generating locally protons through the oxidation of hydroquinone under a constant current, a pH decrease is obtained near the electrode and leads to the continuous buildup of a PSS/PAH film. The different parameters affecting this buildup are discussed. It is shown that when using an enzyme instead of PSS, i.e. enzyme/PAHd solutions, an enzymatically active film is self-constructed whose activity increases with the deposition time. This process is well suitable to functionalize specifically micro-electrodes by enzymes.

4.2 INTRODUCTION.

Materials interact with their surrounding environment through their surface. Catalysis, molecular recognition or cell adhesion are typical examples of such interactions. During the last decades, progress in surface science allowed modifying and tuning material's surface properties in a highly controlled way by the development of new coating methods. Among the numerous surface functionalization strategies, the layer-by-layer (LbL) assembly of polyanions and polycations, leading to so-called polyelectrolyte multilayer films, is certainly the strategy that has attracted most attention (Decher 1997) (Skorb et al. 2013). It opened new avenues in fields such as biomaterials (Crouzier et al. 2010, Hammond 2012), energy storage (Xiang et al. 2012) and optical properties (Bravo et al. 2007). It is based on the stepwise formation of polyanion/polycation complexes held together through electrostatic interactions. It allows the formation of organic films whose thicknesses range from nano to micrometers. Yet, even if LbL buildup is a powerful functionalization tool, it is also a tedious one because often requiring numerous steps. Thus, as mentioned by Prof. Michael Rubner from MIT, one of the world's leading expert in polyelectrolyte multilayers, "*the Holy Grail in the field would be to mix all the film constituents of a multilayer in a single solution, bring it in contact with the surface and have a film that self-assemble*" (August 2008, Philadelphia).

This challenge can be addressed by using the concept of morphogen driven buildup of film. The concept of morphogen is of paramount importance in developmental biology where it is at the basis of morphogenesis (Potter 2007). But the concept can also be extended to chemistry where a

morphogen can be defined as a molecule or an ion that is produced at an interface, that diffuses into the solution, creating a gradient and which induces locally a chemical process. A first example of morphogen driven construction, even if the concept was not formalized by that time, dates back to the 80th: the electrodeposition of anti-corrosion films are triggered electrochemically by a pH change where the production of protons or hydroxide ions leads to a polymer precipitation (Beck 1988). This process was largely developed by Payne for the electro-deposition of biopolymers for biomaterial applications (Payne et al. 2013). In 2010, Johnson et al proposed to use locally induced electrochemical pH changes to deprotect peptides which then form a thin gel-film constituted of self-assembled fibers (Johnson et al. 2010). In 2006, Collman presented the first electrochemically driven functionalization through click chemistry catalyzed by Cu(I) (Devaraj et al. 2006). The catalyst was generated locally at an electrode by reduction of Cu(II). This approach, i.e. Cu(I) catalyzed click chemistry, was used to propose the first morphogen driven film buildup constituted of two interacting polymers (Rydzek et al. 2011). The role of the morphogen was played by Cu(I) generated at the electrode which catalyzed the reaction between azide and alkyne bearing polymers. Yet to overcome Rubner's challenge, the real obstacle is to obtain a self-assembly process of a film whose cohesion is based on electrostatic interactions. This is not obvious to reach since polyelectrolytes of opposite charges directly self-assemble to form polyanion/polycation complexes when mixed together in solution.

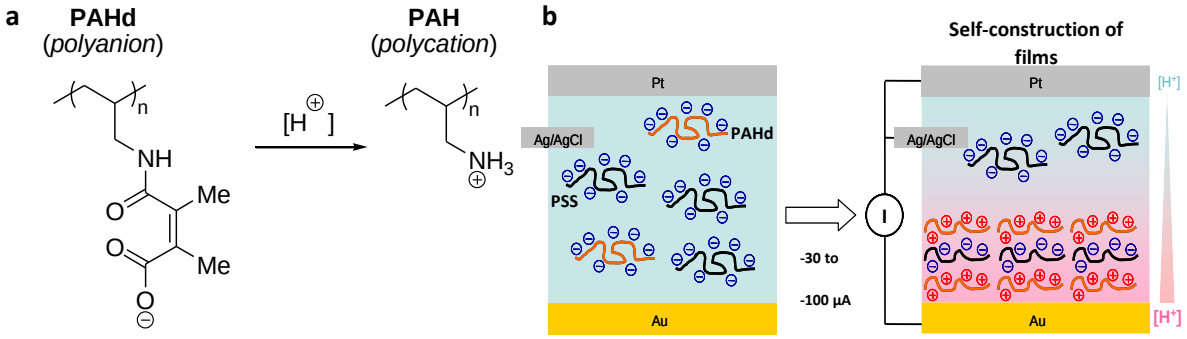

Figure 4.1 Principle of the charge shifting polyelectrolytes: chemical reaction of PAHd deprotection into PAH under acidic conditions (a). Schematic representation of the one pot buildup of electrostatic cohesive films triggered by the application of a constant current leading to a pH gradient (b). In the presence of a mixture of two polyanions (PAHd and poly(styrene sulfonate) (PSS)), this pH gradient allows the transformation of PAHd into polycations PAH that complexes with PSS present in the solution inducing the self-assembly of films.

Here, we present a strategy which merges the fields of polyelectrolyte multilayers and morphogen driven film buildup which allows addressing this challenge. It relies on *charge-shifting polyelectrolytes*, polyelectrolytes that under a pH trigger undergo a chemical transformation leading to an irreversible switch of their overall charge. Lynn introduced this class of polyelectrolytes to disrupt and release in a controlled manner, under a pH trigger, biologically active compounds from polyelectrolyte multilayers

(Liu et al. 2008). A charge shifting polyelectrolyte, negatively charged dimethylmaleic-modified poly(allylamine) (PAHd) was synthesized. At low pH, it transforms spontaneously and rapidly into a polycation poly(allylamine) (PAH) (Figure 4.1a). A solution of hydroquinone and two polyanions, the charge shifting polyelectrolyte (PAHd) and poly(styrene sulfonate) (PSS), is brought in contact with an electrode. A pH gradient is induced electrochemically by oxidation of hydroquinone into paraquinone that produces protons, the morphogens. The local decrease of pH allows the rapid transformation of the charge shifting polyanions (PAHd) into polycations (PAH) that will interact with the other polyanions (PSS), present in solution to form PAH/PSS complexes that grow on the electrode forming the polyelectrolyte film (Figure 4.1b).

4.3 RESULTS AND DISCUSSION.

Negatively charged PAHd was used as charge shifting polyelectrolyte. This polyanion undergoes gradual hydrolysis by decreasing the pH (Figure 4.1b) and transforms into PAH, a polycation widely used in the field of polyelectrolyte multilayers. Amide bond hydrolysis in aqueous solution is not a chemical reaction that occurs rapidly. However, maleic amide derivatives do not respect this rule. This class of amide bonds is cleaved easily at low pH providing free amino groups. The explanation of their ability of hydrolysis lies in the presence of a carboxylic groups close to the amide bond in a relative rigidity. In 2008, Lynn and collaborators have prepared citraconate-modified polyelectrolytes and used them to build multilayer films that erode themselves under a pH trigger (Liu et al. 2008).

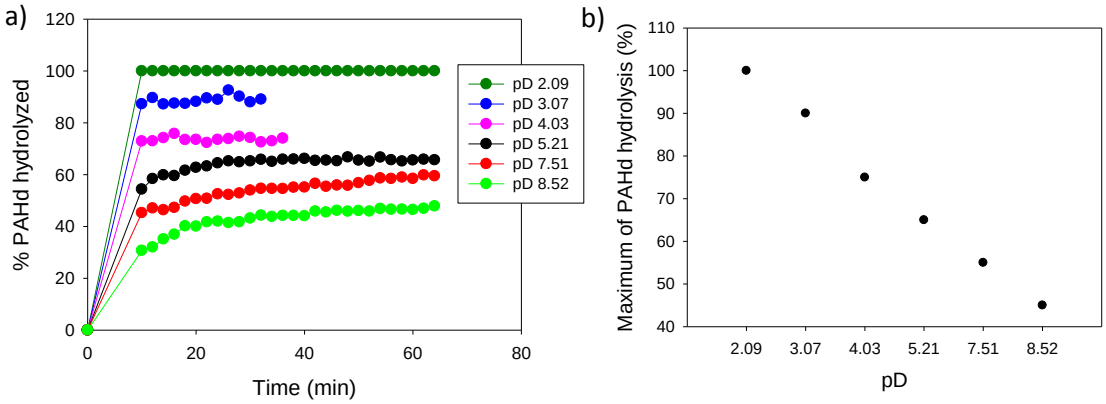

Figure 4.2 Kinetics of side chain amide hydrolysis of PAHd at different pDs determined by NMR spectroscopy (a) and evolution of the PAHd hydrolysis plateau as a function of the initial pD (b).

Based on a preliminary study (cf. chapter 5), PAHd was selected instead of citraconate-modified PAH because it appears to undergo a more rapid hydrolysis under a pH trigger. The hydrolysis of PAHd into PAH in solution as a function of pD (pD = $pH_{reading}$ + 0.41 (Glasoe et al. 1960)) was first investigated by NMR spectroscopy at room temperature. The evolution of the percentage of hydrolyzed PAHd as a

function of time for different pD values is represented in Figure 4.2a. The hydrolysis takes place rapidly (less than 10 min) reaching a plateau value that increases with the decrease of pD. The evolution of the plateau value as a function of the initial pD is represented in Figure 4.2b. For pD values below 3, almost 100% of the dimethylmaleic groups are hydrolyzed. PAHd thus appears to be the charge-shifting polyelectrolyte of choice to overcome Rubner's challenge.

This challenge was first addressed by using a solution containing both PAHd and PSS. PSS is a strong acid, which is fully charged over a large pH range and in particular around the pH at which PAHd undergoes hydrolysis. Moreover, PAH/PSS is a polyelectrolyte pair leading to one of the most robust polyelectrolyte multilayer.

Several methods are described to create a gradient of protons from an electrode. By electrochemical oxidation of hydroquinone into 1,4-benzoquinone, two electrons are transferred to the electrode concomitantly with the production of two protons released in the media. Compared to the electrolysis of water which is another common way to generate protons, the oxidation of hydroquinone allows working with a lower oxidative potential, roughly 0.3-0.4 V and therefore is convenient with the use of gold-coated working electrode. By oxidizing hydroquinone at an electrode, a pH of 3.6 has been calculated in the close vicinity of the surface that increases gradually to neutral away from it (Johnson et al. 2010).

Electrochemical-quartz crystal microbalance (EC-QCM) was used to monitor the buildup *in situ* during the application of the current. The electrode was first covered with a layer of branched poly(ethylenimine) (PEI) to ensure a strong anchoring on the surface followed by the deposition of a PSS layer rendering the surface negatively charged. This is intended to prevent non-specific adsorption of PSS and PAHd. When such a functionalized electrode is brought in contact with PAHd in the presence of hydroquinone at pH 7, a small frequency shift (2Hz) is observed as expected. As soon as a current of -100 µA is applied, the frequency shift decreases rapidly and stabilizes at around -20 Hz (

Figure 4.3), corresponding typically to the deposition of one PAH layer on the previously adsorbed PSS layer.

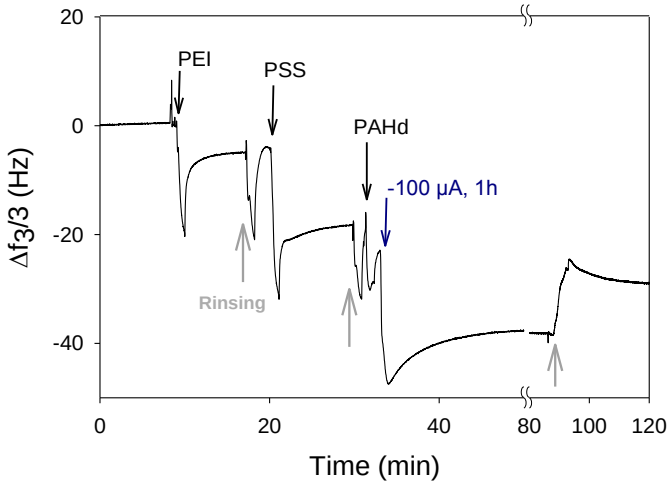

Figure 4.3 Evolution of the frequency shift $\Delta f_3/3$, measured by EC-QCM-D, as a function of time when a current of -100 µA is applied on an aqueous PAHd solution containing PSS (both at 1 mg/ml) and hydroquinone (60 mM) at pH 7.

When this experiment is repeated in the presence of a mixture of PAHd/PSS and hydroquinone under a flow rate of 0.05 ml/min, no signal is observed in the absence of current. The flow rate was imposed to ensure a constant concentration of reactants in the electrochemical cell. The current intensity was first varied from -30 to -100 µA (lower currents rapidly lead to a saturation of the QCM signal) while keeping the pH of the buildup solution at 7. The frequency shift decreases, in first approximation, linearly with time, the slope of this decrease being indicative of the buildup kinetics of the film (Figure 4.4).

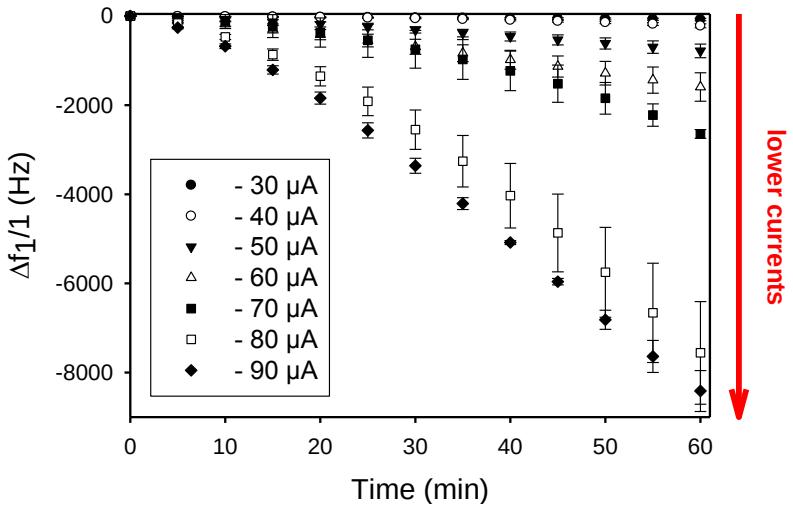

Figure 4.4 Evolution of the frequency shift $\Delta f_1/1$, measured by EC-QCM-D, as a function of time during the self-construction of PAHd/PSS buildup for applied current ranging from -30 to -90 µA. PAHd/PSS solutions were prepared at 1 mg/ml each in the presence of hydroquinone (60 mM) at pH 7.

The PAHd/PSS film buildup kinetic strongly depends on the applied current: lower currents leads to higher buildup kinetic. Such results make sense since lower currents lead to more acidic conditions in the vicinity of the working electrode. For more positive currents such as -30 and -40 µA, almost no

buildup is observed. The frequency shift decrease stops as soon as the current is switch off and starts again when the current is switch on again (Figure 4.5). In the sole presence of PSS and hydroquinone in solution, no frequency change is observed (data not shown). These experiments prove the continuous buildup of a film, in the presence of PAHd and PSS under electrochemical control. Moreover, the presence of both partners is required for the film to construct which strongly indicates the buildup of a PAH/PSS film.

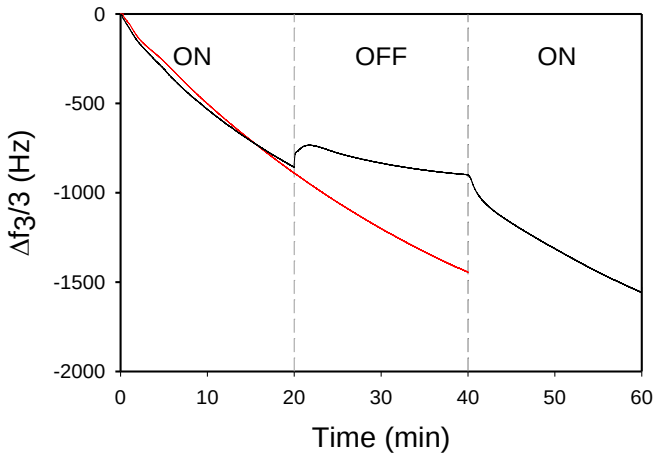

Figure 4.5 Evolution of the frequency shift $\Delta f_3/3$, measured by EC-QCM-D, as a function of time during the self-construction of PAHd/PSS film for a current applied at -70 µA during 40 min. The construction is done continuously (red line) or in two steps of 20 min (black line).

The simultaneous presence of both partners in the film is proven through X-ray photoelectron experiments (XPS). Indeed, atomic composition of films obtained at -40 µA, -60 µA, -80 µA and -100 µA have been analyzed after 60 min of self-construction. For all these films, the presence of both constituting polymers PAH and PSS is confirmed by a ratio between sulphur atom from sulphate and nitrogen from ammonium groups. This ratio S(2p)/N(1s), corresponding to the atomic ratio PSS/PAH, is measured between 1.12 and 1.34 showing a small excess of PSS in the obtained films (Figure 4.6a). The ratio of NHCO/N(1s) allows to get access to the deprotection ratio of PAHd. The hydrolysis of the PAHd is complete for current intensities below -60 µA (Figure 4.6b).

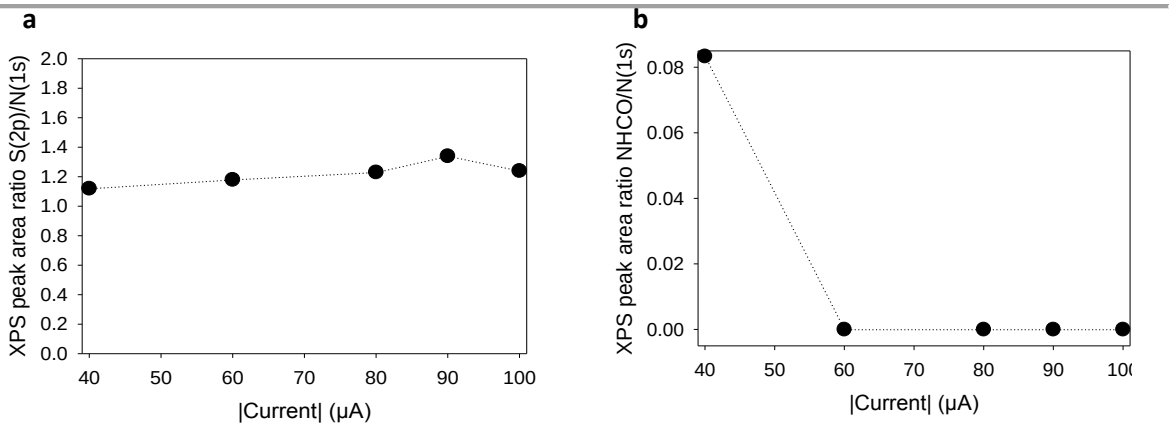

Figure 4.6. S(2p)/N(1s) ratio, corresponding to the atomic ratio of PSS/PAH (a), and NHCO/N(1s) ratio (b), corresponding to the deprotection degree of PAHd, determined by XPS on self-constructed films prepared from PAHd/PSS mixture through the application of different values of current intensity -40, -60, -80, -90 and -100 µA.

The morphology of the deposited film was characterized by Atomic Force Microscopy (AFM) in contact mode and liquid conditions. After scratching, the thickness of the film was also determined. Figure 4.7a shows a typical morphology corresponding to a film constructed during 45 min at pH 7 with a current of -90 µA.

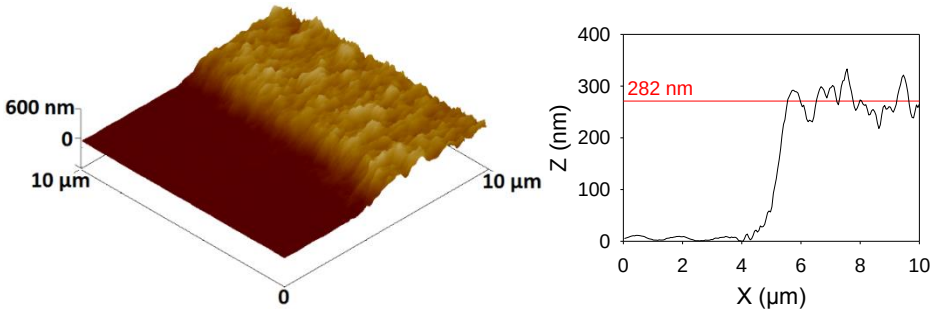

Figure 4.7 Typical 3D AFM image, in contact mode and liquid state, of a scratched film obtained by self-construction of PAHd/PSS solution at -90 µA during 45 min (a). Section profile of the scratched film (b). The mean value of three profile gives a thickness of 282 ± 11 nm.

The film appears homogeneous and rough with a thickness of the order of 282 ± 11 nm (determined on three z section measurements) and a roughness of 43 nm (determined on a 10x10 µm² image). The high roughness observed is due to the self-assembly of PAH/PSS complexes on the substrate. This thickness increases as a function of the time over which the current is applied (Figure 4.8). Figure 4.9 shows the evolution of the film thickness and roughness with respect to the buildup time. This confirms that the steady decrease of the frequency shift with time under application of a constant current corresponds to a continuous increase of the film thickness.

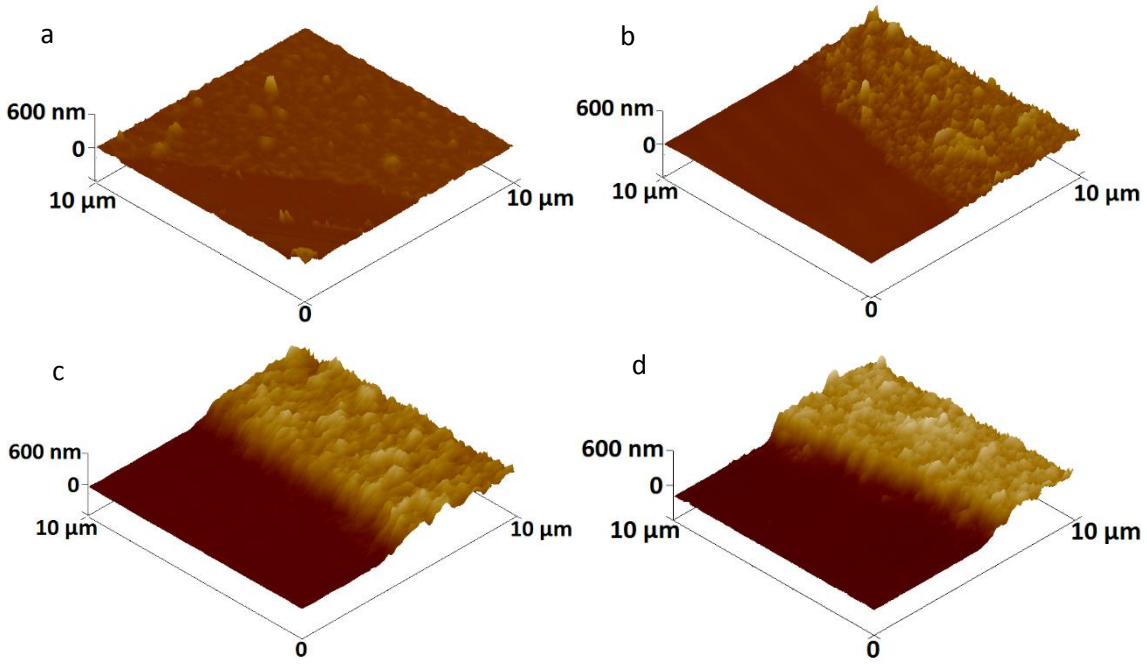

Figure 4.8 Typical 3D AFM image of a scratched film obtained by self-construction of PAHd/PSS solution at -90 µA during 15 (a), 30 (b), 45 (c), and 60 (d) minutes.

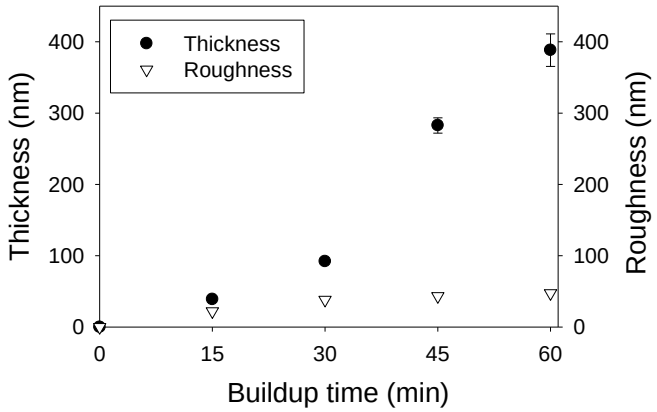

Figure 4.9 Evolution of PAHd/PSS film thickness and roughness for an applied current of -90 µA during 15, 30, 45 and 60 minutes. The film thicknesses were evaluated on three profilometric measurement of the scratch. The roughnesses of the films were evaluated on 10×10 µm² AFM images.

Figure 4.9 shows that the PAHd/PSS film grows over time for a fixed current of -90 µA. The film roughness is high for low construction time but stays constant while the film grows. Thicker films are then smoother than thin films.

To gain more insight of the mechanism several parameters that might influence the buildup process were varied. Figure 4.10 shows that the buildup kinetics, i.e. the frequency shift value after 35 min of construction, increases when the current intensity is decreased. This is expected since a

decrease of the current corresponds to an increase of the proton generation and thus to a stronger lowering of the pH near the electrode.

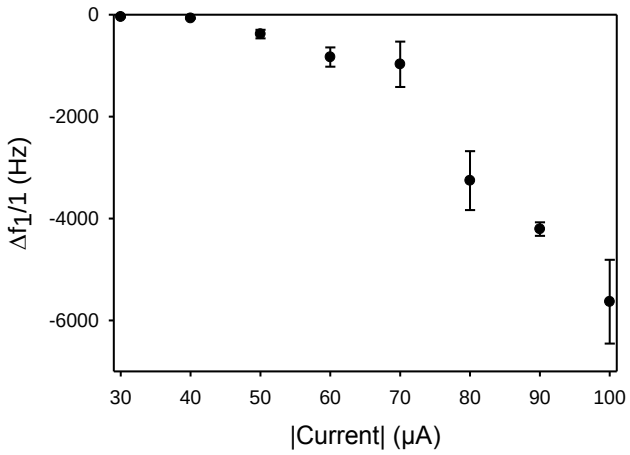

Figure 4.10 Variation of the buildup kinetic with respect to the current applied. The buildup kinetic is defined as the frequency shift $\Delta f_1/1$ obtained after 35 min of self-construction of the PAHd/PSS film at pH 7.

The influence of the pH of the buildup solution was also investigated for an applied current of -100 µA (Figure 4.11). At pH 6.5, the buildup process cannot take place because the PAHd/PSS solution becomes rapidly turbid, indicating the rapid hydrolysis of PAHd into PAH in solution and the formation, in solution, of PAH/PSS complexes. At pH 8, no frequency shift is observed even when a current of -100 µA is applied, indicating the absence of film buildup. At pH 7.5, the buildup kinetic is decreased.

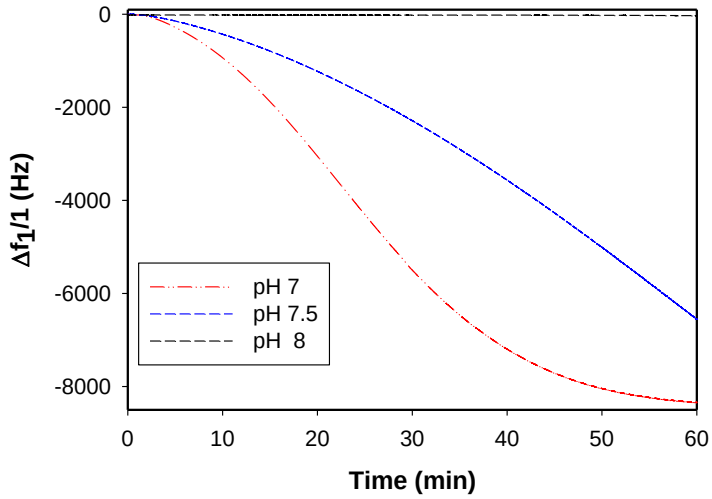

Figure 4.11 Evolution of the frequency shift $\Delta f_1/1$, measured by EC-QCM-D, as a function of time during the self-construction of PAHd/PSS film for a current applied of -100 µA during 1h for different values of buildup pH.

It thus comes out that the pH window allowing the buildup process to take place is fairly narrow, lying between 7 and 8. It must also be noticed that when the experiments were realized in HEPES buffer solution at pH 7, no film buildup was observed (data not shown). This is expected since in a

buffer solution the production of protons at the interface is neutralized by the buffer. The pH change near the electrode is thus strongly reduced, hindering the hydrolysis of PAHd. This also indicates that it is the local pH decrease that must be the film buildup trigger.

PSS interacts strongly with PAH leading to PAH/PSS multilayer that can be constructed over a very large range of conditions (pH, ionic strength…). This is why this system was selected for a proof of principle. To generalize this concept, PSS was replaced by an enzyme, alkaline phosphatase (AP), whose Ip is close to 4. It is thus negatively charged at pH 7. Similarly to the PSS case, almost no frequency shift is observed in the presence of enzyme/PAHd solutions, in the absence of current and as soon as a current of -100 µA is applied frequency shifts take place (Figure 4.12). The buildup kinetic is much slower than for PSS probably due to a different charge ratio between PAHd and AP. This demonstrates that the film buildup platform based on PAHd is versatile and that one can replace negatively charged PSS by other negatively charged macromolecules.

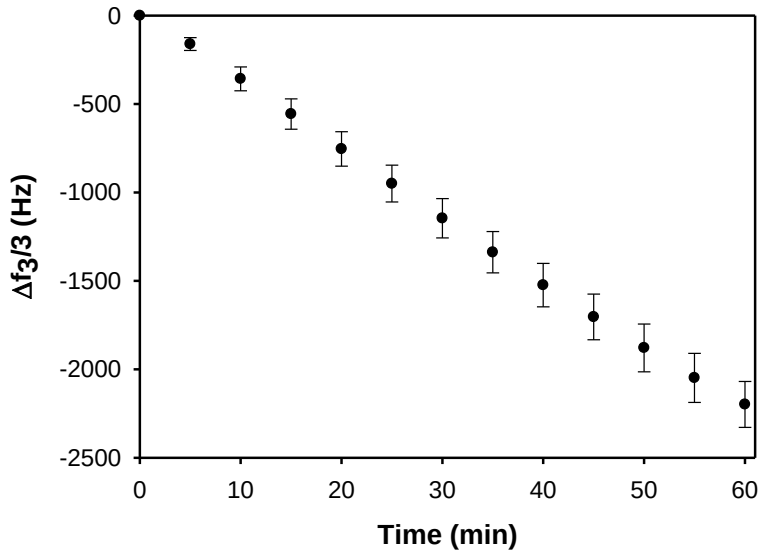

Figure 4.12 Evolution of the frequency shift $\Delta f_3/3$, measured by EC-QCM-D, as a function of time during the self-construction of PAHd/AP film for a current applied of -100 µA during 1h. PAHd and AP were at 1 mg/ml, pH7 in the native solution.

It was verified by AFM that the application of a current indeed leads to a film deposition (Figure 4.13). The obtained PAHd/AP film appears homogeneous and rough with a mean thickness of 19 ± 5 nm.

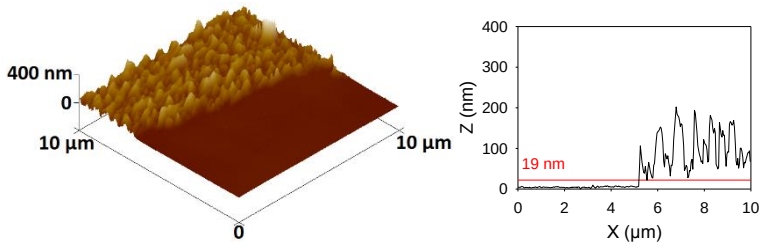

Figure 4.13 Typical 3D AFM image of PAHd/AP film built at -100 µA during 1h. Profilometric measurement on the scratch gives a mean thickness of 19 ± 5 nm.

Using paranitrophenyl phosphate, substrate of AP, it was verified that AP remains enzymatically active in the self-constructed PAHd/AP film. Paranitrophenyl phosphate is transformed into paranitrophenyl and phosphate ions in the presence of AP and the reaction was followed by UV spectroscopy at 405 nm (Figure 4.14a). PAHd/AP films were built by the application of -100 µA during 15, 30 and 45 minutes. The enzymatic activity of the film increases with the construction time (Figure 4.14b). This indicates that not only the enzymes present at the outer part of the film are active but the entire film. This result is extremely interesting for future biosensor applications since it should allow increasing sensor sensitivity simply by increasing the film deposition time.

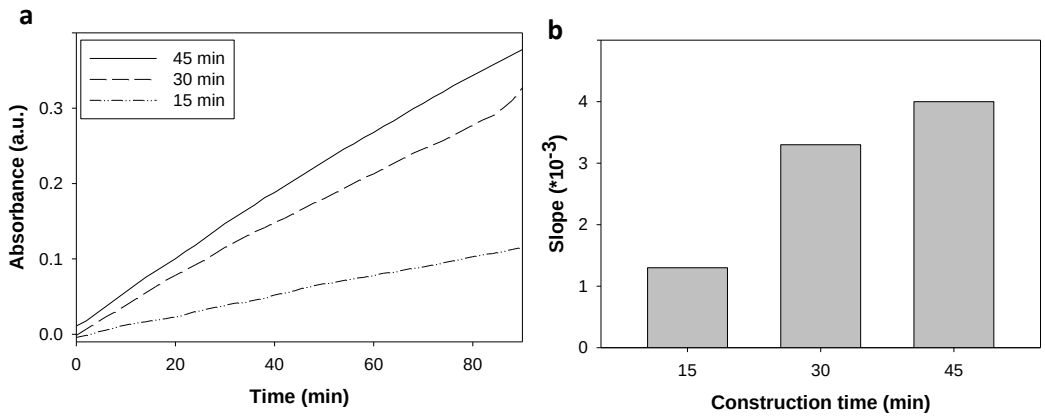

Figure 4.14 Evolution of the absorbance as a function of time of the supernatant of PAHd/AP film, containing paranitrophenyl phosphate (a). Variation of the PAHd/AP film activity for different construction times (b). PAHd/AP films were constructed by applying -100 µA during 15, 30 and 45 minutes. Paranitrophenyl phosphate is transformed into paranitrophenyl and phosphate ions in the presence of AP and the reaction was followed by UV spectroscopy at 405 nm.

Finally since the pH shift is localized near the electrode, it should be adequate to functionalize miniaturized electrode surfaces. Two films bearing a fluorescence dye were buildup on a micro-electrode array. The first film, made of PAHd/PSS labelled with rhodamine, was buildup during one hour by the application of -100 µA on the suited electrode. The second film, made of PAHd/AP labelled with fluoresceine isothiocyanate, was constructed by the application of -100 µA during one hour on another micro-electrode. Fluorescence images were taken on the two micro-electrodes to check the presence of the films and to verify their spatial localization (Figure 4.15).

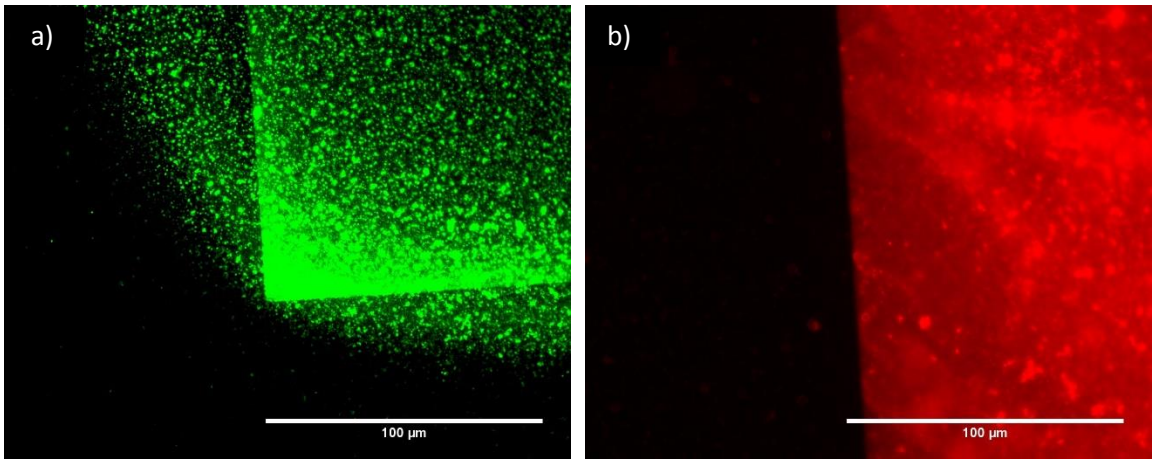

Figure 4.15 Fluorescence images of the PAHd/AP_{fitc} (a) and of the PAHd/PSS_{rho} (b) films constructed on the micro-electrodes.

The fluorescence images show that both of the films constructed on the desired micro-electrode. The PAHd/PSS_{rho} film exhibit a good spatio-selectivity since no fluorescence is observed on the insulating substrate. The PAHd/AP_{fitc} film also displays a good spatio-selectivity but a small gradient of fluorescence is observed on the insulating substrate. This is mainly due to the autofluorescence of the resin that is part of the microelectrodes combined with the low fluorescence of AP. This opens the route towards the functionalization of nanoelectrode arrays.

4.4 CONCLUSION.

Based on the concept of morphogen driven self-construction of films, the self-assembly of polyelectrolyte films was addressed by using a mixture of PSS and a charge shifting-polyelectrolyte PAHd, which transforms into PAH under acidic conditions. By generating locally protons through the oxidation of hydroquinone under a constant current, a pH decrease is obtained near the electrode and leads to the continuous buildup of a PAH/PSS film. The buildup kinetics increases when the current intensity is decreased from -30 µA to -100 µA. The pH window allowing the buildup process to take place is fairly narrow, lying between 7 and 8. XPS allows to determine that the atomic ratio PSS/PAH is lying between 1.12 and 1.34 showing a small excess of PSS in the obtained films. When using an enzyme instead of PSS, i.e. PAHd/enzyme solutions, an enzymatically active film is self-constructed whose activity increases with the deposition time. This process is well suitable to functionalize specifically micro-electrodes by enzymes opening the route towards miniaturized biosensors.

4.5 MATERIAL AND METHODS.

4.5.1 Synthesis of dimethylmaleic-modified poly(allylamine) (PAHd).

PAH (0.5 g, 5.3 mmol, 1.0 eq.) was dissolve in 1M NaOH aqueous solution (15 mL) and stirred overnight. 2,3-Dimethylmaleic anhydride (2.7 g, 21.4 mmol, 4.0 eq.) was added by portion maintaining the pH of the reaction solution above 10 by addition of 6M NaOH aqueous solution. The reaction mixture was stirred overnight at room temperature then dialyzed with a cellulose ester membrane (MWCO 14000-16000) against Milli-Q water (adjusted to pH > 10 using NaOH aqueous solution) for 3 days. The final solution was freeze dried to give the desired PAHd as a white solid (0.938 g, 80%): FTIR (neat): 3264, 2914, 2852, 1630, 1554, 1392, 1305 cm^{-1}; ^{1}H NMR (D_2O, 400 MHz) δ 3.25 (bs, 2H), 1.86 (m, 8H), 1.27 (bs, 2H); ^{13}C NMR (D_2O, 100 MHz) δ 179.1, 175.2, 138.3, 129.5, 43.3, 36.3, 32.7, 16.7, 16.2.

4.5.2 Polyelectrolyte solutions.

Polyelectrolyte solutions at 1 mg/mL were prepared by dissolution of the adequate amount of polyelectrolytes in 150 mM $NaNO_3$ aqueous solution. The PAHd/PSS and PAHd/AP films were built as follow: a bilayer assembly was started onto a bare gold substrate by adsorbing positively charged poly(ethylenimine) (PEI, *M* = 750 000 g/mol) followed by poly(styrene) sulfonate (PSS, *M* = 70 000 g/mol). This first electrostatic bilayer promotes further film buildup. PAHd solution was prepared in presence of PSS or AP (1mg/mL each) in 150 mM $NaNO_3$ aqueous solution with 60 mM Hydroquinone at pH 7.

4.5.3 NMR spectroscopy study of PAHd hydrolysis.

The hydrolysis of PAHd into PAH in solution as a function of pH was first investigated by NMR spectroscopy (Bruker Advance DPX400 spectrometer) at room temperature. The samples were prepared as follows: PAHd (5.1 mg) was dissolved in D_2O (600 µL) containing *tert*-butanol as internal reference (1.24 ppm). The desired pDs were adjusted with a solution of 0.1 M NaOD in deuterium oxide using the equation (Glasoe et al. 1960):

$$pD = pH_{reading} + 0.41$$

The resulting solution was put into a NMR tube and the spectra were recorded at 400 MHz every 2 min for one hour. We calculated the percentage of side chain amide hydrolysis of PAHd by comparing

the relative peak areas of the methyl group in PAHd and the methyl group of hydrolysis residues (dimethylmaleic anhydride and dimethylmaleic acid) using the equations below (Figure 4.16).

$$Z = \frac{x+y-3}{2} \qquad \%PAHd\ hydrolyzed = \frac{100*Z}{3+Z}$$

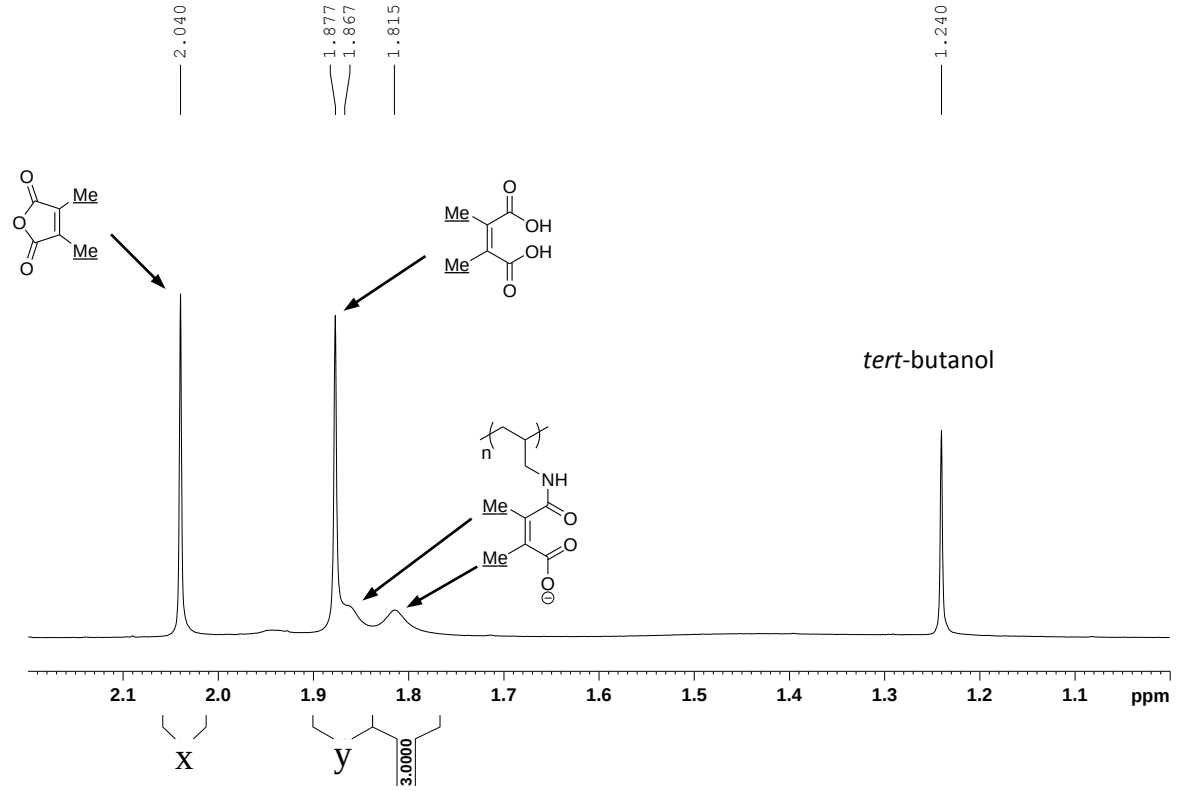

Figure 4.16 NMR spectra of PAHd during its hydrolysis.

4.5.4 Film buildup procedure.

An anchoring bilayer of poly(ethylene imine) (PEI) and poly(styrene sulfonate) (PSS) was deposited onto the gold working electrode by the LbL technique prior to the polyampholyte film buildup.

The aqueous PEI solution (1 mg/ml in 150 mM sodium nitrate) was injected in the electrochemical cell (600 µl) at a flow rate of 600 µL/min with a peristatic pump. The adsorption of the polycation was monitored by EC-QCM-D. Once the signal stabilizes, i.e. after ca. 5 minutes, an aqueous solution of sodium nitrate was injected in the cell to rinse it (600 µl at 600 µl/min) during 2 minutes.

The aqueous polyanion solution (PSS at 1 mg/ml in 150 mM sodium nitrate) was then injected in the cell (600 µL at 600 µl/min) with the peristatic pump. The adsorption of the polyanion on the previous polycation layer was monitored by EC-QCM-D. Once the signal stabilizes, i.e. after ca. 5 minutes, an aqueous solution of sodium nitrate was injected in the cell to rinse it (600 µl at 600 µl/min) during 2 minutes.

An aqueous solution of sodium nitrate (150 mM) containing PAHd (1 mg/ml), PSS (1 mg/ml) and hydroquinone (60 mM) at pH 7 was then injected in the electrochemical cell (600 µl at 600 µL/min). Once the EC-QCM-D signal stabilized, a flow rate of 50 µl/min was established.

A galvanostatic current ranging from -30 to -100 µA was then applied for 1h to trigger the hydroquinone oxidation and start the polyampholyte film buildup. After a construction time of 1h, an aqueous solution of 150 mM sodium nitrate was injected in the cell (600 µL at 600 µl/min). Once the signal stabilizes, i.e. ca. 5-10 minutes, the signal monitoring of the EC-QCM-D was stopped. The gold working electrode was then un-mounted from the EC-QCM-D and dried with a flow of dry air for 5 minutes and the samples were stored in dry state.

4.5.5 Functionalization of microelectrodes.

The microelectrode structure (IDA ref: A-012125, Biologic) was first immersed in a PEI (1 mg/ml in 150 mM $NaNO_3$), buffer and PSS (1 mg/ml in 150 mM $NaNO_3$) solutions. The formation of an anchor bilayer later promotes the film buildup.

An aqueous solution of 150mM sodium nitrate containing PAHd (1mg/ml), PSS (0.9 mg/ml), PSS rhodamine (0.1 mg/ml) and hydroquinone (60 mM) was brought into contact with the microelectrodes. The microelectrode was addressed during 1h through the application of a current (-90 µA) with the CHI 660e potentiostat/galvanostat.

An aqueous solution of 150mM sodium nitrate containing PAHd (1mg/ml), AP (0.9 mg/ml), AP fluoresceine (0.1 mg/ml) and hydroquinone (60 mM) was brought into contact with the microelectrodes. The microelectrode was addressed during 1h through the application of a current (-90 µA) with the CHI 660e potentiostat/galvanostat.

4.6 COMPLEMENTARY RESULTS.

4.6.1 XPS analysis of the PAHd/PSS film.

Table 1. Binding energies and area percentages of nitrogen functionalities of the film prepared from PAHd and built through the application of various intensities: -40, -60, -80, -90 and -100 µA.

I (µA/cm^2)	XPS peak area (%)		
	NH_2 (399.9-400.0 eV)	NHCO (400.9 eV)	NH_3^+ (401.9-402.0 eV)
-40	44	8	48
-60	27	_	73
-80	26	_	74

-90	24	_	76
-100	25	_	75

Table 2. S 2p/NH_3^+ ratio determined by XPS of the film prepared from PAH-D and built through the application of various intensities: -40, -60, -80, -90 and -100 µA.

I (µA/cm^2)	40	60	80	90	100
Area of XPS peak ratio S 2p/NH_3^+	1.12	1.18	1.23	1.34	1.24

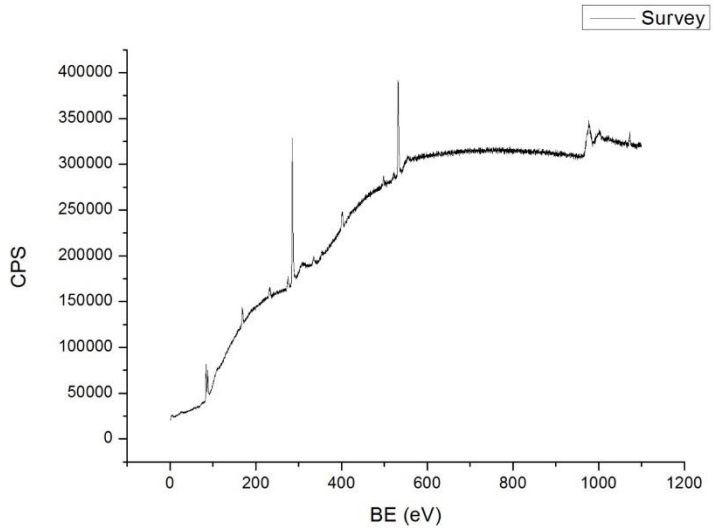

Figure 4.17. XPS survey spectrum of the film prepared from PAHd/PSS solution through the application of a current intensity of -40 µA.

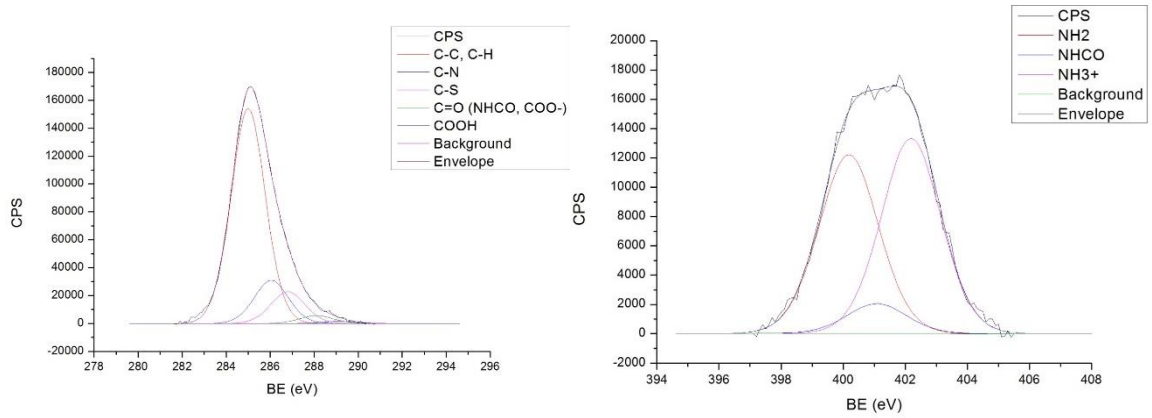

Figure 4.18. XPS (a) C 1s and (b) N 1s peaks of the film prepared from PAHd/PSS solution through the application of a current intensity of -40 µA.

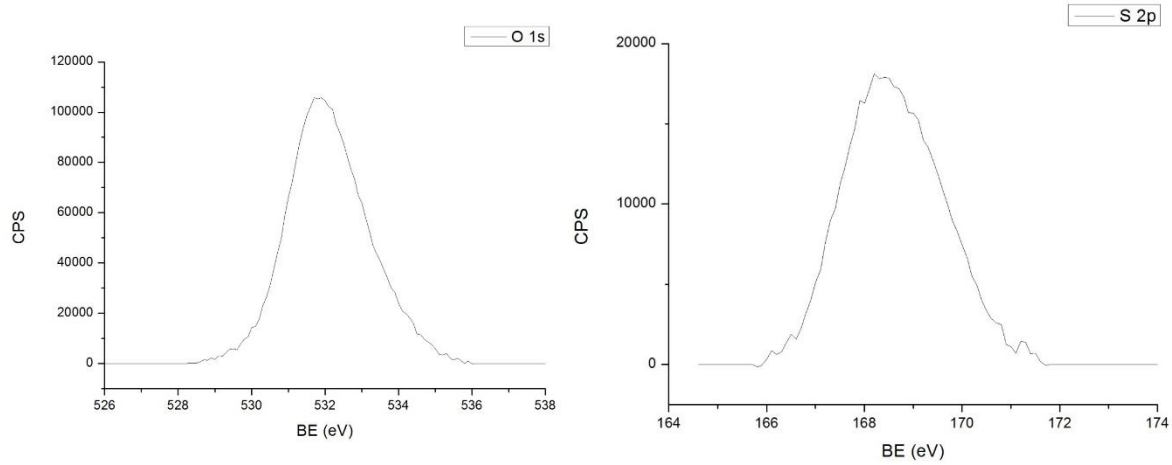

Figure 4.19. XPS (a) S 2p and (b) O 1s peaks of the film prepared from PAHd/PSS solution through the application of a current intensity of -40 μA.

REFERENCES

Beck, F. (1988). "Electrodeposition of Polymer-Coatings." Electrochimica Acta **33**(7): 839-850.

Bravo, J., L. Zhai, Z. Z. Wu, R. E. Cohen and M. F. Rubner (2007). "Transparent Superhydrophobic Films Based on Silica Nanoparticles." Langmuir **23**(13): 7293-7298.

Crouzier, T., T. Boudou and C. Picart (2010). "Polysaccharide-Based Polyelectrolyte Multilayers." Current Opinion in Colloid & Interface Science **15**(6): 417-426.

Decher, G. (1997). "Fuzzy Nanoassemblies: Toward Layered Polymeric Multicomposites." Science **277**(5330): 1232-1237.

Devaraj, N. K., P. H. Dinolfo, C. E. D. Chidsey and J. P. Collman (2006). "Selective Functionalization of Independently Addressed Microelectrodes by Electrochemical Activation and Deactivation of a Coupling Catalyst." Journal of the American Chemical Society **128**(6): 1794-1795.

Glasoe, P. K. and F. A. Long (1960). "Use of Glass Electrodes to Measure Acidities in Deuterium Oxide1,2." The Journal of Physical Chemistry **64**(1): 188-190.

Hammond, P. T. (2012). "Building Biomedical Materials Layer-by-Layer." Materials Today **15**(5): 196-206.

Johnson, E. K., D. J. Adams and P. J. Cameron (2010). "Directed Self-Assembly of Dipeptides to Form Ultrathin Hydrogel Membranes." Journal of the American Chemical Society **132**(14): 5130-5136.

Liu, X. H., J. T. Zhang and D. M. Lynn (2008). "Polyelectrolyte Multilayers Fabricated from 'Charge-Shifting' Anionic Polymers: A New Approach to Controlled Film Disruption and the Release of Cationic Agents from Surfaces." Soft Matter **4**(8): 1688-1695.

Payne, G. F., E. Kim, Y. Cheng, H. C. Wu, R. Ghodssi, G. W. Rubloff, S. R. Raghavan, J. N. Culver and W. E. Bentley (2013). "Accessing Biology's Toolbox for the Mesoscale Biofabrication of Soft Matter." Soft Matter **9**(26): 6019-6032.

Potter, J. D. (2007). "Morphogens, Morphostats, Microarchitecture and Malignancy." Nature Reviews Cancer **7**: 464-474.

Rydzek, G., L. Jierry, A. Parat, J. S. Thomann, J. C. Voegel, B. Senger, J. Hemmerle, A. Ponche, B. Frisch, P. Schaaf and F. Boulmedais (2011). "Electrochemically Triggered Assembly of Films: A One-Pot Morphogen-Driven Buildup." Angewandte Chemie, International Edition in English **50**(19): 4374-4377.

Skorb, E. V. and H. Mohwald (2013). "25th Anniversary Article: Dynamic Interfaces for Responsive Encapsulation Systems." Advanced Materials **25**(36): 5029-5042.

Xiang, Y., S. F. Lu and S. P. Jiang (2012). "Layer-by-Layer Self-Assembly in the Development of Electrochemical Energy Conversion and Storage Devices from Fuel Cells to Supercapacitors." Chemical Society Reviews **41**(21): 7291-7321.

CHAPTER 5: ELECTROCHEMICALLY TRIGGERED MORPHOGEN DRIVEN SURFACE CONFINED SELF-ASSEMBLY OF POLYAMPHOLYTES BASED ON CHARGE-SHIFTING POLYELECTROLYTES

5 ELECTROCHEMICALLY TRIGGERED MORPHOGEN DRIVEN SURFACE CONFINED SELF-ASSEMBLY OF POLYAMPHOLYTES BASED ON CHARGE-SHIFTING POLYELECTROLYTES.

CONTENTS

Chapter 5: Electrochemically triggered morphogen driven surface confined self-assembly of polyampholyte based on charge shifting polyelectrolytes

5.1 ABSTRACT.

We demonstrated that polyampholyte-based films can be efficiently self-assembled onto a surface in a one-pot manner. By using a gradient of protons generated at an electrode surface, a charge-shifting polyelectrolyte present in solution can be transformed in a polyampholyte, leading to the continuous buildup of a film based on electrostatic interactions.

5.2 CONTEXT OF THE STUDY.

Polyelectrolyte multilayers constitute a very powerful and versatile tool allowing the functionalization of almost any kind of substrate, whatever its chemical nature and morphology (Decher 1997). Obtained by the alternate deposition of polyanions and polycations on a surface, they rely on electrostatic interactions between positive and negative charges and can be considered as polyanion/polycation complex assemblies. Because of this alternation between positive and negative charges, polyelectrolyte multilayers necessitate, by essence, the use of two types of polyelectrolytes. Recently, it was however reported that one can also buildup, in a step-by-step manner, films from a single solution containing polycation/polyanion complexes, PEDOT and PSS respectively (PEDOT: poly(3,4-ethylenedioxythiophene); PSS: poly(styrene sulfonate)) (de Saint-Aubin et al. 2012). Yet, this film was obtained by a step-by-step adsorption of each layer of PSS-PEDOT realized by spin-coating and followed by a drying step after each deposition. Powerful and versatile, the layer-by-layer technology suffers from some drawbacks. One of them is that the buildup process can be long and tedious when an important number of deposition steps are required. It is thus of interest to develop alternative buildup strategies, in particular one-pot strategies which are by far more rapid and convenient. Caruso and Qiao have recently developed a concept moving in this direction based on the Continuous Assembly of Polymers (CAP) through sequential and chemical cross-linking steps (Mertz et al. 2011). Yet, the main question is, how to obtain a single solution with constituents that will not interact together but interact exclusively near the interface leading to one-pot film buildups ? The answer can come from a biomimetic inspiration, by simply having a look how nature initiates and creates complex three dimensional morphologies at one pole of an undifferentiated cell during embryogenesis: Nature uses *morphogens* (Millar 2002, Potter 2007). Morphogens can be defined as chemical species that are generated locally, diffuse into solution, through tissues and affect cell fate. In

2011, our group has introduced a new strategy to build, in a one-pot manner, thin films made of polymers of same charge but covalently linked by the azide/alkyne click reaction. This reaction is catalysed by Cu(I) which was electrochemically generated *in situ* at an electrode and played the role of morphogen (Rydzek et al. 2011). This approach of film buildup has been actively developed so far by us (Rydzek et al. 2012a, Rydzek et al. 2012b, Rydzek et al. 2013) and the community (Rydzek et al. 2014). But without formalising it, the morphogen approach is used since long times in the car industry to produce anti-corrosion surfaces. There, one generates electrochemically protons, the morphogens, which diffuse into the solution and interact with polymers rendering them insoluble. Electro-precipitation induced by pH changes has been largely exploited by the group of Payne who developed films based on chitosan, a polysaccharide known to become insoluble in water above pH 6.5 (Wu et al. 2002). Using a charge shifting polymer, namely a negatively charged dimethylmaleate-modified poly(allylamine) (PAHd), we showed that one can construct, in a one pot manner a (PAH/PSS) film starting from a mixture of two polyanions, PAHd and PSS in solution (chapter 4). The pH trigger, localized near an electrode was obtained by oxidizing hydroquinone into 1,4-benzoquinone, releasing two protons from the electrode (cathode). This acidic gradient transforms PAHd in PAH, leading to an electrostatic complexation between PAH and PSS formed in the close vicinity of the electrode.

Herein, we demonstrate that this concept can be extended one step further to obtain a one pot buildup of films made from only one polyelectrolyte. By using citraconate-modified poly (allylamine hydrochloride) (PAHc), a partially charge shifting polyelectrolyte, it is possible to generate *in situ* a polyampholyte. This polymer can be self-assembled due to charge complexation leading to a polyampholyte-based film. This original approach can be considered as the ultimate simplified polymer system leading to a one-pot film deposition.

Amide bonds hydrolysis in aqueous solution is not a chemical reaction that occurs rapidly. However, maleic amide derivatives do not respect this rule. Indeed, this class of amide bonds used to be cleaved easily at low pH providing free amino groups (Kirby et al. 1972). The explanation of its ability of hydrolysis lies in the presence of a carboxylic groups close to the amide bond in a relative rigidity (Aldersley et al. 1974). In 2008, Lynn and collaborators have prepared a citraconate-modified polyelectrolyte (PAHc) and used it to build multilayer films in a step-by-step manner (Liu et al. 2008). The hydrolysis property of the PAHc allows a gradual erosion of the multilayer over time, depending on the pH in the media. This elegant strategy has been used to control the release of biological compounds due to the degradation of the film. It must be noted that the PAHc has two isomers of citranonic acid groups grafted along the polymer backbone: one with the methyl group in α position

(proximal) and the second one in β position (distal). The α/β ratio is 3/7 and can be explained by the easier nucleophilic addition of the free amine of the PAH onto the less hindered carbonyl group of the citraconic anhydride during the synthesis of PAHc (Figure 5.1a).

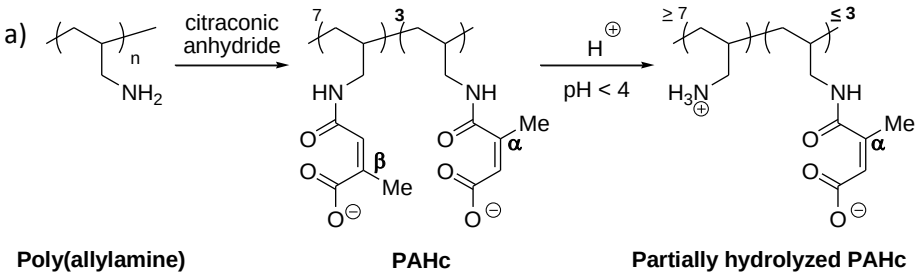

Figure 5.1 Nucleophilic addition of amino groups from PAH with citraconic anhydride. Two isomers derived-citraconate in ratio 3/7 are present along the polymer backbone of PAHc (a); Schematic representation of electrochemically triggered morphogen driven surface confined self-assembly of polyampholytes based on charge-shifting polyelectrolyte (b).

5.3 Results and discussion.

Monitoring the hydrolysis behaviour of PAHc in acid conditions was reported in the literature (Liu et al. 2008). When dissolved in deuterated phosphate buffer at pH 7.4, the side chain hydrolysis occurred slowly with only 25% of conversion after eight days. However, when solubilized in deuterated acetate buffer at pH 5, the side chain hydrolysis reached 55 % within five hours. Close inspections of the data revealed that the rate of hydrolysis of the β isomer that have the methyl group distal to the amide bond was significantly greater than the rate of hydrolysis of the α isomer which have the methyl group proximal to the amide bond. Hydrolysis of the β isomer occurred very rapidly with a conversion of around 70 % in the first five hours and was complete at 95 % after 70 hours. On the other hand, the hydrolysis of the α isomer was much slower with a conversion of only 20% after eight days.

Several days at pH 5 were required to transform entirely PAHc in PAH. Therefore, it seems possible to create *in situ* a polyampholyte in solution at pH below 5 from PAHc, due to the simultaneous presence

of positive and negative charges along the same polymer chain (Figure 5.1a). Going one step further along this line, if a sufficient gradient of protons is generated from a surface (electrode) in the presence of PAHc in solution, the polyampholyte derived from the partial PAHc hydrolysis may self-assemble on itself. This could lead to a polyelectrolyte film based on the solely electrostatic interaction coming from only one polyelectrolyte. This idea constitutes the core strategy for the design of a surface-initiated film construction driven by morphogens (protons, generated from the surface).

Several methods are described to create a gradient of protons from an electrode. By electrochemical oxidation of hydroquinone into 1,4-benzoquinone, two electrons are transferred to the electrode concomitantly with the production of two protons released in the media. Compared to the electrolysis of water which is another common way to generate protons, the oxidation of hydroquinone allows working with a lower oxidative potential, roughly 0.3-0.4 V and therefore is convenient with the use of gold-coated working electrode. By oxidizing hydroquinone at an electrode, a pH of 3.6 has been calculated in the close vicinity of the surface that increases gradually to neutral away from it (Johnson et al. 2010). The self-construction of films was monitored by an electrochemical quartz crystal microbalance (EC-QCM) which was used for both applying a controlled current intensity on the gold electrode and monitoring the film growth. These film buildup were performed under a slight flux (0.05 ml/min) to ensure a constant concentration of reactants. The gradient of morphogens, the protons, was created by electrochemical oxidation of hydroquinone induced galvanostatically from the electrode surface by applying oxidation currents. All experimental details are given in section 5.5. Figure 5.3a shows the evolution of the frequency shift for the third overtone ($\Delta f_3/3$) depending on the different adsorption steps realized on the gold substrate. Successive adsorption step of a first layer of poly(ethyleneimine) (PEI) and then PSS lead to a negatively charged coating onto the gold electrode of the QCM substrate. Rinsing solution was composed of 150 mM $NaNO_3$ solution. This bilayer leads to a decrease of 50 Hz of the frequency shift. PAHc solution (1mg/mL), containing 60 mM of hydroquinone at pH 6, is introduced in the QCM cell. No significant evolution of the frequency shift is observed.

As soon as a constant current is applied between -50 and -150 µA through the electrode, a linear decrease of the frequency shift takes place. The buildup kinetics correspond to the slope obtained by fitting the constructions with a linear model plot. The most important slope, reflecting the faster rate of the film buildup, is obtained when the intensity applied is lower or equal to -100 µA (Figure 5.2a). Figure 5.2b shows the evolution of the polyampholyte films thicknesses and roughnesses for an applied current ranging from -50 to -100 µA and a buildup time of 1h.

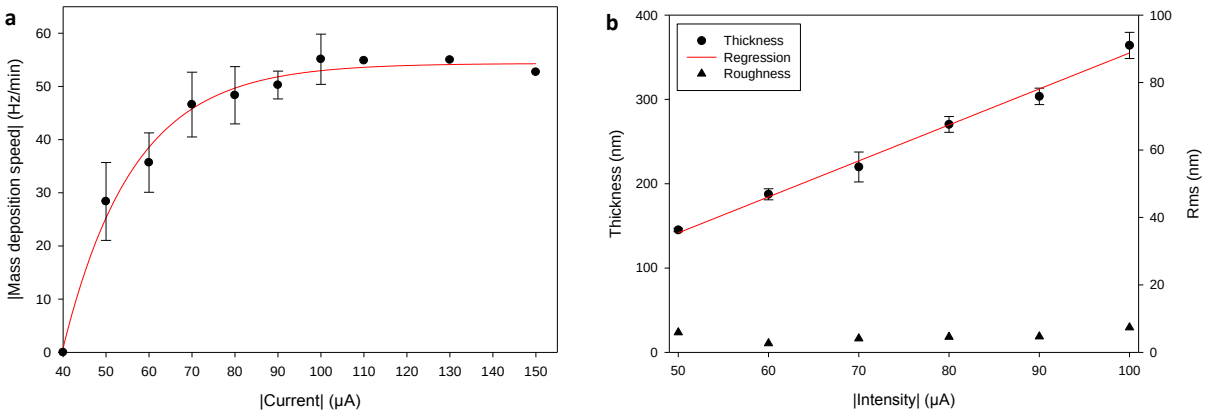

Figure 5.2 Evolution of the mass deposition rate with the variation of the absolute intensity value ranging from 40 to 150 µA, applied during the film buildup. The error bars represent the standard deviation of three independent experiments (a). Evolution of the thickness and roughness of polyampholyte-based films measured by AFM according to the absolute value of the intensity applied to the system to build these films. The buildup was run during one hour for each intensity used. The error bars represent the standard deviation of three independent experiments (b).

Figure 5.3a shows the linear evolution of the frequency shift when -100 µA is applied to the system: a continuous film buildup occurs when applying this current. One hour later, as soon as one rinses the film with 150 mM $NaNO_3$ solution containing hydroquinone while maintaining the current, the film growth stops and the frequency shift remains constant. This film remains thus intact. However, when the film is rinsed with a water solution without hydroquinone or when the current is switched off, an increase of the frequency shift takes place which returns almost to the initial value before the film buildup (data not shown). In the absence of current and thus of pH gradient, the film does not remain stable. It might be due to the fact that when the current is stopped, the pH inside the film is modified and thus also the protonation of the amine and carboxylic groups (from citraconate moieties) along the polymer chains. This affects the anionic/cationic equilibrium leading to a destabilization of the film cohesion. When such a film is built over long periods of time at -100 µA (more than 4 h at -100 µA), after 3 h of continuous buildup, suddenly the frequency shift levels off during 1 hour and then increases rapidly to reach ultimately its value observed before current application (Figure 5.3b). Even in the presence of a current, after a long period of buildup the film is no longer stable and dissolves in solution. This is expected from the full PAHc hydrolysis process leading to the polycation, PAH.

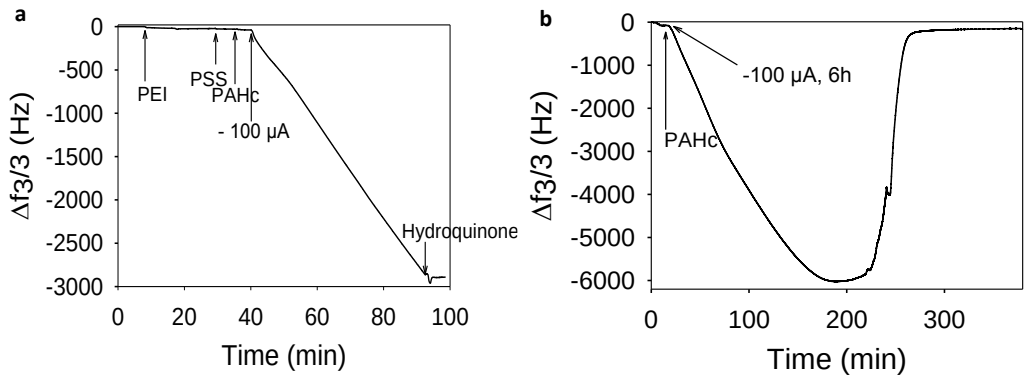

Figure 5.3 Evolution of the frequency shift, $\Delta f_3/3$, as a function of time during the application of -100 µA for 1h in contact with the PAHc solution (a); Evolution of the frequency shift, $\Delta f_3/3$, as a function of time for the application of -100 µA during 6 h. A precursor bilayer of PEI and PSS is adsorbed onto the substrate before the contact with the PAHc solution (b).

The topography of the films was studied by AFM in dry condition by using the contact mode. When built under a current intensity of -100µA, the film growth was stopped after 30, 45 and 60 minutes of buildup: the film-coated crystal was removed from the QCM cell, dried with a stream of nitrogen and imaged. A scratch of the film was performed in order to get its profile. The film is extremely smooth and growth linearly with time to reach 360 nm (Figure 5.4). Moreover, its thickness linearly correlates to the intensity applied to build the film. For the same time of buildup, lower applied intensities lead to thicker films as shown in (Figure 5.2b).

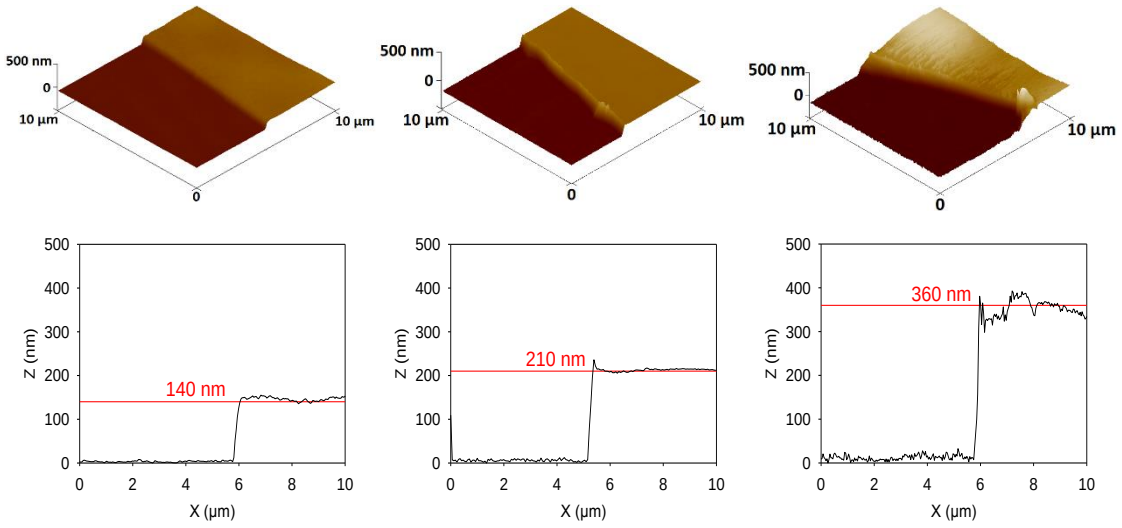

Figure 5.4 Three-dimensional scratched images and profilometric sections (10 µm × 10 µm) obtained in AFM contact mode and dry state of films obtained from PAHc solution after the application of -100 µA during 30 (a), 45 (b) and 60 (c) min. The zero-value line in Z is arbitrarily defined by the apparatus.

In situ composition of the film prepared by using -100 µA intensity was determined by XPS after 30, 45 and 60 min of film buildup (section 5.6.1). This analysis allows the measurement of amino ($\underline{N}H_2$) and ammonium ($\underline{N}H_3^+$) group proportions along the partially hydrolysed PAHc backbone through

the detection of nitrogen atoms. The nitrogen involved in the citraconamide bond (NHCO) is also measurable. Evolution of the ratio between the proportion of the citraconamide group (NHCO) and all nitrogen-containing groups (N_{1s}), NHCO/N_{1s}, allows to determine the degree of hydrolysis of PAHc that composed the film. After 30 min, 64% of the PAHc has been hydrolysed (ratio NHCO/N_{1s}= 0.36), going to 73% of hydrolysis measured both at 45 and 60 min of construction (ratio NHCO/N_{1s}= 0.27 in both cases). The PAHc seems to be hydrolysed partially and rapidly in the first minutes of the film buildup, going to a plateau close to 73% (Figure 5.5).

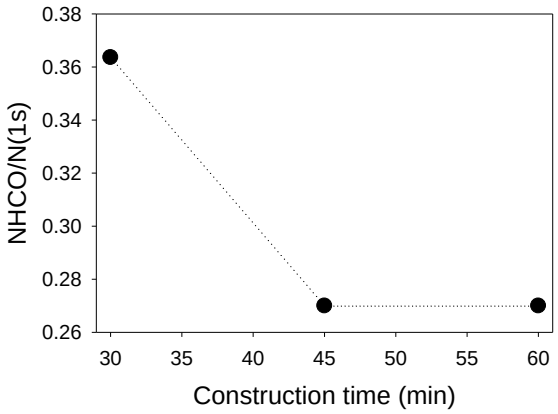

Figure 5.5 Evolution of NHCO/N1s areas ratio determined by XPS of the films prepared from PAHc and built through the application of -100 µA during 30, 45 and 60 minutes.

This value of hydrolysis is in agreement with the literature where the β isomer (70%) present all along the PAHc is quickly hydrolysed, leaving the pH-insensitive citraconamide α isomer (30%) anchored onto the polymer backbone. This XPS analysis confirms the polyampholyte nature of the constituting polymer of the film. Furthermore, it validates our buildup strategy based on the chemical transformation of a polyelectrolyte into a polyampholyte, leading to a film buildup.

To avoid a dissolution of a so-prepared polyampholyte-based films when brought in contact with aqueous solution, we chemically crosslinked them by heating treatment at 150 °C which is a common way to reticulate polyamine and polycarboxylic acid in thin polymer films (Harris et al. 1999). Indeed, chemical reaction occurs leading to stable amide bonds formation from the amine and the carboxylic groups both presents along the hydrolysed PAHc. After thermal crosslinking of the polyampholyte based film (at 150°C for 12 h), its thickness decreases by half of its initial value. In contact with water, the film thickness remains constant even after two cycles of drying-hydrating steps, indicating that the crosslinking provided a robust architecture (Figure 5.6).

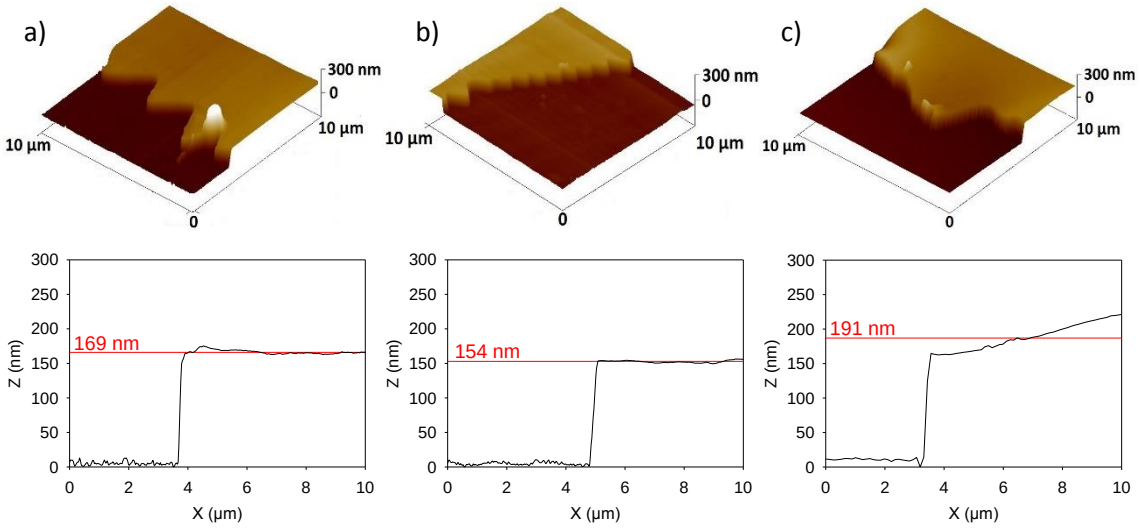

Figure 5.6 AFM images and thicknesses measurements on a scratch of a polyampholyte film buildup at -100 µA during 1h and crosslinked by a heat treatment at 150 °C during 12 h. Three z sections measurements on the scratched film in dry condition at the exit of the oven gives a mean thickness of 168.7 ± 5.2 nm (a). After immersion of the film in MilliQ water during 2h, the three z sections measurements on the scratched film in dry condition gave a mean thickness of 154.5 ± 1.7 nm (b). AFM image in liquid state during a second immersion of the film returned a mean thickness of 191 ± 11 nm for the three z section measurements (c).

5.4 CONCLUSION.

Morphogen-driven film buildup is herein illustrated by a new way of polyelectrolyte-based film design in a single-step process with only one polyelectrolyte. Protons, playing the role of morphogens, are gradually generated from an electrode and diffuse into the environment to induce the chemical transformation of a polyanion into a polyampholyte. Hydrolysed at a level of 73%, due to the presence of two citraconamide isomers having different sensitivity to the local pH, the polyampholyte generated *in situ* adsorbs on the substrate and complexes with itself. Resulting films are extremely smooth with thicknesses going to several hundred nanometers after one hour of -100 µA of current application. Thicknesses can easily be tuned by varying the application time of the intensity. Robust polyampholyte based films can be obtained after thermal crosslinking.

5.5 MATERIAL AND METHODS.

5.5.1 List of chemicals.

PAH (Mn= 60kDa), PSS (Mn=70 kDa) and branched PEI (Mn=60 kDa) are purchased from Sigma-Aldrich Hydroquinone. Deuterated water was purchased from Eurositop and DCl from Sigma-Aldrich. Hydroquinone was purchased from Sigma-Aldrich.

PAHc was prepared according to Lynn and coll. (Liu et al. 2008).

5.5.2 Preparation of solutions.

Polyelectrolyte solutions at 1 mg/ml were prepared by dissolution of the adequate masses of polyelectrolytes in 150 mM $NaNO_3$ solution. PAHc solution was prepared in 150 mM $NaNO_3$ with 60 mM Hydroquinone at pH 5.

5.5.3 Film buildup procedure.

An anchoring bilayer of poly(ethylene imine) (PEI) and poly(styrene sulfonate) (PSS) was deposited onto the gold working electrode by the LbL technique prior to the polyampholyte film buildup.
The aqueous PEI solution (1 mg/ml in 150 mM sodium nitrate) was injected in the electrochemical cell (600 µl) at a flow rate of 600 µL/min with a peristatic pump. The adsorption of the polycation was monitored by EC-QCM-D. Once the signal stabilizes, i.e. after ca. 5 minutes, an aqueous solution of sodium nitrate was injected in the cell to rinse it (600 µl at 600 µl/min) during 2 minutes.
The aqueous polyanion solution (PSS at 1 mg/ml in 150 mM sodium nitrate) was then injected in the cell (600 µL at 600 µl/min) with the peristatic pump. The adsorption of the polyanion on the previous polycation layer was monitored by EC-QCM-D. Once the signal stabilizes, i.e. after ca. 5 minutes, an aqueous solution of sodium nitrate was injected in the cell to rinse it (600 µl at 600 µl/min) during 2 minutes.
An aqueous solution of sodium nitrate (150 mM) containing PAHc (1 mg/ml) and hydroquinone (60 mM) at pH 5 was then injected in the electrochemical cell (600 µl at 600 µL/min). Once the EC-QCM-D signal stabilized, a flow rate of 50 µl/min was established.

A galvanostatic current ranging from -50 to -100 µA was then applied for 1h30 to trigger the hydroquinone oxidation and start the polyampholyte film buildup. After a construction time of 1h, an aqueous solution of 60 mM Hydroquinone in 150 mM sodium nitrate was injected in the cell (600 µL at 600 µl/min) while the electrochemical stimulus was still applied in order to maintain the low pH in the vicinity of the electrode. Once the signal stabilizes, i.e. ca. 5-10 minutes, air was injected in the electrochemical cell while the fixed current was still applied. The absence of reactive species in the cell lead to an increase of the tension from 0.3-0.4 V (oxidation potential of hydroquinone) to 0.7 V, the defined value at which the potentiostat stops.

The gold working electrode was then un-mounted from the EC-QCM-D and dried with a flow of dry air for 5 minutes and the samples were stored in dry state.

5.5.4 Crosslinking of polyampholyte-based film through heat treatment.

At the end of the buildup, the polyampholyte-supported QCM crystal were placed in an oven at 150°C for 12 hours. The so-cross-linked film were imaged by AFM in dry conditions at the exit of the oven (Figure 5.6a). After the imaging, they were fully immerged in 5 mL of MilliQ water for 2h and dried to be imaged by AFM again a second time (Figure 5.6b). The sample were then hydrated again in the same conditions as previously water and imaged by AFM in liquid state for the third time (Figure 5.6c).

5.6 COMPLEMENTARY RESULTS.

5.6.1 XPS analysis.

The binding energies and area percentages of nitrogen included-functionalities are gathered in the following table. The film was prepared from PAHc and built through the application of -100 µA intensity during 30, 45 and 60 minutes. Area measurements corresponding to amino (NH_2), ammonium (NH_3^+) and citraconamide groups (NHCO) are reported for the three films (Table 1).

t (min)	**XPS peak area (%)**		
	NH_2 (399.7 eV)	**NHCO** (400.6 eV)	**NH_3^+** (402.0 eV)
30	46	36	17
45	57	27	16

60	57	27	16

Table 1 XPS area measurement of the amino (NH_2), ammonium (NH_3^+) and citraconamide groups (NHCO) for polyampholyte films prepared at -100 µA during 30, 45 and 60 minutes.

REFERENCES

Aldersley, M. F., A. J. Kirby, P. W. Lancaster, R. S. McDonald and C. R. Smith (1974). "Intramolecular Catalysis of Amide Hydrolysis by the Carboxy-Group. Rate Determining Proton Transfer from External General Acids in the Hydrolysis of Substituted Maleamic Acids." Journal of the Chemical Society, Perkin Transactions 2(12): 1487-1495.

de Saint-Aubin, C., J. Hemmerlé, F. Boulmedais, M. F. Vallat, M. Nardin and P. Schaaf (2012). "New 2-in-1 Polyelectrolyte Step-by-Step Film Buildup without Solution Alternation: From Pedot-Pss to Polyelectrolyte Complexes." Langmuir **28**(23): 8681-8691.

Decher, G. (1997). "Fuzzy Nanoassemblies: Toward Layered Polymeric Multicomposites." Science **277**(5330): 1232-1237.

Harris, J. J., P. M. DeRose and M. L. Bruening (1999). "Synthesis of Passivating, Nylon-Like Coatings through Cross-Linking of Ultrathin Polyelectrolyte Films." Journal of American Chemical Society **121**(9): 1978-1979.

Johnson, E. K., D. J. Adams and P. J. Cameron (2010). "Directed Self-Assembly of Dipeptides to Form Ultrathin Hydrogel Membranes." Journal of the American Chemical Society **132**(14): 5130-5136.

Kirby, A. J. and P. W. Lancaster (1972). "Structure and Efficiency in Intramolecular and Enzymic Catalysis. Catalysis of Amide Hydrolysis by the Carboxy-Group of Substituted Maleamic Acids." Journal of the Chemical Society, Perkin Transactions 2(9): 1206-1214.

Liu, X. H., J. T. Zhang and D. M. Lynn (2008). "Polyelectrolyte Multilayers Fabricated from 'Charge-Shifting' Anionic Polymers: A New Approach to Controlled Film Disruption and the Release of Cationic Agents from Surfaces." Soft Matter **4**(8): 1688-1695.

Mertz, D., C. J. Ochs, Z. Y. Zhu, L. Lee, S. N. Guntari, G. K. Such, T. K. Goh, L. A. Connal, A. Blencowe, G. G. Qiao and F. Caruso (2011). "Atrp-Mediated Continuous Assembly of Polymers for the Preparation of Nanoscale Films." Chemical Communications **47**(47): 12601-12603.

Millar, S. E. (2002). "Molecular Mechanisms Regulating Hair Follicle Development." Journal of Investigative Dermatology **118**: 216-225.

Potter, J. D. (2007). "Morphogens, Morphostats, Microarchitecture and Malignancy." Nature Reviews Cancer **7**: 464-474.

Rydzek, G., T. Garnier, P. Schaaf, J.-C. Voegel, B. Senger, B. Frisch, Y. Haikel, C. Petit, G. Schlatter, L. Jierry and F. Boulmedais (2013). "Self-Construction of Supramolecular Polyrotaxane Films by an Electrotriggered Morphogen-Driven Process." Langmuir **29**(34): 10776-10784.

Rydzek, G., L. Jierry, A. Parat, J. S. Thomann, J.-C. Voegel, B. Senger, J. Hemmerlé, A. Ponche, B. Frisch, P. Schaaf and F. Boulmedais (2011). "Electrochemically Triggered Assembly of Films: A One-Pot Morphogen-Driven Buildup." Angewandte Chemie-International Edition **50**(19): 4374-4377.

Rydzek, G., A. Parat, P. Polavarapu, C. Baehr, J.-C. Voegel, J. Hemmerlé, B. Senger, B. Frisch, P. Schaaf, L. Jierry and F. Boulmedais (2012a). "One-Pot Morphogen Driven Self-Constructing Films Based on Non-Covalent Host-Guest Interactions." Soft Matter **8**(2): 446-453.

Rydzek, G., P. Polavarapu, C. Rios, J. N. Tisserant, J. C. Voegel, B. Senger, P. Lavalle, B. Frisch, P. Schaaf, F. Boulmedais and L. Jierry (2012b). "Morphogen-Driven Self-Construction of Covalent Films Built from Polyelectrolytes and Homobifunctional Spacers: Buildup and Ph Response." Soft Matter **8**(40): 10336-10343.

Rydzek, G., T. G. Terentyeva, A. Pakdel, D. Golberg, J. P. Hill and K. Ariga (2014). "Simultaneous Electropolymerization and Electro-Click Functionalization for Highly Versatile Surface Platforms." Acs Nano **8**(5): 5240-5248.

Wu, L. Q., A. P. Gadre, H. M. Yi, M. J. Kastantin, G. W. Rubloff, W. E. Bentley, G. F. Payne and R. Ghodssi (2002). "Voltage-Dependent Assembly of the Polysaccharide Chitosan onto an Electrode Surface." Langmuir **18**(22): 8620-8625.

GENERAL CONCLUSION

Fast deposition on a substrate of organic coatings with an easy and cheap setup is a crucial point towards their applications in the industrial sphere. The one-pot morphogenic approach represents one of the promising ways to achieve these requirements. The first work of this PhD was focused on the one-pot morphogenic buildup of polymer brushes by an eSI-ATRP process. In this part, the morphogen role was played by electrochemically generated copper (I) ions thus generalizing the application of this type of morphogen to other reactions than the Huisgen-Sharpless click chemistry. In the second and third part of this work another type of morphogen was used, namely, protons. The change of the morphogen chemical nature demonstrated the versatility of this concept to other chemical processes. In the second part, the proton morphogen was used to deprotect a polyanion and form a polycation near an electrode. This class of polymers, known as “charge shifting” polymers, was used concomitantly with another polyanion which maintained its charge in acidic media. The two polyelectrolyte of oppositely charges formed complexes on the electrode surface thus leading to the buildup of polyelectrolyte films. In the last part of this work, a partial “charge shifting” polymer was used together with the proton morphogen. In this case, only a fraction of the polyanion was hydrolysed in the electrochemically generated acidic media. The presence of both positive and negative charges on the polymer backbone leads to the complexation of the generated polyampholyte at the electrode and thus to a film buildup.

In the first part of this study, the morphogenic buildup of polymer brushes by eSI-ATRP was investigated. This was intended to show that the copper (I) morphogen used in the Huisgen-Sharpless click chemistry could be adapted to other chemical processes such as SI-ATRP. In that case, it was expected to form polymer brushes by eSI-ATRP with well-defined structure and properties. The materials used to conduct such an experiment were studied to determine the best suited initiator, monomers and transition metal complex. The buildup of the polymer brushes was obtained at an electrode bearing a polyelectrolytic macroinitiator by applying a CV onto a monomer solution containing the transition complex and a bromide salt. The chemical nature of the buildup at the electrode was indirectly verified to be the polymer brushes by testing their anti-fouling properties. Moreover, the influence of the CV scan rate and of the bromide salt present in solution was studied. Increasing the bromide salt concentration allowed to slow down the buildup kinetic and thus to obtain a better control of the polymerization process. The decrease of the CV scan rate was correlated to longer and thicker film buildup. AFM analysis on the polymer brushes displayed thin and smooth coatings. All these parameters influencing the buildup kinetic were discussed with regard to the ATRP process mechanism. Closer investigation of the polymer brushes buildup kinetic revealed that such a

kinetic is in good agreement with the expected one for an ATRP process. However, competitive papers were published in the meantime of this study which lead us to stop further investigation. Nevertheless, it was noted that the experimental parameters used by the competitive team to conduct an eSI-ATRP experiment were close to ours. This also confirms that the results obtained during our experiments were indeed coming from the wanted eSI-ATRP process.

In the second part of this work, the one-pot morphogenic buildup was extended to the formation of films whose integrity is based on polycation and polyanion electrostatic interactions. The chemical nature of the morphogens, i.e. protons, was different from the previous work showing the versatility of this buildup strategy. The protons were produced by the electrochemical oxidation of a small organic molecule at an electrode. In presence of two polyanions, one being a “charge shifting” polymer, i.e. a polymer whose negative charges change into positive ones in acidic media, a film was constructed whose thickness increased with the deposition time. The influence of the applied galvanostatic current intensity was demonstrated to impact the buildup kinetic. Lower currents were shown to lead to higher buildup kinetics and thus to thicker films for a given construction time. The deprotected “charge shifting” polymer (the polycation) was shown to lead to a film formation in presence of a polyanion but also an enzyme. The enzyme films constructed at the electrode were demonstrated to retain their catalytic activity. Furthermore, it was also proved that this catalytic activity increased with the film deposition time, i.e. with its thickness, confirming that the whole film contributed to the measured activity. The versatility of this platform towards different negatively charged macromolecules was used to buildup films with different chemical compositions on microelectrodes.

In the last part of this work, polyampholyte films were constructed by the one-pot morphogenic approach. As in the second work, the proton morphogen was generated electrochemically at an electrode by the oxidation of a small organic molecule. In presence of a partial “charge shifting” polyanion which contains two isomers with different lability in acidic media, a partial hydrolysis of the polymer occurred. The polyampholyte formed at the electrode leads to a film construction whose thickness increased with the deposition time. Chemical analysis of the deposited film confirmed its polyampholytic nature. It was then demonstrated that the film buildup kinetic could be controlled by tuning the applied current intensity. Lower current intensity lead to faster deposition rate and to thicker films for a given construction time. These films can be later cross-linked by a thermic post treatment in order to obtain more robust coatings.

The results obtained during this PhD shows the versatility of the one-pot morphogenic approach to obtain organic thin films or polymer brushes. This strategy presents the advantage of being fairly simple since all the non-interacting species are mixed together and brought at an electrode. Once the electrochemical stimulus is applied, the generated morphogen triggers the fast buildup of the brushes or films. Furthermore, this process could be used to provide spatially functionalized materials with biosensing properties.

The easy setup, the fast tunable deposition kinetic, the spatio-selectivity of the buildups and the ability to form bioactive surfaces all represents strong arguments in favour of this approach and for its potential scale up in industrial applications. This strategy could be further developed to other chemical system in order to provide faster deposition rates of robust films with tuneable properties. It would be of particular interest to develop self-constructed films based on crosslinking reactions between polymers. For this purpose, we have to select a fast and effective chemical reaction that could be obtained after an electro-activation of one of the polymers.

UNIVERSITÉ DE STRASBOURG

Alexandre DOCHTER

Polymer films and brushes self-construction by electrochemically triggered morphogens.

Résumé

Résumé. Les multicouches de polyelectrolytes, systèmes auto-assemblés par adsorption successive de polycations et de polyanions, constituent un matériau d'intérêt pour la fonctionnalisation de surface. Ce type de revêtement possède toutefois quelques limitations majeures : leur construction est lente et fastidieuse ; leur tenue mécanique et chimique est faible. Récemment, une méthode basée sur l'auto-construction de films par l'utilisation d'un morphogène, i.e. un gradient de catalyseur généré depuis une surface, a été développé permettant ainsi une rapide construction de revêtements robustes. Cette technique reste toutefois limitée à des systèmes particuliers basés sur la chimie click ou sur des interactions hôtes-invités.

Nos travaux ont permis de diversifier cette approche de construction tout-en-un par l'utilisation de morphogènes. Dans un premier temps, des brosses de polymères ont été construites en une étape depuis une surface par la réaction de polymérisation ATRP. Cette réaction a été catalysée par la formation d'ions Cu(I) (le morphogène) par électrochimie depuis la surface de travail.

L'approche morphogénique a également été utilisée afin de construire des films de polyélectrolytes et de polyampholytes en une étape par la génération électrochimique d'un gradient de protons (le morphogène) depuis la surface de travail. Ces films ont été fonctionnalisés pour présenter une activité enzymatique.

Mots clés: Auto-assemblage, interface, polyéléctrolytes, enzymes, biomatériaux, électrochimie, morphogène, ATRP, microbalance à cristal de quartz

Résumé en anglais

Abstract. Polyelectrolyte multilayers, i.e. self-assembled systems based on successive polycation and polyanion adsorptions, constitute interesting materials for surface functionalization. These coatings possess several limitations: they are weak towards chemical and mechanical constraint and their buildup is long and tedious. Recently, a new method based on the self-construction of films by the means of a morphogen (a catalyst gradient generated from a surface) has attracted attention since it allows the quick self-assembly of robust films. Nevertheless, this technique was quite limited to peculiar systems based on click chemistry or on host-guest interactions.

This present work generalize the one-pot morphogenic approach to other systems. In the first place, polymer brushes were built up from a surface by ATRP polymerization. The Cu(I) catalyst (the morphogen) was electrochemically generated at the interface.

The morphogenic approach was later used to buildup polyelectrolytes and polyampholyte films in a one-pot manner by electrochemically generating protons (the morphogens) at the interface. These films exhibited an enzymatic activity.

Key words: Self-assembly, interface, polyelectrolytes, enzyme, biomaterials, electrochemistry, morphogen, ATRP, quartz crystal microbalance